To the Graduate Council:

I am submitting herewith a dissertation written by William L. Holt entitled "High Temperature Combustion of Pulverized Coal." I recommend that it be accepted in partial fulfillment of the requirements for the degree of Doctor of Philosophy, with a major in Mechanical Engineering.

Y. C. L. Wu

Y. C. L. Wu, Major Professor

We have read this dissertation and recommend its acceptance:

Floyd W. Crawford

Kenneth R. Kimble

Kenneth E. Harwell

J. B. Dicks

Accepted for the Council:

L. Evans Haworth

Vice Chancellor
Graduate Studies and Research

HIGH TEMPERATURE COMBUSTION OF PULVERIZED COAL

A Dissertation

Presented for the

Doctor of Philosophy

Degree

The University of Tennessee, Knoxville

William L. Holt

March 1981

DEDICATION

This dissertation is dedicated to Patsy, who provided the inspiration, encouragement and love required to complete this work and to my children, Katie, Ashley and Lee.

ACKNOWLEDGEMENTS

In a work of this nature, it is impossible to recognize all of the contributors. During the author's tenure at the University of Tennessee Space Institute (UTSI), many people have contributed to his professional growth. Sincere gratitude and appreciation are expressed to his major advisor, Dr. Susan Wu, for her patience, interest and encouragement. Grateful appreciation is expressed to Dr. John Dicks for his personal interest, encouragement and patience. Without the interest of Drs. Wu and Dicks this work would not have been possible. Special thanks goes to Dr. Kenneth Harwell whose interest and genuine concern were most appreciated. To the other members of the committee, Dr. Lloyd Crawford and Dr. Kenneth Kimble, sincere appreciation is expressed.

Other members of the staff of the Energy Conversion Division at UTSI also contributed to this work. The foremost of these is Mr. John Lanier. To John, the author would like to express his appreciation for his interest and the many hours spent discussing the topic and relevant data. Mr. Bob Clemons spent many hours reducing the data and for this the author is grateful.

The author was fortunate to have beneficial discussions with Dr. Paul Chung of the University of Chicago, to whom he expresses his appreciation.

Of notable value, the author expresses his appreciation and graditude to the hard work and patience of the typist, Ms. Mary Ann Decker. Without her help and that of the Energy Conversion Division secretarial staff this work would not have been completed.

This research was supported by the United States Department of Energy under contract DE-AC02-79ET10815.

ABSTRACT

During recent years there has been mounting interest in the combustion of coal under conditions of high heating rates and high final temperatures. This has resulted from the national interest in coal utilization due to the present energy crisis.

This research was conducted in conjunction with a magnetohydrodynamics (MHD) coal combustor development program conducted at The University of Tennessee Space Institute. During the course of this development program, studies were made on the effects of mixing rate and residence time on the combustion of bituminous coal. Nominal heating rates of 10^5 degrees K per second with final combustion temperatures on the order of 3000°K characterized the typical test conditions. The stoichiometry was nominally 0.90 with oxygen concentrations in the oxidant above 55%. The experimental results were compared to a theoretical coal combustion model involving a one-step, first order Arrhenius reaction rate constant. This model proved to be adequate for the test conditions being studied.

Conclusions were reached as to the behavior of pulverized coal under flame conditions such as those that might be experienced in an MHD coal combustor. Qualitative information is presented as to the behavior of the coal particles during combustion and subsequent burn-out of the carbon.

Recommendations for further work are presented along with recommendations for improving the coal combustion model.

TABLE OF CONTENTS

LIST OF TABLES

LIST OF FIGURES

NOMENCLATURE

A_c	Cross-sectional area of combustor
A_w	Surface area of cylinder combustor wall
A_s	Surface area of a particle
A	Stoichiometric coefficient of oxidant
AVCO	AVCO Everett Research Laboratory
B	Stoichiometric coefficient of fuel
C	Stoichiometric coefficient of Products
C_i	Gaseous i th species mass fraction based on the total gaseous species
$\bar{C}$	Mean molecular speed
$\bar{C}_o$	Constant defined by $\bar{C} / \sqrt{Ts}$
c_p	Constant pressure specific heat
D	Binary diffusion coefficient
DAF	Dry Ash Free Coal
D_c	Diameter of cylindrical combustor
E_s	Representative activation energy for surface reaction with CO_2 and H_2O
E_v	Representative activation energy of volatilization
F	Normalized relative mass flux of the slag in coal particle
$\hat{F}$	Total mass flow rate per combustor
$\hat{F}_{air}$	Air flow rate per combustor at entrance to combustor (I)
$\hat{F}_b$	Fuel flow rate per combustor at I
$\hat{F}_o$	Total oxidant flow rate per combustor at I
h	Total enthalpy of the mixture defined by Eq. 3-67
Δh°	Heat of combustion of coal per unit mass of the gaseous combustible defined by Eq.3-99
Δh_o	Heat of combustion per unit mass of gaseous combustion produced defined by Eq. 3-99

Δh_3	Heat of dissociation of CO_2 into CO per unit mass per unit mass of CO_2 according to Eq. 3-2
Δh_5	Heat of dissociation of NO_2 into NO per unit mass of NO_2 according to Eq. 3-3
Δh_{10}	Heat of dissociation of H_2O into H_2 and O_2 per unit mass of H_2 according to Eqs. 3-2 and 3-4
HV	Lower heating value of coal per unit mass of coal
HHV	Higher heating value of coal per unit mass of coal
J_s	Rate of surface reaction with CO_2 and H_2O
K_o, K_{wo}	Pre-exponential rate constant for volatilization
K_1, K_2, K3	Equilibrium constants defined in Eq. 3-91
L	Latent heat of volatilization of combustible in coal
L_g	Latent heat of volatilization of slag in coal
$\hat{L}$	Mass weighted latent heat of volatilization defined by Eq. 3-34
Le	Lewis number
M_i	Molecular weight of i <u>th</u> species
$\hat{M}$	Molecular weight of the gaseous mixture $(\Sigma_i C_i)M_i)$
M_i	Mass fraction of i <u>th</u> species including the solid particles
$\dot{m}$	Mass rate of generation of total gaseous species per unit volume
$\dot{m}$	Mass rate of generation of total gaseous species per coal particle
$\hat{m}_s$	Instantaneous combustible particle mass
$\hat{m}_{so}$	Initial coal particle mass
$\Delta m'_s$	Mass of the coal per unit mass of the mixture burned during ignition
N_s	Number density of the particles
P	Static pressure of the gaseous mixture

P_b	Partial pressure of the volatilized coal at the coal-gas interface due to heating
P_{bs}	Partial pressure of the volatilized coal at the coal-gas interface due to chemical surface reaction with CO_2 and H_2O
P_9	Partial pressure of ash vapor at the coal gas surface
Q	Rate of heat loss from the mixture per unit volume
Q_{Rg}	Rate of heat loss from the mixture per unit volume based on the gaseous radiation
QRS	Rate of heat loss from the mixture per unit volume based on the particulate radiation
q_R	Rate of radiant heat loss from each particle
R	Particle radius
R_o	Initial particle radius prior to ignition
Re	Reynolds number based on the particle diameter and gas-solid relative velocity
R_u	Universal gas constant
r	Radial coordinate based on particle center
Sc	Schmidt number
T	Absolute temperature
t	Time
u	Flow velocity of the mixture
V	Mass fraction of the coal volatilized
V*	Maximum mass fraction of coal that could be volatilized
V_c	Combustor volume
V	Convection velocity in the direction of r
W_i	Rate of production of i th species by gas phase chemical reaction

x	Coordinate in the flow direction
Z_i	Mass fraction of i th species in ash-free coal given by Eq. 3-97
Z_v	Mass fraction of combustible in coal given by Eq. 3-98
$Z''_i)$	Mass fraction of i th species in coal as given by ultimate analysis
Z_{bs}, Z_{9s}	Defined by Eq. 3-35
$Z'bs$, $Z'9s$	Instantaneous mass fractions of combustiles and ash, respectively, in coal particle
β	$= 3\hat{\beta} + 1$
$\hat{\beta}$	Exponent defined in Eq. 3-5
γ	Function defined by Eq. 3-42a
δ_s	Average density of burning coal
ϵ_g	Emissivity of gaseous mixture
ϵ_s	Emissivity of particulate surface
ϵ_w	Emissivity of combustor wall for particle radiation and that of gas at wall for gas radiation
$\hat{\epsilon}_s$	Parameter defined below Eq. 3-73
ζ	Integral function defined by Eq.3-49
γ	Thermal conductivity of the gaseous species
ρ	Global density of the gas-solid mixture
ρ_g	Density of gaseous species
σ_a, σ_b	Functions defined by Eq. 3-42a
$\overline{\rho D}$	Average constant value of ρD

Subscripts

a, b, d, e	Oxidant, fuel, combustion product, and inert species respectively
C	Carbon

g	Gaseous
H	Hydrogen
I	Entrance to combustor
i	i th species
N	Nitrogen
O	Oxygen
S	Sulfur
s	solid
w	Inner wall surface of combustor
o	x = 0 at the end of ignition, value of parameter at this point
1, 2, 3	O_2, CO, and CO_2 respectively
4,5,6	N_2, NO_2, and NO, respectively
7, 8, 10	H_2O, SO_2, and H_2 respectively
9	Ash
∞	Outside of the diffusion layer surrounding the particle

CHAPTER 1

INTRODUCTION

In combustion systems employing pulverized coal as fuel the combustion process is very complex. The combustion of coal has usually been viewed as occurring by means of gas phase reactions of thermally produced coal volatiles and heterogeneous surface reaction with surrounding oxygen. Volatile release terminates when the original coal organic structure has been reduced to more or less swollen or shattered carbonaceous char with some mineral content. The char thus produced will continue to oxidize due to radiative heat transport from the gas phase reaction and at a rate controlled by diffusion of oxygen. The reactions that are taking place are occurring simultaneously and thus mathematical modeling of the process becomes very difficult.

In general, combustion phenomena can be classified into two categories, i.e., "diffusion controlled" and "kinetically controlled"[1][1]. Diffusion controlled combustion processes are those in which the rate of diffusion is substantially less than the chemical reaction rate. In diffusion controlled processes, phenomena such as mixing and vaporization play the dominant roles. Examples of diffusion controlled combustion processes are liquid droplet

---

[1]Numbers in brackets refer to similarly numbered references in the Bibliography

combustion in rockets and laminar and turbulent diffusion flames. Combustion processes that are kinetically (kinetics as used in this work refer to chemical reactions) controlled are those in which the combustion rate depends on the path of the reaction, i.e., the chemical reaction rate is less than the rate of diffusion. Combustion of pulverized coal in a conventional burner is an example of kinetically controlled combustion.

During the combustion of pulverized coal, volatiles, which consist of hydrocarbon gases, are released when the coal particle temperature is raised. This process differs greatly from that of vaporization which occurs in the combustion of liquid fuels. The release of volatiles depends on chemical reactions that take place on the surface and within the coal particle and thus is not a simple phase change as is the case of liquid fuel vaporization. When the temperature is lowered, the products of combustion of coal do not condense so as to reconstitute the same coal substance.

During the release of volatiles the process may be exothermic rather than endothermic as in the case of vaporization. For a coal particle there is no distinct temperature at which the volatile release occurs. Volatile release depends on the rate at which the temperature of the particle is increased and will continue until all of the volatiles are driven off. After release of all the volatiles, the substance that is left has a very high carbon con-

tent with some mineral matter. This substance is generally referred to as char. Therefore two general processes take place (usually simultaneously) in the combustion of a coal particle, one of volatile release (devolatilization) and one of burning of char.

Of the processes that take place during the combustion of coal the least known are the reactions and their rates that lead to the devolatilization of coal particles. In studies [2] that have been made, devolatilization is most often assumed to occur instantaneously. Further, it is assumed that the amount of volatiles to be produced is fixed based on a value given by the proximate analysis or some other estimated value. Devolatilization is known to exert a strong influence on the combustion of pulverized coal since the rate at which devolatilization proceeds and its yield affects both ignition and flame stability. Recent studies [3-5] indicate that the volatile yield depends on both heating rate and combustion temperature of the coal particle. As with any chemical reaction, the final pyrolysis reaction product (volatile yield) depends on the path of the reaction as well as its degree of completeness.

Objectives

The objectives of the present investigation were as follows:

a) To identify the rate controlling mechanism and determine experimentally the effect of mixing on pulverized coal combustion under conditions of high heating rates ($\approx 10^5$ °K/sec) and high final temperature (≈ 3000°K).

b) To determine experimentally the effect of residence time on pulverized coal combustion with high heating rates and final temperatures.

c) To verify a theoretical combustion model that assumes perfect mixing of fuel and oxidant.

d) To use the theoretical model to establish parametrically the operating parameters for a coal-fired MHD combustor.

e) To use the theoretical model to demonstrate the dependence of carbon conversion on residence time, oxidant preheat temperature, oxygen concentration in the oxidant and stoichiometry.

Organization

The remainder of this dissertation is organized into five chapters. Chapter 2 presents a review of previous theoretical and experimental research on the devolatilization of pulverized coal. The discussion is limited to studies of small coal particles ($\simeq$ 50 μm in diameter), high heating rates, high final temperature, and short residence times. Chapter 3 is a detailed description of a theoretical coal combustion model developed by Chung and Smith [6]. This model was developed without experimental verification and represents a significant simplification when compared with other theoretical models. In Chapter 4, the experimental apparatus and procedures are described. Chapter 5 presents a comparison of the theoretical predictions and experimental results along with a discussion of the limitations of the model. The model is used parametrically to assess the impact of various parameters on carbon conversion. A summary of the present work is presented in

Chapter 6 with a discussion of the conclusions. Recommendations are made for improvement of the theoretical model and for future research.

CHAPTER 2

REVIEW OF RELATED WORK

In this chapter, previous work that is related to the rapid devolatilization of coal particles will be discussed both from an experimental as well as theoretical viewpoint. No attempt will be made to describe the entire subject since this is well documented elsewhere [2-5], but consideration will be given to rapid devolatilization that is relevant to the combustion of pulverized coal particles. With this is mind, the discussion will be limited to studies that consider the following parameters:

1) coal particle diameters less than 100 microns,
2) heating rates of 10^4 degrees K per second or greater,
3) final temperatures in excess of 10^3 degrees K,
4) residence times less than a few seconds.

Pyrolysis or devolatilization is a name given to any process which subjects a thermally degradable material to heat or thermal energy resulting in the release of gases. The primary gaseous products that are released in such a process, which can be liquids or even solids at certain conditions, are referred to as volatiles. The residual solid that is left after devolatilization will be a material that has a very high carbon content with some mineral matter. It has been shown [7,8] that this residual matter can be further devolatilized if the heating process continues. This residual matter is normally referred to as char.

With the restrictions that have been imposed, such as small particles being heated at very high rates with very high final temperatures, the devolatilization process is very complex. This difficulty arises because the coal particles are not homogeneous. If one examines various particles from the same "batch" of coal, it will be found that the chemical and physical properties of the various particles vary greatly. The existence of a broad range of coal types, such as bituminous and anthracite, further complicates the problem since each type will decompose in a slightly different manner. Therefore, it is difficult to develop a model that will completely characterize the decomposition and combustion of any type of pulverized coal. Thus it is necessary to develop a model that attempts to characterize the "average" devolatilization. Further, this model must be limited to a specific type of coal and will be subject to limitations imposed by the experimental variables. In the following discussion, some previous experimental results will be described along with the results of previous theoretical work.

Previous Experimental Work

Parameters that are known to be important in rapid devolatilization of coal include coal type, oxygen concentration, average particle size and size distribution. In addition, the thermal history of a particle is known to be

important and this includes the heating rate as well as the final temperature. In examining a given experiment, the duration of the heating as well as the quench process becomes influential as well as the composition and pressure of the ambient gas.

Most previous experiments have relied on the collection and analysis of quenched gas and/or char samples gathered after devolatilization. The char has normally been analyzed using the proximate or ultimate analysis. The proximate analysis determines the volatiles, fixed carbon and ash while the ultimate analysis determines the elemental composition.

There are basically three types of experiments that have been performed that are applicable to the analysis of the devolatilization of pulverized coal. In the first type of experiment, coal particles are embedded on a wire screen and electrically heated. In this type of experiment, both the heating rate and the ambient conditions can be controlled since they are not affected by the devolatilization of the coal. However, the largest uncertainty lies in the fact that there is an unknown lag time and temperature difference involved in the heating of the coal particle by the wire screen. Anthony [8] reported results from this type of experiment where the heating rate and final temperature were independently controlled.

Stickler [9] performed experiments that involved injecting coal particles into a preheated, hot gaseous

stream. This is representative of the second type of experiment. The advantages offered by this type are that the ambient atmosphere, final temperature and particle concentration can be easily controlled; however, the major disadvantage is that the heating rate of the particle is not known precisely because this depends on the ambient conditions experienced by the particles.

Howard [10] performed experiments in which the coal particles were burned in a flame. This third type of experiment is the subject of the present work. The obvious advantage of this type of experiment is that it represents the type of environment encountered by pulverized coal combustion in commercial processes. The distinct disadvantage lies in the fact that the only variables that can be controlled during the process are those associated with the input streams. In these experiments the heating rate, final temperature, and ambient conditions are determined by the resulting flame.

One of the first important results that was obtained using the wire mesh technique was the work done by Loison and Chavin [7] when they determined that higher heating rates and higher final temperatures produced a higher volatile yield. The problem with their experiment was that the heating rate and final temperature could not be independently controlled. Thus, it was not possible to determine which variable was responsible for the higher yield of volatiles.

Since those experiments, much work has been directed towards investigating this type of phenomenon due to its fundamental importance to the high temperature combustion of pulverized coal as well as to coal gasification processes. Upon examination of the various work that has been done it can be concluded that the devolatilization process at atmospheric pressure occurs in what may be viewed as a two-step process [7,8].

In the experiments of Anthony [8] the coal particles are heated to a high final temperature at a very high heating rate and held at those conditions for a short time. After heating, the particles are rapidly cooled and collected with the residual volatile matter being determined by the proximate analysis. The proximate analysis involves heating the coal particles at a relatively slow rate (15°C/sec) to a temperature of 1273° Kelvin and held for seven minutes. In these experiments the coal particles had reached some quasi-equilibrium state prior to being quenched and the proximate analysis performed. However, during the proximate analysis further devolatilization occurred in the proximate furnace. The implication of these results is that if the coal particles had been maintained at the elevated temperature for a longer period of time, further devolatilization would have occurred. These results imply that there is a two-step process; one that occurs at a fast rate and one that occurs at a much slower rate.

Most of the work that has been done on rapid devolatilization has been directed toward an understanding of the first step. This results from the fact that it is difficult to maintain the coal particles at the high temperatures for sufficient periods of time for the second process to take place.

This type of behavior was found in experiments by Anthony [8] with lignite and bituminous coal. Figure 2-1 shows the effect of time on devolatilization weight loss from Montana lignite at different heating rates and final temperatures. Anthony found that the final weight loss from lignite, independent of final temperature, was 41% at a final temperature of 1000°C and 31% at a final temperature of 700°C. Proximate analysis of the same coal indicated that the weight loss was 44.71% at 950°C when the residence time was seven minutes. Thus his data indicated the existence of a fast process and a slower second process during devolatilization. He reported a similar type of behavior for bituminous coal. However, the behavior for bituminous coal was quite different from that of lignite when subjected to varying ambient pressures. He noted that in the case of lignite there was no change in weight loss when the pressure was varied from 0.001 to 100 atmospheres. In the case of bituminous coal, shown in Fig. 2-2, the weight loss decreased substantially with increasing pressure. His data indicated that at pressures below about 5 atmospheres the volatile yields exceed that which would be found by proximate analy-

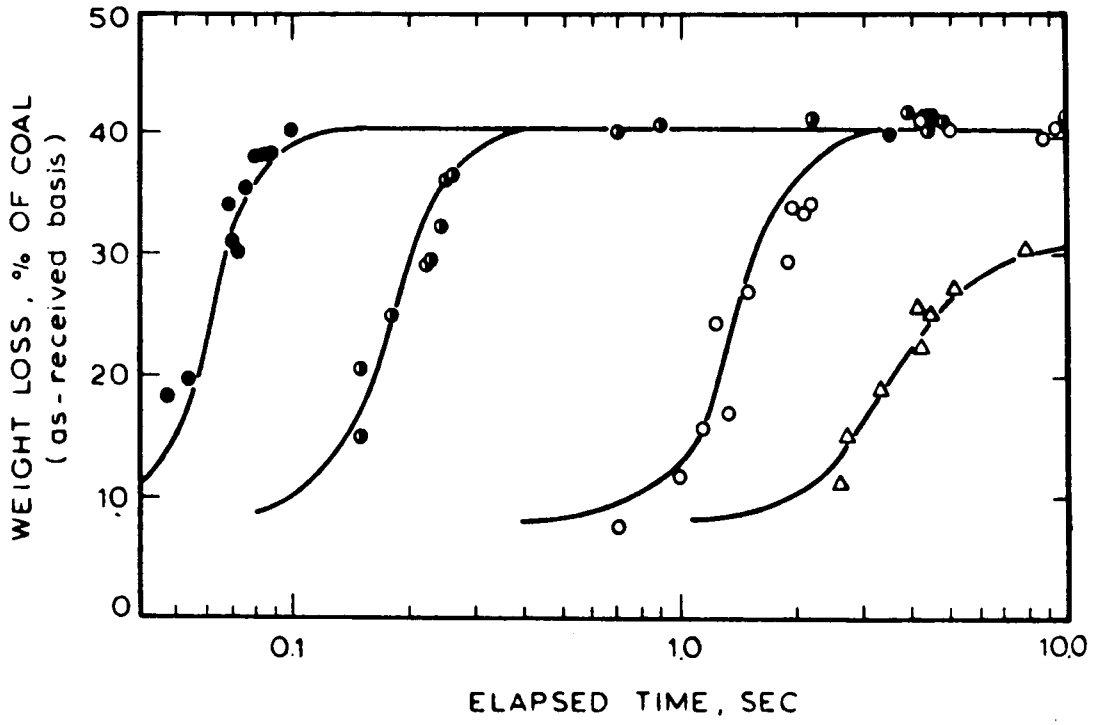

Figure 2-1. Effect of time on devolatilization weight loss. From lignite at different heating rates and final temperatures [t=0 at initiation of heating; pressure - 1.0 atm helium; mean particle diameter = 70 μm; final temperature (if attained) - 1000°C (●, ◑, ○), 700°C (Δ); nominal heating rate (C·sec) - 10,000 (●), 3000 (◑), 650 (○) 180 (Δ)] [8]

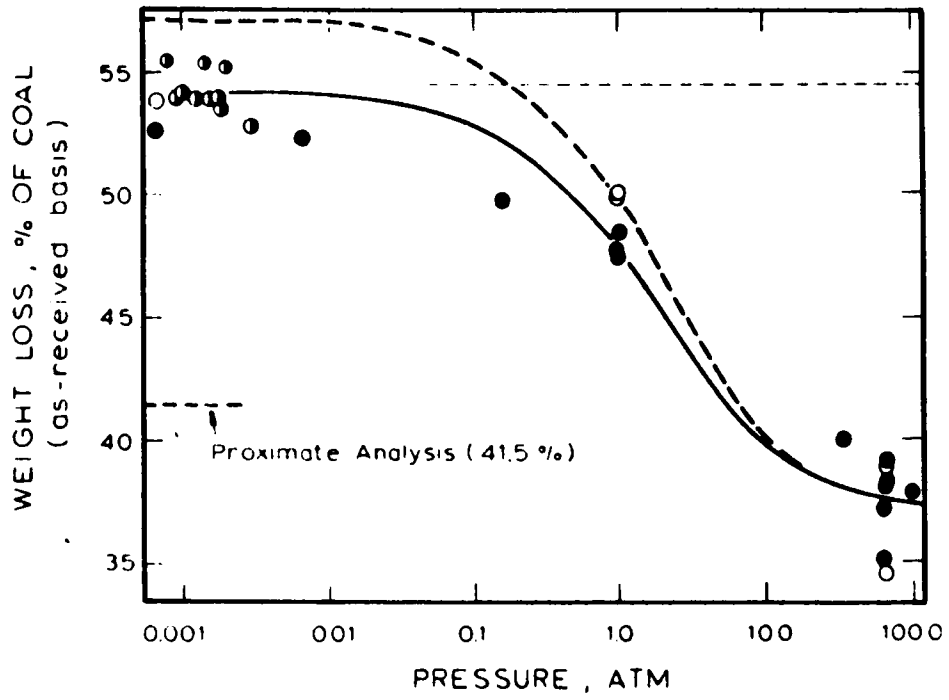

Figure 2-2. Effect of pressure on devolatilization weight loss. From Pittsburgh seam bituminous coal [final temperature = 1000°C; experimental time = 5 to 20 sec; mean particle diameter = 70 μm; atmosphere = helium; nominal heating rate (°C/sec)-10,000 (○), 3000 (◑), 650 to 750 (●); curves (solid-uncorrected for cracking deposition; dashed-corrected for cracking deposition)] [8]

sis. The data also indicate that higher heating rates increased the weight loss at pressures below 1 atmosphere by about 2 percent, but at higher pressures the effect of the heating rate was trivial. Tar condensation occurred during the devolatilization of the bituminous coal but did not occur with the lignite.

Anthony's data thus showed that the second process in the reaction is so slow that its effects would not be seen during rapid devolatilization. His data further indicated that the total volatile loss was apparently independent of the heating rate or the residence time. This conclusion can be supported by other experiments and seems to apply to temperature ranges other than those examined by Anthony.

Using a hot gas particle heater, the most comprehensive data on the first fast step of rapid devolatilization were obtained by experimenters at BCURA [2]. Their results have been supported by other experimenters using small flames [11]. Figure 2-3 is a typical devolatilization curve for different heating rates and final temperatures taken from the work by BCURA. These data illustrate the general devolatilization behavior that is observed in the first fast step of the reaction. As indicated in the figure, the residual volatiles in the char, as determined from proximate analysis, decreased exponentially with residence time in the reactor. However, as the coal particles reached what seems to be a quasi-equilibrium state in the reactor, further devolati-

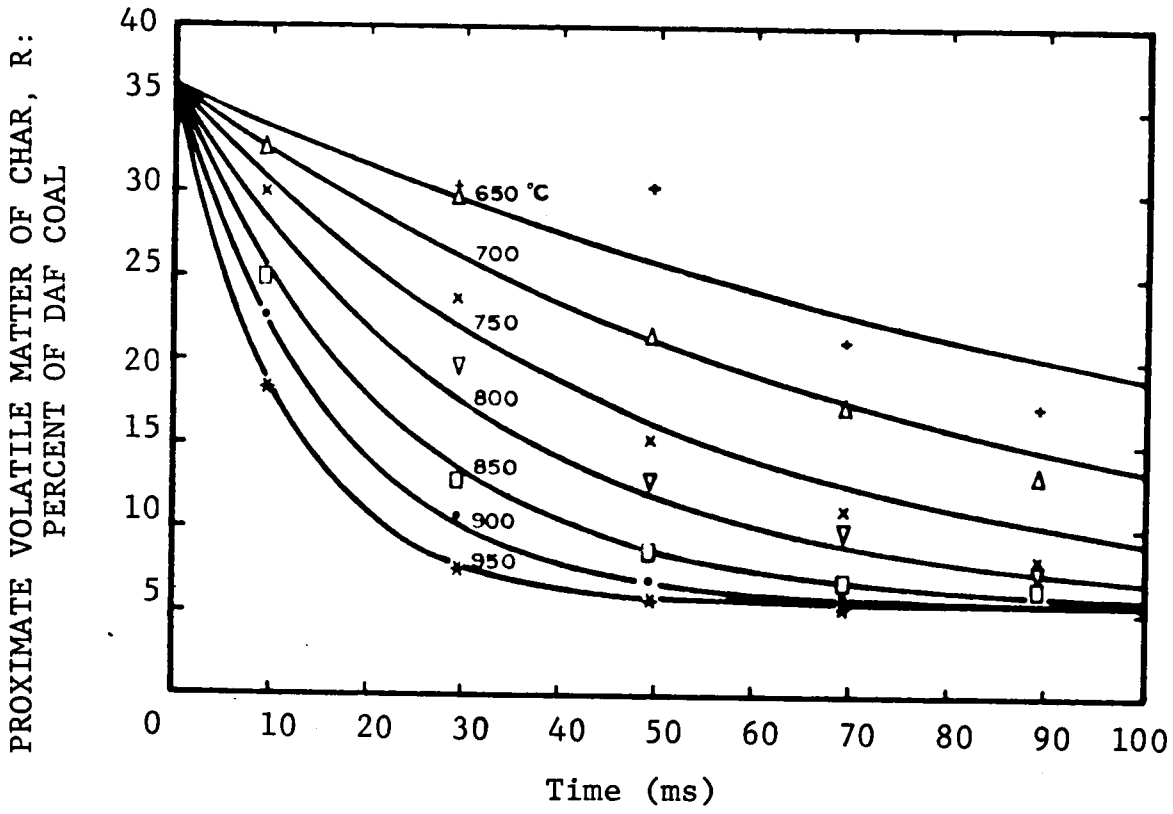

Figure 2-3. Variation of proximate volatile matter of char with time at various temperatures. [2]

lization of the residual char occurs during the proximate analysis. From these data it is seen that the rate of devolatilization is lower at lower temperatures and/or heating rates while the amount of residual volatiles decreases as the reactor temperature is increased. It should be pointed out that both the rate of devolatilization and the amount of residuals that are left in the char depend upon the coal type.

Anthony's results did not agree with the results found by BCURA; however, his work was done with a wire grid rather than a hot gas particle heater. Referring back to Figure 2-1, it will be noticed that the degree of devolatilization was independent of the time required for completion of the first process. In the Figure, three heating rates are indicated for the same final temperature. As shown by the data, the degree of devolatilization was the same in all three cases. These results obviously do not agree with the results of BCURA as presented in Figure 2-3; however, the time dependent nature of devolatilization has been observed by other researchers [11,12] in at least two types of experiments.

Up to this point we have discussed experiments that were concerned primarily with the volatile matter left in the residual char; however, equally important is the liberated volatiles. In examining the work of various experimenters it is generally agreed that the rate of heating not only influences the amount of volatiles that are

produced, but it also affects the composition. The work of BCURA and Anthony both showed that high heating rates and high final temperatures yield an increasing amount of volatiles that can exceed that found by the proximate analysis. Both Anthony and BCURA concluded that the maximum yield of volatile matter increases with heating rate and carbon content of the feed coal. Based on these observations, BCURA introduced the "Q factor" which is defined as the ratio of the weight loss to the change in volatile matter. The "Q factor" is expressed as:

$$\text{"Q factor"} = \frac{\text{Weight Loss}}{VM_{coal} - VM_{char}}$$

where VM_{coal} = Proximate volatiles in the coal

VM_{char} = Proximate volatiles in the char

Weight Loss = Total Pyrolysis Weight Loss.

It is significant to observe that the same conclusions were reached with two different types of experiments; i. e., one in which a grid was used and the other in which a hot gas particle heater was used. Anthony concluded that the volatile yield depended more upon final temperature rather than heating rate and this led to the conclusion that any increase in final temperature would result in an increase of volatile production. These conclusions were supported by further work in the same type of experiments by Suuberg [13].

Howard and Essenhigh [10] found results that appear to conflict with the previous discussion. They concluded that

the ignition and early reaction of coal particles in a flame involve heterogeneous reactions occurring at the solid surface. The defect in this experiment was their conclusion that the amount of reacted volatiles could be calculated as the difference between the volatiles found during the proximate analysis of the feed coal and that found during proximate analysis of residual char. Based on findings of the other researchers showing that the proximate analysis of the feed coal volatiles is not a true indication of the amount of volatiles that can be produced during rapid devolatilization, their assumption cannot be substantiated.

Char (as previously defined) consists of carbon with some insignificant amounts of hydrogen, oxygen, and other trace elements. Many experiments, such as those conducted by Howard and Suuberg, have shown that the composition of volatiles is also a function of temperature and the heating rate. There have been various attempts to identify the various chemical species in the volatiles, but this has proven to be difficult because the devolatilization process is very complex so that a simple description is probably not applicable. However, Ubhayakar [14] made an attempt to give some simple description of the devolatilization process with the provision that it would not be comprehensive.

In his work Ubhayakar approximated a typical coal, such as bituminous, with the chemical formula $CH_{0.8}$. The basis of this assumption is the fact that coal is predominantly carbon and hydrogen with smaller amounts of oxygen (except

lignites), nitrogen and sulfur. Based on these statements it is assumed that the volatiles are essentially hydrocarbons with different carbon/hydrogen ratios. Figure 2-4 is a qualitative range of hydrocarbons one can expect via different pyrolysis routes. He chose to represent the reaction of the coal as:

$$CH_{0.8} \longrightarrow x\,C + C_{1-x}::H_{0.8} \qquad (2\text{-}1)$$

(Coal) (Char) (Volatiles)

This relationship can be written if it is assumed that an x amount of carbon remains as char at the completion of the devolatilization reaction. In this relationship the carbon/hydrogen ratio will be that of all the volatiles inclusive of tars, oils and gases and will be (1-x)/0.8. In this same context, volatile yield can be expressed as a weight percent of the original dry ash-free coal as [12(1-x) + 0.8]/12.8. These two quantities are shown in Figure 2-4 as a function of x. In the figure the carbon/hydrogen ratios of certain common hydrocarbons are indicated in the upper part. The figure illustrates what types of hydrocarbons one might expect to find over a range of carbon remaining in the residue and would indicate the types one would expect to find with various carbon/hydrogen ratios. This is not an exact representation but does give an overview of the kinds of hydrocarbon that one could expect. In general Ubhayakar was able to determine that under conditions of fast pyrolysis one

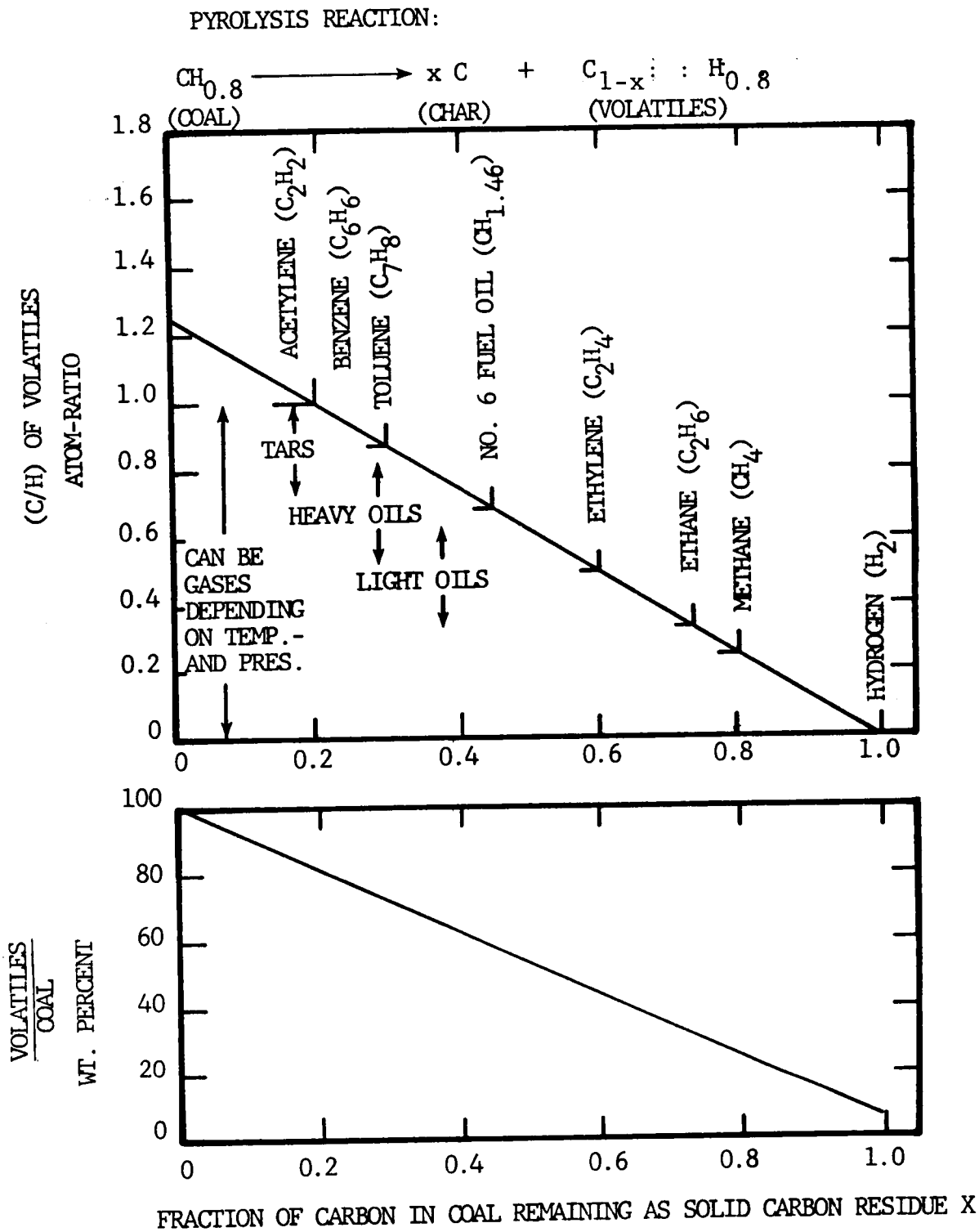

Figure 2-4. A simplified Picture of the Composition of Volatiles [14]

would have volatiles that exhibit higher carbon/hydrogen ratios than those found by proximate analysis. This fact has been determined by other experimenters [4,13]. The volatiles that are first released are much richer in carbon than those that are liberated at some later time. All of the volatiles driven off under conditions of rapid devolatilization turn out to be richer in carbon than those that would be found by proximate analysis.

This type of behavior is further pointed out by referring to Figure 2-5 which was taken from the work of Badzioch [2]. Badzioch showed that essentially all of the hydrogen is driven from the coal when the volatile matter is determined by proximate analysis. But in the case of rapid devolatilization, more volatiles are produced than by proximate analysis. This means that since the evolving hydrogen carries with it a larger amount of carbon the carbon/hydrogen ratio must be higher than the value found by proximate analysis. The type of behavior shown in Figure 2-5 was taken under conditions of an inert atmosphere; however, the same type of behavior has been found by other experimenters [11] using flame pyrolysis. Upon comparison of Smoot's [11] work with the work shown in Figure 2-5, it can be concluded that the rapid devolatilization was not strongly affected by the ambient conditions. Apparently this is true over the range of conditions that were studied in both experiments. However, other experiments [15] have shown that the composition of the volatiles varies greatly with the composition of the feed gas. It was concluded by

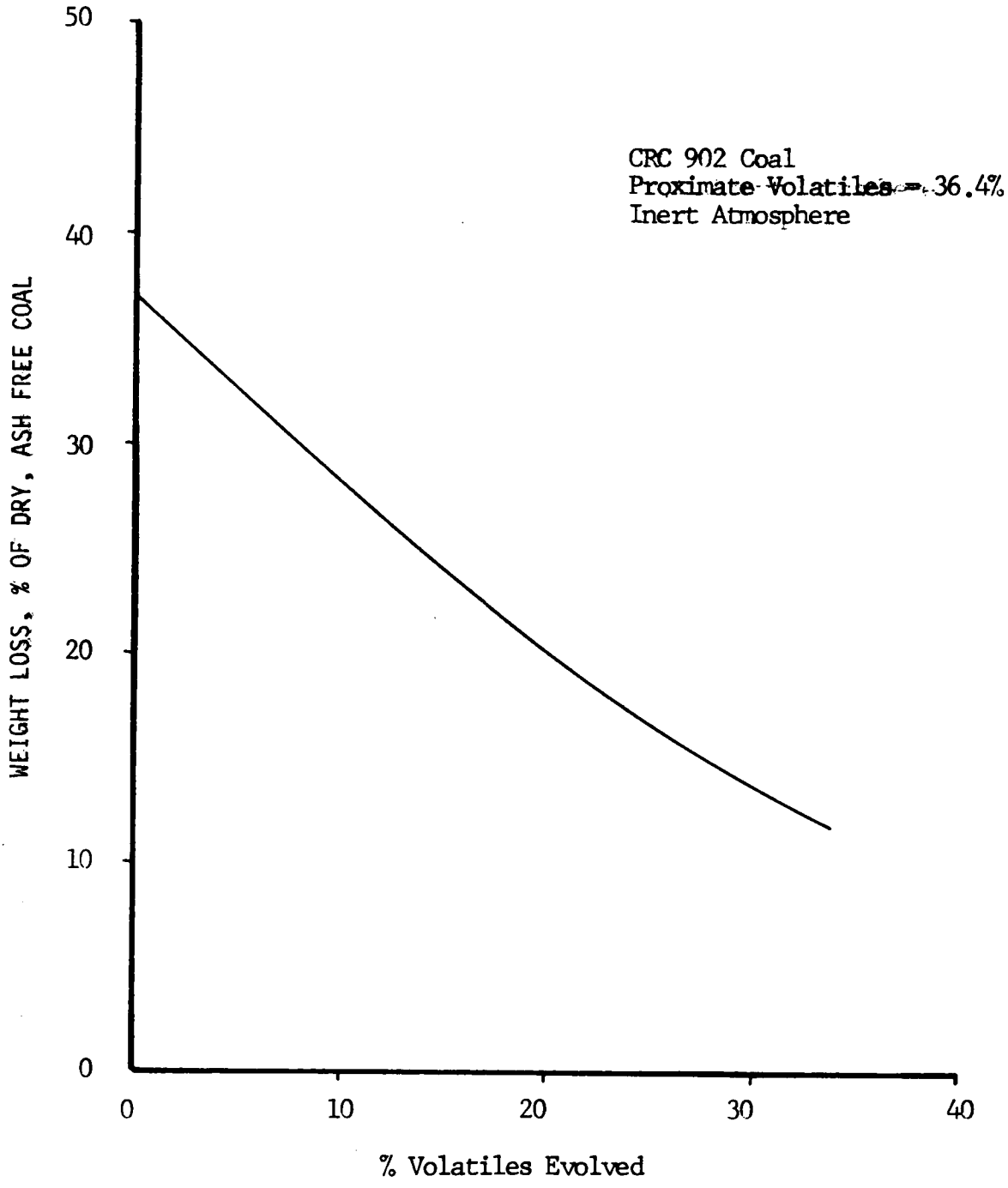

Figure 2-5. Total Weight Loss As A Function Of Residual Volatiles In Char [2]

Coates and Glassett [15] that the emerging volatiles probably reacted with the ambient gas so that the final gas composition depended upon ambient gas composition. However, the primary volatile products do not.

Most of the experimental work referred to so far depended upon using ash as a tracer. This appears to be satisfactory as long as the amount of residual ash is independent of the devolatilization reaction. Padia [16] suggests that this is not always the case but at lower temperatures this approach would be satisfactory.

There have been many experiments [13,15] in which the devolatilization products have been sampled and analyzed using the gas chromatograph. The composition measured in this manner may not be a true indication of the primary devolatilization products since secondary reactions might occur which are dependent on the sampling method. In spite of this source of error, it seems to be the best available method to determine the gas composition. The apparent products of rapid devolatilization at a temperature of 1300°K are given in Table 2-1. The primary products consist of H_2O, CO_2, and CO as well as some light hydrocarbons that are primarily CH_4 and H_2. In addition, depending upon the type of coal and the ambient gas, heavy hydrocarbons, referred to as tars, are also produced.

Certain experimental work [8,9] has shown that the composition of the volatiles depends to some extent on the particle size and proximity of the pulverized coal particles.

TABLE 2-1

APPARENT PRODUCTS OF FAST PYROLYSIS AT 1300°K

Coal	Ambient Gas	Tar	Mole percent of product gas CH_4	H_2	C_2-C_4	CO and CO_2	
Bituminous	Vacuum	9.9	50.3	13.1	-	26.7	[7]
Bituminous	O_2	-	8	59	-	26.7	[15]
Bituminous	Vacuum	53	6	31	3	8	[5]
Lignite	He	13	3	1	3	38	[49]

These conclusions are not supported by all experiments; however, on examining the work of Anthony [8] and Ubhayakar [9], the effect of particle size on volatile composition is shown. It is generally accepted [4,5] that large particles behave quite differently than pulverized coal particles. The explanation is that the char surface provides a site where a secondary reaction occurs. It is thought that the devolatilization products generated near the center of the particle must migrate to the outside for escape. It is felt that during this migration the volatiles crack, condense, or possibly polymerize with some carbon deposition taking place during the process. When larger particles are used, the deposition is felt to increase and therefore one finds less volatile yields for the larger particles. One would expect the same kind of behavior when there was a high particle

density. This conclusion was reached by Ubhayakar [9] as a result of his experiments.

As previously mentioned, in Anthony's work with bituminous coals, it was shown that lower pressures tended to favor increased volatile production. It would thus appear that lower pressures would tend to decrease the amount of time required for the internally generated volatiles to migrate to the surface of the particles and therefore the lower pressure would have the same type of effect as decrease in particle size. Figure 2-6 presents a comparison of data taken by Anthony and Suuberg which indicates the effect of ambient gas pressure. In both of these experiments the coals were heated on wire grids in a helium atmosphere under similar conditions. The data indicate the volatile yields that would be expected for a caking bituminous coal and a non-caking lignite. In both cases higher pressures tended to reduce the volatile yield; however, in the case of the caking coal, the effect was much more pronounced than that found for lignite. An explanation for this behavior given by Ubhayakar was that this effect is based on the secondary cracking or condensation reactions of the volatiles as they escape from within the coal particles through the coal char matrix to the outside. Both Anthony and Suuberg suggested that the higher pressures tended to reduce the mass transfer coefficients for volatile escape and to increase the residence time within the particles. Additional time for the volatiles to crack and to deposit carbon within the particle

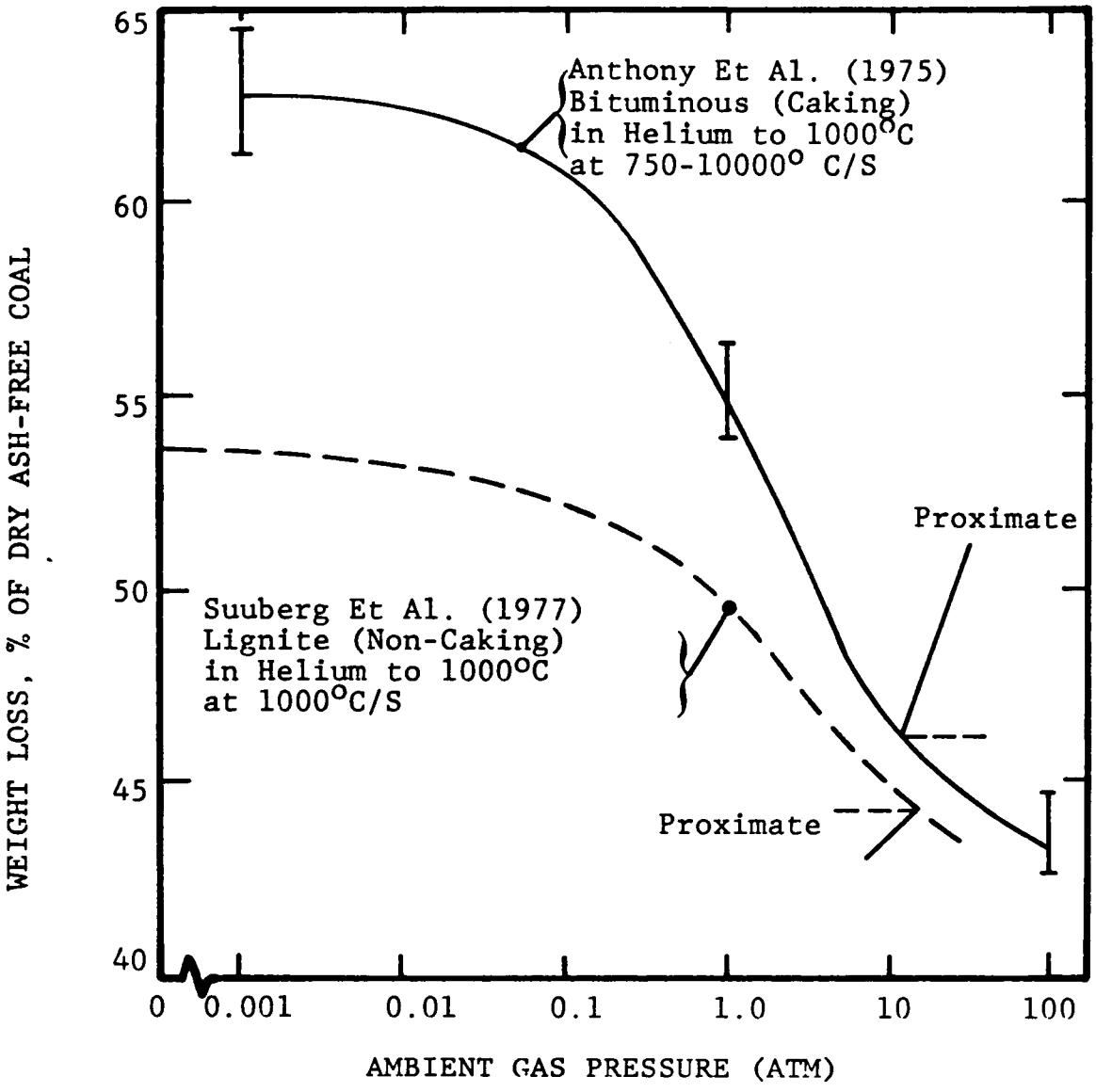

Figure 2-6. Influence of Ambient Gas Pressure [14]

itself by condensation would result in the release of smaller amounts of volatiles. Ubhayakar attempted to explain the difference in caking and non-caking coals. Ubhayakar stated that the mass transfer coefficient for the escape of the volatiles increases with pressure difference between the volatiles and the ambient gas. For the case of caking coals, this pressure difference is probably smaller than that for non-caking coals because during devolatilization the caking coals tend to swell and therefore to reduce the internal pressure. The net result is that the mass transfer rate for the caking coal will be somewhat lower than that for the non-caking coal. Therefore, in the case of the caking coal, the secondary cracking will be higher. This explanation is not without drawbacks. For example, in the case of caking coals it is felt by some experimenters [14] that the caking coals tend to explode and in this manner release volatiles much faster than non-caking coals. If this argument is true, then the previous explanation does not explain the effect of pressure. If the caking coals do not explode under conditions of rapid pyrolysis, then the data in Figure 2-6 becomes valid.

The secondary cracking and condensation reactions of the volatiles, which have been shown by some experimenters [14] to reduce volatile yield, depend on pressure and ambient gas composition as well as the physical characteristics of the coal. Of the various physical characteristics of coal that

have been shown to be important, the following four are thought to be the most significant [14]:

1. Size of the coal particles
2. Internal porosity of the particles
3. The plasticity of the coal
4. The packing density of the particles in the sample.

Figure 2-7, from work by Ubhayakar, illustrates the effect of these four characteristics on the time that the volatiles spend in contact with the residual char. The fundamental conclusion is that the net volatile yield will be lower if the contact time between the volatiles and the char is longer. In the case of particle size for smaller particles a shorter transient time exists for volatile release than for the larger particles. Porosity affects the devolatilization from the standpoint that for coals with large inner-connected pores, i. e., large porosity, then there is less resistance to the flow of the volatiles when compared to coals that have small inner connected pores, i. e., coals with low porosity. The plasticity of the coal affects devolatilization as in the case of non-caking coals where the pore size gradually increases. On the other hand for caking coals, the pore size decreases and the coal particles become plastic. The effect of packing affects the residence time of the volatiles on the char surface since in lightly packed conditions there is less surface area and very high inner particle distances. In this case the con-

	Less Time Spent In Contact With Char Surface	More Time Spent In Contact With Char Surface
Size	Volatiles 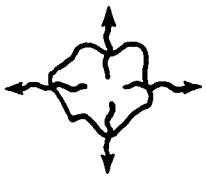 Shorter Transit Time	Volatiles 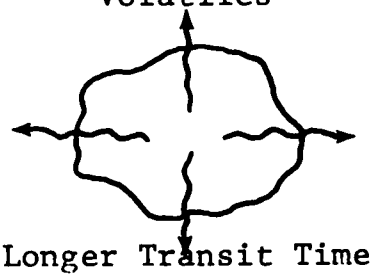 Longer Transit Time
Porosity	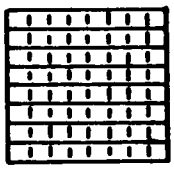 Large Inter-Connected Pores Less Resistance to Flow	 Small Inter-Connected Pores More Resistance to Flow
Plasticity	Non-Caking Coals  Pore Size Gradually Increases	Caking Coals  Pore Size Decreases and Coal Becomes Plastic
Packing	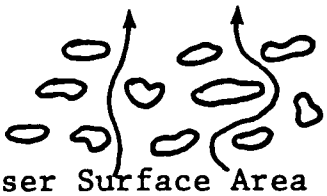 Lesser Surface Area Higher Inter-Particle Distance	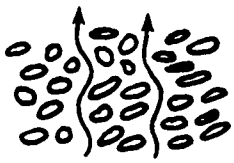 Higher Surface Area Lower Inter-Particle Distance

Figure 2-7. Influence of Physical Characteristics [14]

densation and cracking of the volatiles will occur outside the particle of origin.

Gray [17] showed using an ASTM proximate analysis that if the sample weight was increased, i.e., higher packing density, then the net volatile yield would decrease. Kobayashi [18] ran several crucible tests in an attempt to repeat the results of Gray and found no significant influence of packing depth on the net volatile yield. These results have not been explained. However, the answer to this discrepancy probably lies in the differences in the experiments. Ubhayakar [14] pointed out the low yields that are produced in coke ovens as compared to the various experiments. These low yields indicate that secondary cracking on the surface of the particles is a significant phenomenon under certain types of test conditions.

From the foregoing discussion it is quite plausible to assume that not only the composition but the appearance of the coal particles change as the volatiles are given off. There is a considerable amount of data available which describes these changes as all of the volatiles are given off. But there is very little data on the changes experienced by the coal particles themselves during the process in which the volatiles are evolved.

Previous Theoretical Modeling

In any chemical reaction the kinetics of the process are a measure of the rate of reaction in terms of kinetic constants as well as physical parameters such as pressure

and temperature. Kinetic data for chemical reactions are usually obtained by conducting carefully controlled experiments. Even for a simple bimolecular reaction, such as a methane reacting with oxygen, obtaining kinetic data is quite difficult as shown by Penner [19] and other experimenters [20]. In looking at the complex chemical structure of coal, kinetic modeling of the devolatilization reaction becomes as complex as the chemical structure of coal itself. If one tries to analyze each of the bond breakages from the atomic and molecular point of view the representation becomes quite complicated. Because of this difficulty it has been a generally accepted practice to approximate the complex kinetics of coal devolatilization by pseudo-kinetic constants. Most researchers have tried to model the kinetics of coal devolatilization by using an overall Arrhenius type relationship shown in equation 2-2.

$$K = K_o \exp(-E/RT) \qquad (2\text{-}2)$$

In this expression the pre-exponential or frequency factor, K_o, as well as the activation energy, E, are such pseudo-constants. Most of the kinetic modeling that has been done has used this type of relationship or some variation of the Arrhenius relationship. These will be discussed later. These kinetic schemes have been useful in explaining the performance of certain coal combusting devices.

Figure 2-8 a summary of various reaction rate constants that have been used by various researchers [21]. On examining the figure one notices a wide variation in reaction rate

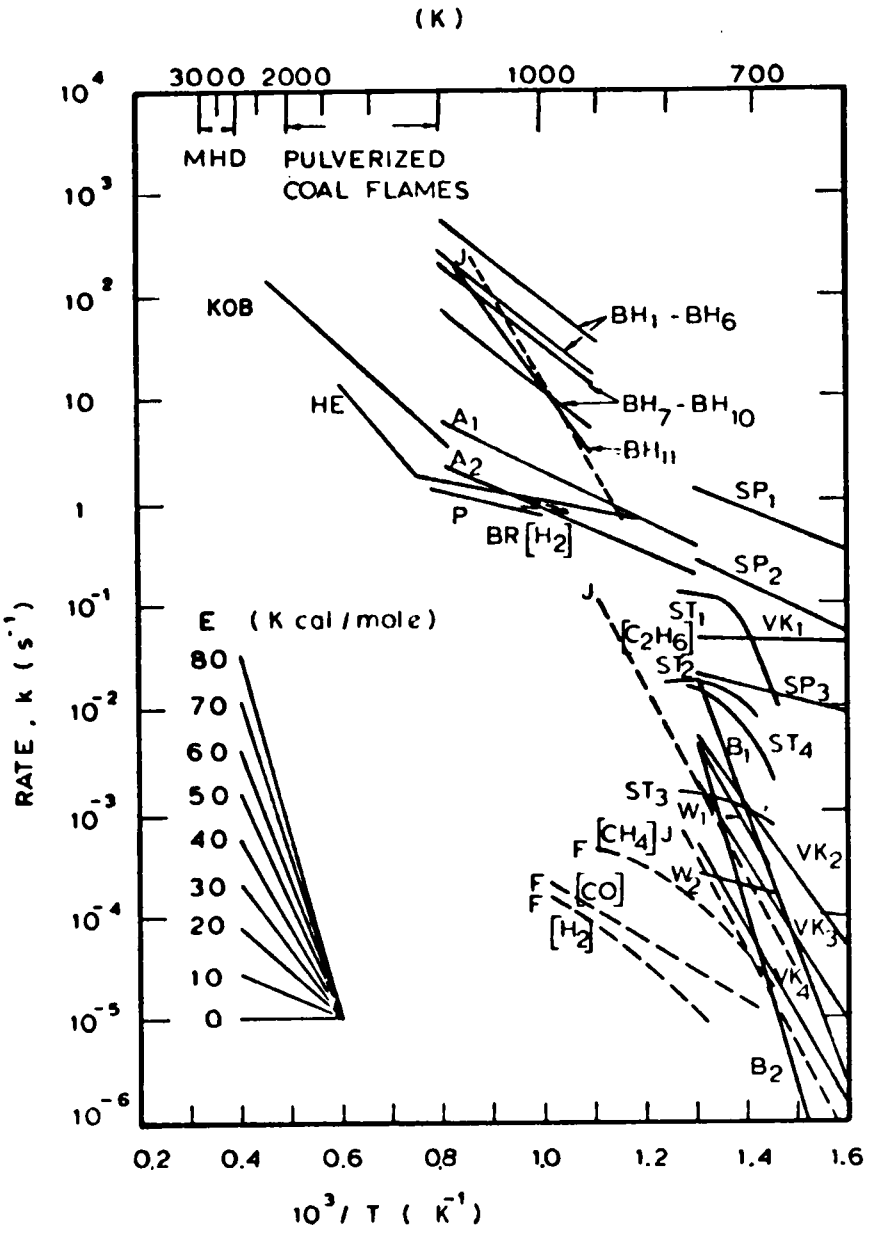

Figure 2-8. Comparison of pseudo-first order rate constants obtained by different investigators [21]

constants. Table 2-2 is a summary of the coal types and sources of data that are given in Figure 2-8. Part of the variations that are shown for the rate constants can be explained by the various types of coal considered, the proximate volatile matter contents and also the temperatures at which the experiments were conducted. However, in considering the various schemes employed it is necessary that one understands the experiments from which the analyses were developed. For these reasons there exists a variety of schemes in the literature that attempt to model coal devolatilization. As previously stated, the modeling of the kinetics of coal devolatilization is very complex so that it is probably impossible to develop just one scheme that will model devolatilization in a simple manner.

Because of the complexity of the problem it becomes necessary to develop basic guidelines to make the problem tractable. The guidelines that have normally been used are:

1. To make the model as simple as possible with as few kinetic parameters as necessary and
2. To try to make it applicable to "all conditions".

Obviously these two guidelines tend to work against each other.

In trying to gather the kinetic data, the weight loss of the coal particle has been determined as a function of the various experimental conditions. If this type of approach is to be viable, it must take into account the

TABLE 2-2

COAL TYPES AND THE SOURCES OF THE DATA SHOWN IN FIGURE 2-8 [21]

		VM (%d.a.f.)
A_1A_2:	Anthony (1974)	
	A_1:Pittsburgh Seam Bituminous Coal	46.2
	A_2:Montana Lignite	46.2
B_1B_2:	Böyer (1952)	
	B_1:Dourges Coal	22.5
	B_2:St.Fontaine Coal	36.0
BH_1-BH_{11}:	Bâdzioch and Hawksley (1970)	
	BH_1-BH_6:Coal "E"-"K"(highly swelling bituminous coals)	17.7-35.3
	BH_7-BH_{10}:Coal "A"-"D"(weakly swelling bituminous coals	36.1-42.0
	BH_{11}:Coal "L"(semi-anthracite)	11.5
BR:	Berkowitz and Den Hertog (1962)	
	"No.1" (a low volatile bituminous coal from the Cascade area of Southern Alberta)	-
	(H_2 evolution from devolatilized coal)	
F:	Fitzgerald (1956)	
	(CH_4,CO, H_2 evolution)	
	"Coal E" (vitrinite of a coking coal)	23.3
HE:	Howard and Essenghigh (1967)	
	Pittsburgh Seam Bituminous Coal	37.4
J:	Juntgen and Van Heek (1967)	
	Ethane evolution at three different heating rates	19.1
P:	Peters and Bertling (1965)	
	"From Fig. 8"	-
SP_1-SP_3:	Shapatina, et al. (1960)	
	Moscow District Brown Coal (Three different stages of devolatilization)	50.2
ST_1-ST_3:	Stone, et al. (1954)	
	ST_1-ST_3:Pittsburgh Seam Bituminous Coal (three different stages)	42.2
	ST_4:Colorado Coal	41.5
VK_1-VK_4:	Van Krevelen, et al. (1951)	
	VK_1:Brown Coal	51.0
	VK_2:Bituminous Coal, low rank	39.5
	VK_3:Bituminous Coal, high rank	18.8
	VK_4:Semi-anthracite	14.2
W_1,W_2:	Wiser, et al. (1967)	
	Utah High Volatile Bituminous Coal (W_1:first 60 min;W_2:60-160 min)	47.5(% dry)
KOB	Kobayashi, et al (1976)	
	Lignite and Bituminous Coal	

effect of all of these parameters such as temperature, heating rate, ambient gas pressure and physical characteristics. The major test parameters that have been used in trying to determine the influence of test parameters on weight loss data are given in Table 2-3. In most theoretical work that has been done, the major amount of emphasis has been on weight loss as a function of temperature since most experimental work indicates that this is the largest influence. The various schemes employed can be listed in broad general categories as follows:

1. Single Reactions
2. Multiple parallel reactions
3. Multiple competing reactions
4. Complex schemes
5. Schemes involving secondary char forming reactions.

Most of the single reaction schemes have assumed a single Arrhenius reaction of first order. This type of reaction is given by the following expression:

$$\dot{V} = K\,(V^{*} - V) \qquad (2\text{-}3)$$

In this expression $\dot{V}$ is the rate of the volatile production, V is the total volatiles produced at any instance of time, V^{*} is the volatile yield as time approaches infinity, and K is the kinetic constant as previously defined in equation 2-2. Certain researchers such as Badzioch [22] assumed one reaction holds at all instances of time while others used different kinetic "constants" in different tem-

TABLE 2-3

INFLUENCE OF TEST PARAMETERS ON WEIGHT LOSS DATA
(TO BE EXPLAINED BY COAL PYROLYSIS KINETICS MODELS)

A. Weight Loss vs. Temperature				
B. Weight Loss vs. Heating Rate				
1:	Temp. < 1000°C Rate < 0.5°C/s	Volatile Yield	<	ASTM Proximate VM
2:	Temp. ~ 1000°C Rate ~ 50°C/s	Volatile Yield	~	ASTM Proximate VM
3:	Temp. > 1000°C Rate > 500°C/s	Volatile Yield	>	ASTM Proximate VM
C. Weight Loss vs. Ambient Gas Pressure				
1:	Higher Ambient Pressure -- Lower Volatile Yield			
2:	Pressure Effect in Non-caking coals is less than that in caking coals.			
D. Weight Loss vs. Physical Characteristics				
	Volatile Yield of Density Packed Coal Particles	$\leq$	Volatile Yield of Lightly Packed Coal Particles	
	Volatile Yield From Large Particles	$\leq$	Volatile Yield From Small Particles	

poral zones as dictated by the experimental results (Stone [23]). However, in referring back to Figure 2-8 it is quite obvious that such a simple approach is not sufficient to obtain any kind of consistent predictive behavior of coal devolatilization. Pitt [24] deviated from the single Arrhenius type of scheme and proposed another in which he assumed that the rate of devolatilization was given by the following:

$$\dot{V} = B\, V^{*}\, /t \qquad (2\text{-}4)$$

where B = Experimentally Determined Constant

t = time

However, this type of approach is limited to the experimental conditions.

In looking at a single reaction scheme the primary difficulty lies in the assumption of V^{*}. Usually this value is taken as the amount of volatiles given off during proximate analysis or some other value that is consistent in aiding the scheme to predict quantitative results. The problem with this method is that at high rates of devolatilization, it is impossible for the single reaction schemes to predict the enhanced volatiles yields. To model high rate devolatilization with a single reaction scheme, it becomes necessary to know what the volatile yield will be at the high rate conditions. V^{*} becomes a parameter that can be adjusted to make the theory fit the experimental results, and thus in this manner has no real physical meaning.

It is now generally accepted that coal is formed by a very slow pyrolysis or thermal degredation of prehistoric plants and trees under conditions of very high pressure. If this process, which is often referred to as the coalification process, is continued to completion, then the final product becomes pure carbon or natural graphite. Coal is thus known to be composed of various fragments of prehistoric life. Each fragment has its own physical and chemical characteristics. It then becomes plausible to assume that the devolatilization of these fragments occurs simultaneously and in parallel. These assumptions led to the development of the schemes proposed by Pitt, [24] Anthony, [8] and Nsakala [25] and referred to as multiple parallel reactions.

Nsakala [25] proposed using two first order parallel reactions based on the two component hypothesis of Essenhigh and Howard [3]. Essenhigh and Howard considered coal to be composed of an amorphous component, C_1 in a lamellar component, C_2. Nsakala assumed that the amorphous component devolatilized to volatiles referred to as V_1 and the lamellar component devolatilized to volatiles, V_2 leaving behind a solid residue. This scheme employs the following reactions.

$$\text{COAL} \begin{cases} \xrightarrow{k_1} C_1 \longrightarrow S_1 + V_1 \\ \xrightarrow{k_2} C_2 \longrightarrow S_2 + V_2 \end{cases} \qquad (2\text{-}5)$$

$$\dot{C}_1 = -k_1 C_1 \; ; \; k_1 = A_1 \exp(-E_1/RT)$$

$$\dot{C}_2 = -k_2 C_2 \; ; \; k_2 = A_2 \exp(-E_2/RT)$$

The deficiency in the results obtained by this method is that the scheme was forced to correlate with the data; that is, in looking at components 1 and 2 they had to assume that the initial proportions were not the same depending on the various size coal particles. For a 64 micron particle they assumed that the ratio of C_1 to C_2 was 25 to 75 whereas for a 180 micron particle they assumed that the ratio was 4 to 96. In examining a given coal this reasoning does not seem plausible even though the fragment distribution in a given size particle may be different. It is not expected that the difference would be quite as drastic as that required to have their scheme fit their experimental data.

Anthony [8] and Pitt [14] also used multiple parallel first order Arrhenius reactions with a constant frequency factor but with a statistical distribution for the activation energies. With this method it is possible to recognize that there would by many constituents in the coal devolatilizing at different rates. This method has the advantage in that the number of constants is reduced to three, i.e., the frequency factor, the mean activation energy and the standard deviation in activation energy. In Anthony's work, a Gaussian distribution of the activation energy was employed whereas Pitt used a rectangular distribution. The formulation was

$$\text{Coal} \rightarrow \sum_{i=1}^{n} C_i \xrightarrow{k_i} \sum_{i=1}^{n} (S_i + V_1) \rightarrow S + V$$

$$\dot{V}_i = k_i (V_i^* - V_i); \quad k_i = A_i \exp(-E_i/RT) \qquad (2\text{-}6)$$

$$E_i = f\left(E_o, \sigma, f(E)\right) \text{ where } \int_0^\infty f(E)\, dE = 1$$

However, with the multiple parallel reaction scheme the difficulty lies in that the asymptotic yield of the volatiles, V^*, is not coupled to the heating rate and therefore the scheme does not explain the Q-factor effect. Kobayashi conducted an experiment that obtained data which disqualified the multiple parallel reaction scheme. The results of his work are shown in Figure 2-9. The hydrogen/carbon ratio in char is shown as a function of weight loss for two types of coal, i. e., Pittsburgh seam bituminous and Montana lignite. The Figure shows the results obtained for two different heating rates and two different final temperatures for each coal. The lower heating rates were done in crucibles whereas the higher heating rates with higher final temperatures were obtained in an entrained flow experiment. In examining these data, it can be seen that at any particular weight loss the hydrogen/carbon ratio in the char is always higher for the higher heating rates for both types of coal. Since for a given type of coal, i. e., Pittsburgh seam bituminous or Montana lignite, the original composition is the same, the data imply that the hydrogen/ carbon ratio of the volatiles produced in the high heating rate experiment is lower than that in the lower heating rate experiment. When looking at the point in which the hydrogen carbon ratio is equal to zero the volatile yield is quite different in

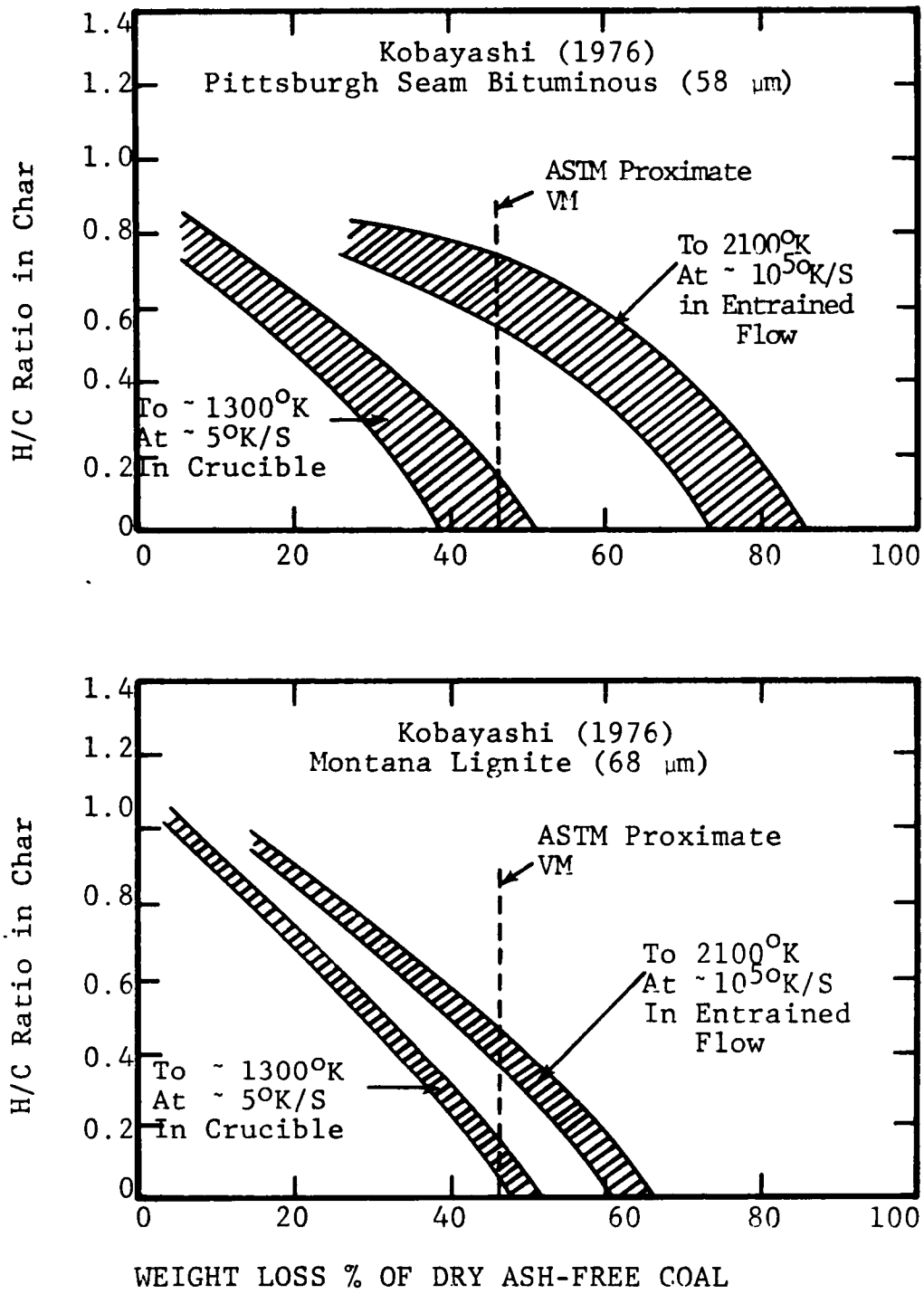

Figure 2-9. H/C Ratios in Chars from Two Coals [21]

the two experiments. Anthony attempted to explain these effects by modifying his scheme to include secondary char forming reactions. The secondary char forming reactions were taken to compete with the volatiles as they were escaping from the particles. This type of scheme will be discussed later.

In the multiple parallel reaction scheme it was assumed that the coal consisted of a mixture of constituents that were devolatilized independently but yet in parallel. In contrast to this, the multiple competing reaction scheme assumes that the coal itself is the only constituent that is devolatilizing. It devolatilizes to different products by different reactions that are significant at different temperatures and simultaneously compete with each other. With this type of approach there is built in a provision for explaining the enhanced volatile yields that occur under conditions of rapid devolatilization.

Kobayashi [21] proposed two first order competing reactions and used this model to correlate data of Kimber and Gray [26] and Badzioch and Hawksley [22] with his own data. The two first order reactions used are as follows:

$$\text{COAL (mass m)} \xrightarrow{k_1} (1 - a_1)S_1 + a_1 V_1 \qquad \text{COAL (mass m)} \xrightarrow{k_2} (1 - a_2)S_2 + a_2 V_2 \tag{2-7}$$

$$\dot{m} = (a_1 k_1 + a_2 k_2)m$$

$$k_{1,2} = A_{1,2} \exp(-E_{1,2}/RT)$$

In his representation, a_1 and a_2 are

stoichiometric constants that are chosen based on the experimental conditions and k_1 and k_2 are kinetic parameters that have high and low activation energies respectively these corresponding to high and low temperatures. By choosing the proper stoichiometric constant 2 to be larger than 1 then the Q-factor effect found by BCURA can be explained. Ubhayakar extended the meaning of the stoichiometric constants proposed by Kobayashi by expressing them in terms of the hydrogen/carbon ratios of the coal and of the expected volatile yield at low and high temperatures. However, with this type of scheme these constants still fall into a category of adjustable constants which have no physical meaning.

Gray [17] proposed a physico-chemical model that involved extensive hydrogen atom migration in the carbon linkage structure of coal. The preceding kinetic representation can be reconciled with this description in the lower activation energy case. The higher activation energy route occurs on a shorter time scale and thus the model possibly may correspond to less hydrogen migration which will allow unsaturated carbon atoms to rupture the high energy multiple bond structures.

Complex schemes have been proposed by Fitzgerald and Van Krevelen [27]. Their model, done at relatively low temperature devolatilization, consists of a series of consecutive reactions illustrated by the following:

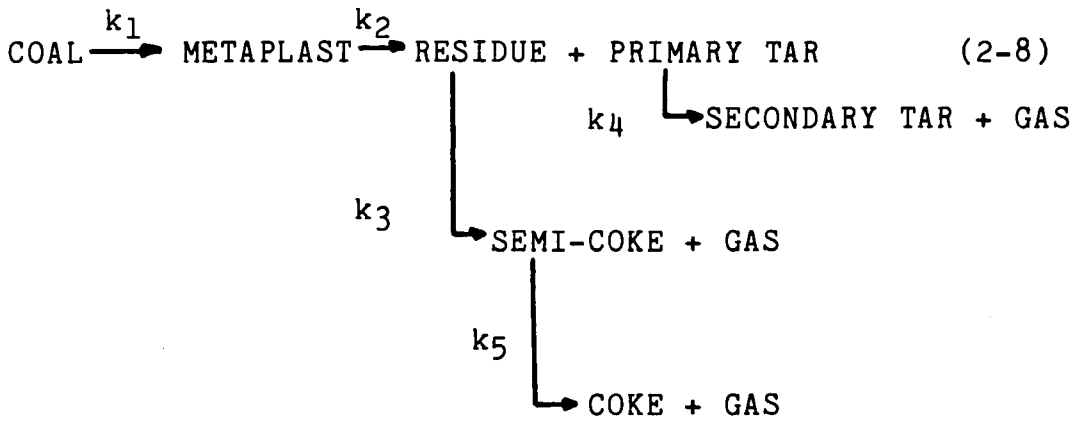

(2-8)

$$k_i = A_i \exp(-E_i/RT), \quad i = 1,5$$

This type of representation appears to be plausible for their experimental observation; however, in examining the relationship, there are 10 unknowns in the model which are rather difficult to relate to the weight loss data. Again the Q-factor effect is not predicted directly by this scheme so that their model would not be valid for high temperature devolatilization conditions.

Johnson [28] proposed a similar scheme which is somewhat simpler in that it includes just a single competitive step.

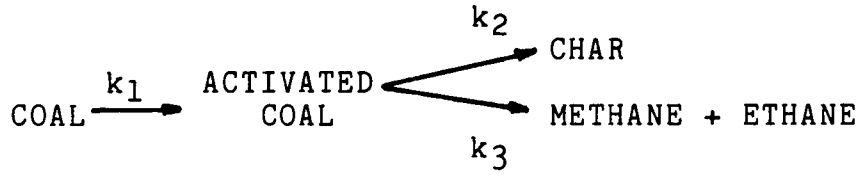

(2-9)

$$k_{1-3} = A_{1-3} \exp(-E_{1-3}/RT)$$

Based on the experimental results it seems that this scheme is suitable for predicting devolatilization in a hydrogen atmosphere producing specifically methane and ethane as a final product gas.

Reidelbach and Summerfield [29] visualize the coal devolatilization process at various temperatures under dif-

ferent heating conditions as being very complex. They proposed the following scheme which involves consecutive and competing char forming reactions:

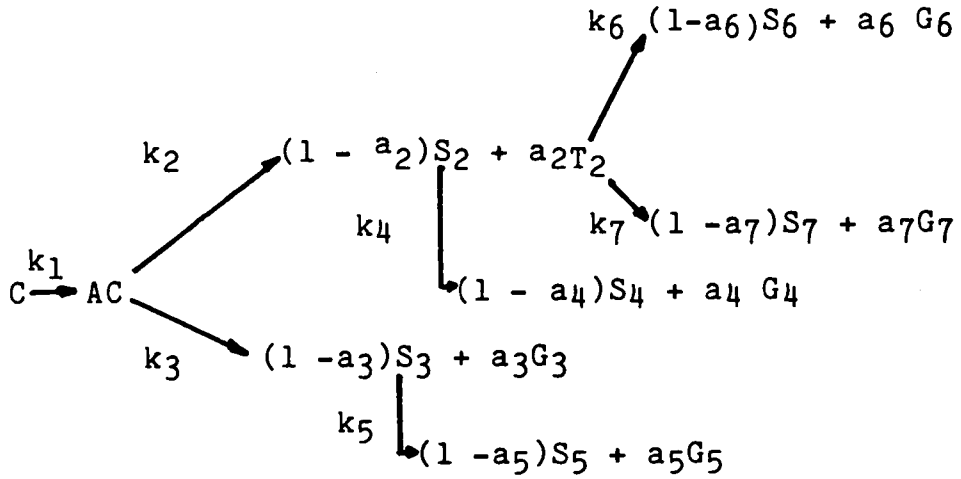

(2-10)

C = COAL
S = SOLID RESIDUE
T = TAR
G = GAS

$k_i = A_i \exp(-E_i/RT)$, i=1,7

a_i = Stoichiometric Constants

In this scheme the constants k_6 and k_7 are the secondary char forming reactions by which the volatiles crack and deposits condensate on the char structure. It has been shown that this type of scheme can predict most of the observed devolatilization phenomena both at low and high temperatures and including the Q-factor effect. But the difficulty with this scheme lies in the 21 unknown parameters that are indicated in the previous relationships.

Anthony [8] expanded the original multiple parallel schemes to include an additional rate equation for the escape of the volatiles from the particle and for the thermal decomposition of the volatiles. This scheme is repre-

sented as:

$$\text{Coal} \quad \sum_{i=1}^{n} C_i \xrightarrow{k_i} \sum_{i=1}^{n} (S_i + V_i) \rightarrow S + V \begin{cases} \xrightarrow{k_e} S + V \\ \xrightarrow{k_c} (S+S_c)+V_c \end{cases} \qquad (2\text{-}11)$$

$$k_i = A \exp(-E_i/RT); \quad E_i = f\left(E_o, \sigma, f(E)\right) \text{ where } \int_o^{\infty} f(E)\, dE = 1$$

k_e = Rate of Escape of Volatiles

k_c = Rate of cracking of Volatiles to Solids (S_c) and Cracked Volatiles (V_c)

This type of representation depends on the relative magnitudes of the additional rate constants. For instance, with the lower heating rates, the scheme forces the rate of cracking to be higher than the rate of escape. However, at higher temperatures it makes the rate of escape higher than the cracking rate. This type of scheme was criticized by Kobayashi [21]. He stated that at high temperatures the rate of cracking, which probably is very sensitive to temperature, may very well be higher than the rate of escape (probably less sensitive to temperature). At this point neither of these phenomena has been proven by experimental data.

Stickler [30] proposed that devolatilization could be described by a model based on two competing reaction schemes that consisted of a pair of parallel first order irreversible reactions, i.e.

$$\text{COAL} \xrightarrow{k_1} (1- a_1)\, S_1 + a_1 V_1$$
$$\text{COAL} \xrightarrow{k_2} (1- a_2)\, S_2 + a_2 V_2$$

$$k_i = A_i \exp(-Ei/RT) \quad i = 1, 2 \qquad E_1 < E_2 \qquad (2\text{-}12)$$

with the rate equations given as

$$\frac{dc}{dt} = -(k_1 + k_2)\, C$$
$$\frac{dv}{dt} = (dv_1 + dv_2)/dt = -(a_1 k_1 + a_2 k_2) C \qquad (2\text{-}13)$$

He proposed that one of the reactions be dominate at a slow heating rate and lower temperatures while the second reaction would be dominate at the higher heating rates and the higher temperatures. The results were that the proper behavior was predicted in that there was a dependence on coal heating history. This scheme allowed the volatiles from the coal to react with the exhaust gases to give the equilibrium composition and temperature of the products. In addition, this scheme accounted for particle size, exhaust temperature, coal loading, and differences in residence time and their effects on the volatile yield, product gas temperature and composition.

An attempt was made to correlate this scheme with experimental data taken at AVCO [14]. In some areas there was agreement; however, upon comparison with the experimental results, the measured particle temperatures were higher than those computed. The volatile yields were ascertained by gas analysis and char analysis. There was a disproportionate increase in difference between the two

types of analysis with coal loading. Detailed examination of the data suggested that the quantities actually being measured by the two analyses were different and that certain key phenomenological aspects were ignored. The analytical scheme did not allow for thermal cracking of the volatiles into soot and hydrogen after the volatiles escaped from the coal particles. Qualitatively, the difference in the computed and measured particle temperature could be explained. If the volatiles released by the particle were allowed to react completely with the combustion gases, the final equilibrium temperature would agree with that computed by the analytical model. If the volatiles crack into soot and hydrogen during the devolatilization process, the soot (being relatively unreactive) would not have been available for endothermic reaction with the combustion gas. As a result, the remaining portion of the volatiles and hydrogen released by cracking would react with the gases. The final temperature of the particle would be decreased by a lower magnitude or the particle temperature would be higher than if all of the volatiles could react with the combustion gases.

After realizing the effects of this phenomenon and noting the discrepancy between the char and the gas analysis, the experimental set-up was examined. If the spray-quench system operated efficiently, the char and gas analysis should agree; that is, if the spray quench captures all of the solid particles. These solid particles would be

used in the char analysis and would indicate the weight fraction of the original amount of coal that was lost as gases. This is the type of result indicated by the gas analysis; however, it is well known that soot particles are sub-micron in size. Smaller particles of soot behave more like gases and thus are not totally captured by the spray quench system. It was assumed that the soot particles were carried away with the gaseous part of the exhaust. Therefore the char particle analysis indicated the amount of volatiles which escaped from the char particles. The gas analysis only accounted for that portion of the volatiles which reacted with the exhaust gases and did not consider any cracking phenomena. The resulting conclusion is that the differences in the gas analysis and char analysis can be explained by the formation of sub-micron soot particles in the gas phase.

With this type of reasoning, Ubhayakar [31] modified a model developed by Stickler to include thermal cracking of the volatiles. Further experiments were performed and the comparison of computed data with analytical data did not show good agreement. A cracking fraction was defined and the experimental data were fitted to the analytical data by allowing the cracking fraction to increase exponentially with coal loading. There was a difference in the measured soot which resulted from the difference between the gas and the char analysis. However, the measured soot was smaller in magnitude than that computed. An attempt was made to

explain this phenomenon by others [32] as ash vaporization or soot deposition within the char structure. These processes were discussed by Ubhayakar [14]. By correlating the analytical model with the data, an empirical relationship for the cracking fraction was developed as a function of coal loading which seemed to apply only to the particular reactor being used.

Table 2-4 is a summary of all of the devolatilization models discussed listing the merits and demerits of each model. All models give primary importance to the temperature effect. The right hand column in the table indicates the number of unknown, adjustable parameters that must be used with each model.

In all of the models that have been discussed, a significant amount of experimental data is required to determine the various adjustable parameters that are used in the computations. In every case the ultimate extent of devolatilization must be determined experimentally. This value is used as an input to the various devolatilization models. This means that there is no model that can be used to apply to a new and different coal where there are no experimental data.

Another limiting factor of the models is that the temperature history must be specified before the temperature-dependent devolatilization can be computed. This means that the devolatilization equations must be coupled to the various transport equations for general use. If this is achieved, the solution of the coupled equations will be

TABLE 2-4

MERITS AND DEMERITS OF COAL PYROLYSIS MODELS

		TEST PARAMETERS ON WEIGHT LOSS DATA TO BE EXPLAINED BY PYROLYSIS MODELS: TABLE III				NO. OF ADJUSTABLE CONSTANTS
		A TEMP.	B HEATING RATE	C AMBIENT GAS PRESSURE	D PHYSICAL CHARACTERISTICS	
COAL PYROLYSIS MODELS:	2-3	YES	NO	NO	NO	$\geq$ 3
	2-4	YES	NO	NO	NO	2
	2-5	YES	P	NO	NO	4
	2-6	YES	P	NO	NO	3
	2-7	YES	YES	I	I	6
	2-8	YES	NO	NO	NO	10
	2-9	YES	YES	NO	NO	6
	2-10	YES	YES	I	I	21
	2-11	YES	YES	I	YES	6
	2-12	YES	I	NO	NO	4

P: Partially. However, given enough time, asymtotic yields are independent of temperature and heating rates.

I: Indirectly. Data elements can be explained by adjusting constants.

able to describe the interdependent histories of temperature, volatile yields and their evolution.

In attempting to choose a best model for a given situation, it would depend heavily upon the amount of experimental data that would be available for a specific coal of interest that is being analyzed. For most cases, a set of first order, irreversible, parallel reactions would be appropriate. Badzioch [22] reduced the treatment to a set of one while Suuberg's [13] treatment required a set of 15. Stickler's approach required basically the use of two sets. In many cases, this may be appropriate.

The major difference between the types of experiments, which have been discussed previously and are the subject of this work, is that most of the data have been taken in either inert atmospheres, in flames using air or by injecting the coal particles into a preheated neutral gas.

In the case of the present work, the coal particles are injected into a high temperature, substoichiometric flame that allows for the ignition of the coal particles under hypergolic conditions. The effects of this type of experiment will be discussed in detail later. The present work considers the effects of mixing on the rapid devolatilization of pulverized coal particles. Up to the present time, these types of experiments have not been performed under conditions of high temperature combustion. In this work the experimental data will be compared to a model developed by Chung [6] which differs somewhat from the models

that have been previously discussed. The model of Chung will be discussed in detail in the next chapter.

CHAPTER 3

ANALYTICAL MODEL

The analytical model presented in this chapter is that presented by Chung and Smith [6]. This model had not previously been supported by experimental results. The theory as presented is a one-dimensional, coal combustion model that incorporates a unique approach to the reaction rate. This approach will be discussed in detail.

The chapter contains a discussion of the simplified combustion chemistry used as well as the devolatilization model. The combustion theory is developed for the one-dimensional case and includes radiative heat transport in a simplified sense.

Simplified Chemistry

Chung and Smith assumed that the combustible elements react with oxidant at an infinitely fast rate according to the following stoichiometric relationships:

$$\begin{aligned} C + O_2 &\longrightarrow CO_2 \\ 2H + (1/2)\ O_2 &\longrightarrow H_2O \\ N + O_2 &\longrightarrow NO_2 \\ S + O_2 &\longrightarrow SO_2 \end{aligned} \qquad (3\text{-}1)$$

The combustion products are then assumed to readjust according to the following equilibrium relationships:

$$CO_2 \longrightarrow CO + (1/2)\ O_2 \qquad (3\text{-}2)$$

$$1/2\ N_2 + NO_2 \longrightarrow 2\ NO \qquad (3\text{-}3)$$

$$CO + H_2O \longrightarrow CO_2 + H_2 \qquad (3\text{-}4)$$

These gas phase chemical reactions are those simplified

reactions considered by Lewis [33], along with the dissociation reaction introduced by Chung. It is well known that these reactions are the predominant ones that influence the thermal aspects of combustion.

The combustible part of coal consists primarily of carbon, hydrogen, nitrogen, oxygen, and sulphur, in proportions that can be determined by ultimate analysis. However, it has been pointed out by Spaulding [34] that in solid fuels, oxygen is usually bound with hydrogen in the form of H_2O. Chung chose to modify the relative mass of hydrogen in coal combustibles to be that given by the ultimate analysis reduced by one-eighth of the oxygen mass in the coal combustibles.

The chemical reactions indicated by equations 3-1, 3-2 and 3-3 are those that were used by Lewis. However, Chung included the shift reaction indicated by equation 3-4, since Spaulding determined this reaction to be important in high temperature combustion.

The coal is assumed to contain H_2O in an amount equal to that associated with the oxygen content of the coal. When evaporated, the H_2O will participate in the shift reaction given by equation 3-4 along with the H_2O that is generated in the combustion reaction of equation 3-1.

If it is assumed that the combustion reaction given in equations 3-1 through 3-4 proceed at an infinitely fast rate, then this implies that the combustion of the coal particle is controlled by the following:

a) rate of coal devolatilization

b) diffusion of the reactants across the diffusion layer surrounding the coal particles

c) conduction of heat across the conduction layer

d) diffusion and conduction within the coal particles.

The coal particle combustion model is illustrated in Figure 3-1. An examination of the relative orders of magnitude of the known rates given for the combustion reactants listed and compared to the devolatilization and diffusion rates justifies the assumption of infinitely fast rates [35]. At this point the only additional rates involved are the surface gasification rates of the char by CO_2 and H_2O. This will be discussed later.

Devolatilization

Of the phenomena that take place during the combustion of coal the least known is the rate of devolatilization of the coal particles. In the previous sections, this was discussed in some detail. In these studies [7,8] it was most often assumed that the devolatilization occurred instantaneously with the burn-out of the char being the single rate controlling step. In many of these studies it was assumed that the amount of volatiles to be produced was given by proximate analysis or some other estimated value. Devolatilization is known to exert a strong influence on the combustion of pulverized coal since devolatilization rate and its yield affects both ignition and flame stability. Volatile yield depends on both heating rate and combustion

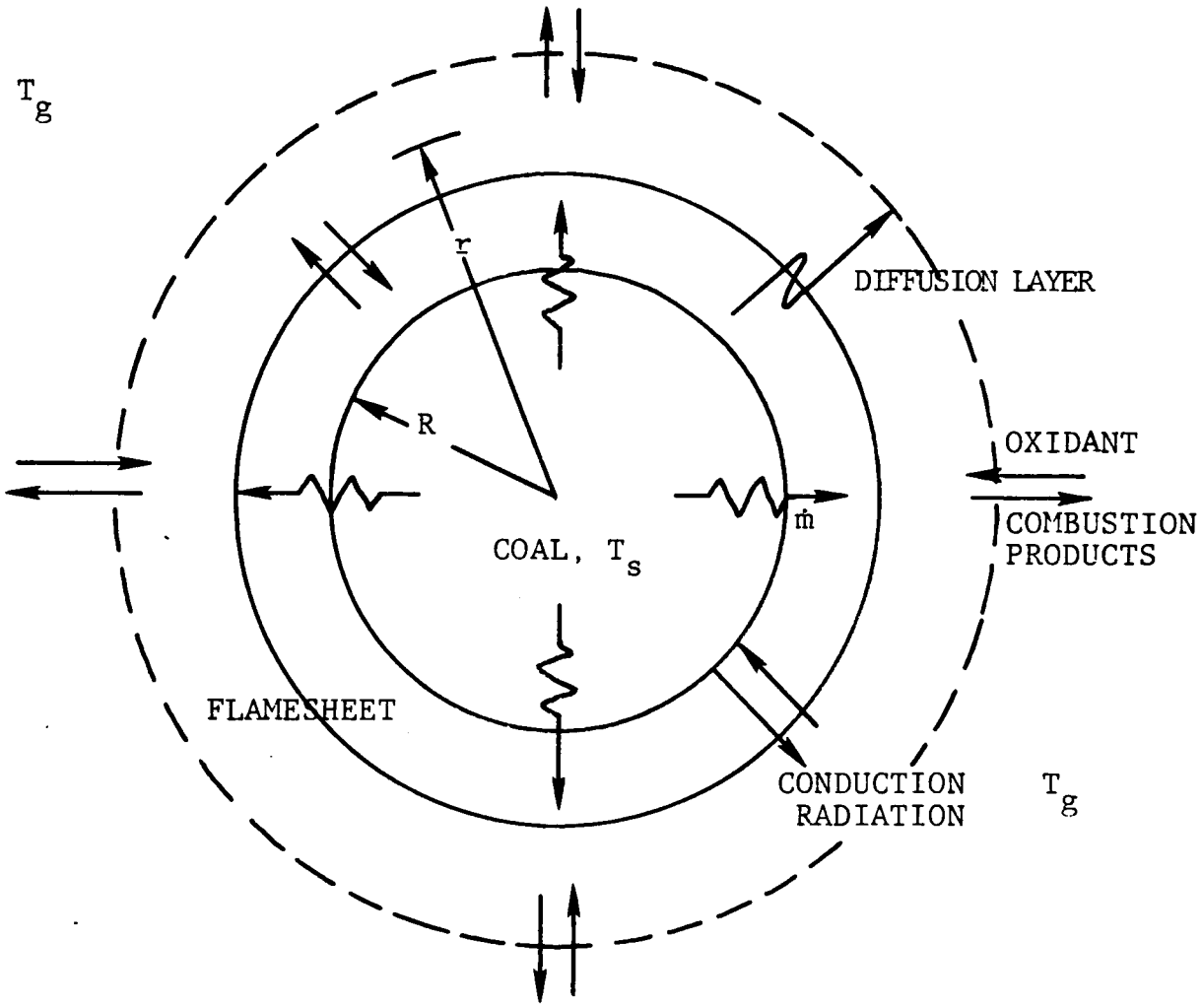

Figure 3-1. Coal Particle Combustion Model [6]

temperature of the coal particle. This type of behavior is indicative of all chemical reactions in which the final pyrolysis reaction product (volatile yield) depends on the path of the reaction as well as its degree of completeness. In previous work [8] the rate of devolatilization has been given as a first order Arrhenius reaction or

$$\dot{V} = K (V^* - V) \qquad (2\text{-}3)$$

In the previous analyses that have been discussed, one significant deficiency is that the combustion reaction was not included. In any real situation, this reaction is taking place simultaneously with devolatilization. As a result, it has been impossible to develop any type of analytical description of the devolatilization process that has general applicability. As was pointed out, the analyses are strongly tied to the availability of empirical data. Previous attempts to model the devolatilization process using a single first order rate equation have been defective from the standpoint that the asymptotic value, V^*, of the volatiles was based on the proximate analysis or fixed by some experimental constraint. With the single step reaction it was impossible to predict the ultimate volatile matter in the coal because the ultimate yield was fixed by the asymptotic value. The fraction of volatile matter that can be volatized from a coal is not fixed. As stated previously, with increasing heating rates and final temperatures, the amount of volatile release varies greatly. The combustible component of coal cannot be viewed as consisting of material

that can be volatilized and/or portions that cannot be volatilized. In principle, it should be possible to volatilize all of the combustible components of coal; i. e., at high temperatures the so-called fixed carbon portion of the coal combustibles will also volatilize. It seems plausible to assume that the rate of volatilization is a function of the total particle mass at any given instant of time rather than some fixed fraction of the initial particle mass. Therefore, it is possible to model the rate of devolatilization with a single reaction if the rate of devolatilization is formulated as a function of the coal particle mass. As the volatilization proceeds, there is a decrease in the devolatilization rate since a greater fraction of the remaining coal mass consists of those volatiles that have higher activation energies.

Chung modified the rate law in the following manner:

$$\frac{1}{\hat{m}_s}\frac{d\hat{m}_s}{dt} = \left(\frac{\hat{m}_s}{\hat{m}_{so}}\right)^{\hat{\beta}} K_o \exp[-E_v/(R_u T_s)], \qquad (3\text{-}5)$$

where $\hat{m}_s$ is the mass of the combustible portion of the coal particle at any time, t, $\hat{m}_{so}$ is the initial portion of the coal particle that is combustible and $\hat{\beta}$ will be determined from experimental results.

If it is assumed that the coal particle is spherical and homogeneous and that the diffusion of the volatile matter through the layer surrounding the coal particle is

subsonic, then the partial pressure of the volatile matter at the gas-solid interface is that corresponding to saturation. Therefore, the saturation partial pressure for the volatile matter can be given as:

$$P_b = \frac{K_o}{3\bar{C}_o} \frac{R_u}{M_b} \delta_s R \left(\frac{m_s}{\hat{m}_{so}}\right)^{\hat{\beta}} \sqrt{T_s} \exp[-E_v/(R_u T_s)] Z'_{bs} \qquad (3\text{-}6)$$

There is a given ash content of coals considered, so that any combustion model must include ash vaporization. It is assumed here that the partial pressure of the ash at the coal-gas interface is proportional to the instantaneous mass fraction of the ash within the coal particle. This is the same basic assumption as used in computing the partial pressure of the volatiles at the gas solid interface. In this context, the partial pressure of the ash is given by the following relationship:

$$P_g = Z'_{gs} \exp(A_g - B_g/T_s) \qquad (3\text{-}7)$$

The constants A_g and B_g are chosen such that the partial pressure of the ash corresponds to the saturation pressure of SiO_2. Silicon dioxide is chosen since it is the major ash constituent.

The analysis includes the surface reaction of CO_2 and H_2O with the char particle. It is well known that the rates of surface reaction of CO_2 and H_2O in the char are very

small at low temperatures. This is not true at the higher temperatures which are encountered in this work. Higher coal particle temperatures exist due to the fact that near stoichiometric amounts of oxygen are present at the particle surface. When the char temperature is above approximately 2500°K throughout the combustor, there is a sufficient amount of oxygen present to cause the surface combustion reaction to be the predominant reaction. In this case, the surface reaction of the oxygen with the char will be much greater than that between the char surface and CO_2 and H_2O. In the case of a fuel rich mixture, such as that investigated in this work, the oxygen is depleted by combustion as indicated in equation 3-1 which in turn results in the the conversion of CO_2 to CO and O_2 via the equilibrium gas phase reactions of equations 3-2 and 3-4. The oxygen that is generated thus diffuses towards the surface for additional combustion according to equation 3-1. This is the major char gasification mechanism in a fuel rich combustor of finite size. However, it is possible in fuel rich combustion that the direct surface gasification of the char by CO_2 and H_2O may become important if a long residence time occurs.

Due to the suspected secondary nature of the CO_2 and H_2O reactions with the char surface, Chung proposed to include these reactions in an approximate manner. An assumption was made that the gasification reaction between the CO_2, H_2O and the char is chemically rate controlled in a

regime where it is significant when compared to the other combustion reactions. If this assumption is true, then the surface reaction rate will be given by

$$J_s = K_w Z'_{bs} \rho_g \frac{(m_3 + m_7)}{m_g} \qquad (3\text{-}8)$$

In keeping with the assumptions made previously about the reaction rates of the combustibles, the surface reaction by the CO_2 and H_2O gasifies combustibles whose constituents are carbon, hydrogen, nitrogen and sulfur. The combustibles thus given off then proceed through infinitely fast reactions described by equations 3-1 thru 3-4. The gasification rate due to the H_2O and CO_2 was then determined by equation 3-8 and the particular chain of reactions leading to the final equilibrium state described by 3-2 thru 3-4 is not important since these reactions are assumed to take place instantaneously.

Using the reaction rate equation for the H_2O and CO_2, an equivalent partial pressure is deduced in the same manner as the partial pressure for the volatiles at the gas/solid interface, so that the following relationship results:

$$P_{bs} = \frac{\sqrt{T_s}}{C_o} \frac{R_u}{M_b} K_w Z'_{bs} \rho_g \left(\frac{m_3 + m_7}{m_g} \right) \qquad (3\text{-}9)$$

Thus the total partial pressure of the combustible gas at the gas/solid interface is a sum of the partial pressure of

the volatiles at the gas/solid interface plus the partial pressure of the gases given off by the surface reactions of CO_2 and H_2O. This type of formulation is used in the subsequent analysis of coal particle combustion.

Development of the Model

The following assumptions were made:

1) the coal particles were assumed to be spherical and uniform in size,

2) the proximity of the coal particles was such that a single particle combustion analysis would be valid for each particle,

3) the oxidation reactions represented by equation 3-1 could be taken as a single one-step irreversible reaction,

   A (oxidant) + B (fuel) $\longrightarrow$ C (product) where the coefficients, A, B, and C are representative stoichiometric coefficients,

4) the combustion products of the above reaction immediately redistribute themselves by meams of equilibrium reactions represented by equations 3-2, 3-3 and 3-4 when the products enter the gaseous stream,

5) the diffusion flame sheet solution is valid,

6) the coal density remains constant during combustion,

7) the rate of volatilization is represented by the modified Arrhenius reaction rate law incorporating rate of devolatilization as a function of the particle mass,

8) temperature and material composition are uniform in the solid particle and a quasi steady state analysis is valid through the combustor following ignition.

The assumption of a single, one step irreversible reaction is valid because of the extremely fast chemical kinetics in the gas phase reaction.

In assuming that the diffusion flame sheet solution is valid, it will be noted that at high rates of devolatilization the flame sheet will be established in the diffusion layer at some distance from the coal particle, but as the coal devolatilization rate decreases the flame sheet will tend to be located on the surface. In other work by Chung [37] this flame sheet description of combustion gives results which are identical to those obtained from the description of the diffusion controlled surface combustion. Thus if the diffusion controlled flame description is correct then automatically the diffusion controlled surface combustion will be correct in the limit of small volatilization rates.

In previous coal combustion models [47], two limiting assumptions have been made concerning the coal density during devolatilization and combustion. One assumption is that the coal particle size remains constant and that the density is allowed to decrease as the devolatilization and combustion proceed. The other assumption is that the coal density remains constant, but the coal particle size is allowed to decrease with the process of devolatilization and combustion. Neither assumption is correct, but no detailed understanding of the behavior of coal size and density exists during combustion. Either assumption would introduce the same order of magnitude of discrepancy in the calcula-

tions [47]. Therefore for convenience Chung chose to use the constant density assumption in his analysis.

The characteristic time for the diffusion layer surrounding the particle to adjust itself to the changing properties in the free stream is much less than that required to change the properties of the free stream. It is reasonable to assume that a quasi-steady state combustion analysis will be valid for all periods except ignition.

Any accurate analytical formulation of the ignition characteristics of coal particles is quite formidable due to the very rapid increase in the particle surface temperature which is associated with ignition. Chung employed an aymptotic technique that was used by Ahluwalia [36] to obtain the ignition solution. In this analysis it is assumed that the solid fuel is a sphere immersed in some gaseous environment with a given oxidant concentration. At time t = 0, a constant radiative flux is applied uniformly to the surface. The solution then describes the particle surface temperature variation with time.

Ignition is fundamentally an asymptotic process which describes the transformation of fuel from a state of no chemical reaction to one of self-sustained combustion [36]. The point of ignition is defined as the point where an inflection is first observed in the temperature time history of the particle. This point represents the end of the predominantly external heating period and the beginning of predominant combustion.

Consider the representation of the coal particle in Figure 3-1 showing a particle of radius R located in some gaseous mixture of oxidant, combustion products, and chemically inert species. In the layer around the particle, the thermal chemical interaction is taking place and it is this region that is defined as the diffusion layer.

If chemical changes are assumed to occur by a single reaction step then the Shvab-Zeldovich [35] form of the conservation equation is particularly useful. For species conservation

$$\nabla \cdot (\rho \vec{v} C_i - \rho D \nabla C_i) = W_i \qquad i - 1 \ldots, N \tag{3-10}$$

Using the expression for the divergence in spherical coordinates we find

$$\frac{d}{dr}(r^2 \rho v Y_i) = \frac{d}{dr}(r^2 \rho D \frac{dY_i}{dr} + W_i \tag{3-11}$$

For the case where four species are being considered, i.e., oxygen, fuel, ash and inerts, one can write the following specie conservation equations:

Conservation of Oxidant

$$\frac{d}{dr}(r^2 \rho v C_a) = \frac{d}{dr}(r^2 \rho D \frac{dC_a}{dr}) + W_a \tag{3-12}$$

Conservation of Fuel

$$\frac{d}{dr}(r^2 \rho v C_b) = \frac{d}{dr}(r^2 \rho D \frac{dC_b}{dr}) + W_b \tag{3-13}$$

Conservation of Ash Vapor

$$\frac{d}{dr}(r^2 \rho v C_g) = \frac{d}{dr}(r^2 \rho D \frac{dC_g}{dr}) \tag{3-14}$$

Conservation of Inerts

$$\frac{d}{dr}\left(r^2 \rho v C_e\right) = \frac{d}{dr}\left(r^2 \rho D \frac{dC_e}{dr}\right) \qquad (3\text{-}15)$$

The conservation equations for ash and inerts do not contain rate terms for gas phase reaction since the model assumes no gas phase chemical production of these species. Based on the formulation for the four species then it follows for the combustion products:

Conservation of Combustion Product

$$C_d = 1 - (C_a + C_b + C_g + C_e) \qquad (3\text{-}16)$$

Conservation of Energy

For conservation of energy the Shvab-Zeldovich equation is

$$\nabla \cdot \left[\rho v \left(\int_{T_o}^{T} C_p dT\right) - \frac{\gamma}{C_p} \nabla \left(\int_{T_o}^{T} C_p dT\right)\right] = - \sum_{i=1}^{n} h_i^o W_i \qquad (3\text{-}17)$$

Using the expression for divergence in spherical coordinates then

$$\frac{d}{dr}\left(r^2 \rho v c_{pg} T\right) = \frac{d}{dr}\left(r^2 \rho D c_{pg} \frac{dT}{dr}\right) + W_d \Delta \hat{h}_o \qquad (3\text{-}18)$$

As previously stated, the model assumes two component devolatilization of the combustion products and of the vaporization of the ash. Referring to Figure 3-2, the mass fraction and temperature profiles between the gas solid interface, W, and the interior location of coal particle, S, can be visualized.

Considering the i^{th} species continuity relationship

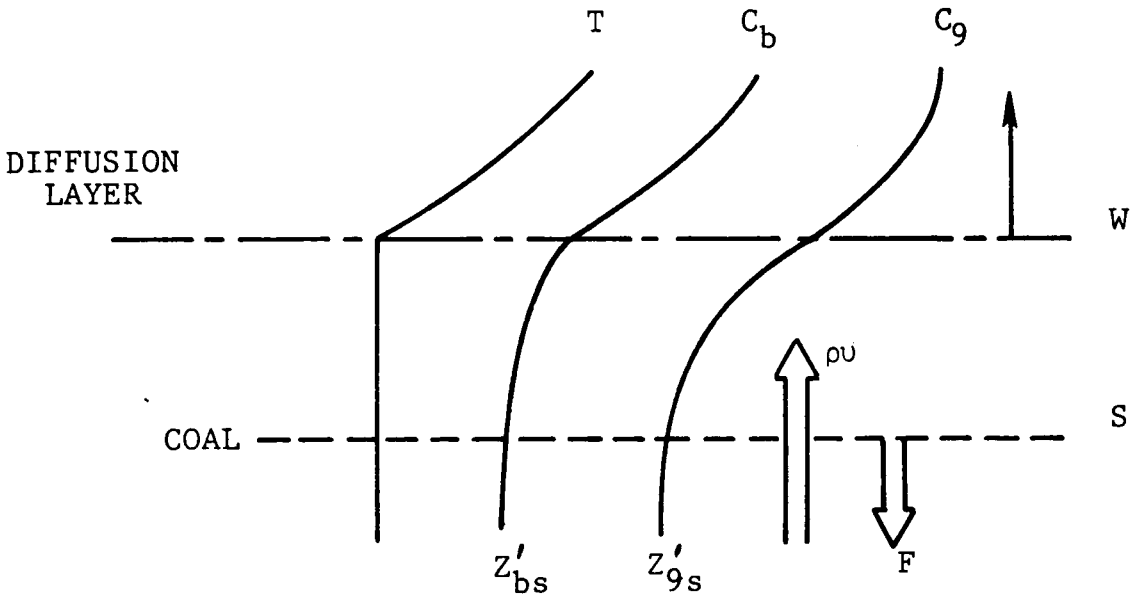

Figure 3-2. Profiles of Fuel and Ash Mass Fraction and Temperature [6]

$$(\rho_i v_i)_s = (\rho_i v_i)_w \tag{3-19}$$

where $$v_i = v_o + \bar{V}_i \tag{3-20}$$

and $$v_o = \frac{\Sigma \rho_i v_i}{\rho} \tag{3-21}$$

Introducing equation 3-20 into 3-19 and write the following:

$$(\rho_i v_o)_s + (\rho_i \bar{V}_i)_s = (\rho_i v_o)_w + (\rho_i \bar{V}_i)_w \tag{3-22}$$

In the above equations, v_i, $\bar{V}_i$ and v_o represents the r directional absolute and relative velocities of the ith species and the mass averaged velocity respectively. It should be noted that these equations will be valid irrespective of the states of the materials.

Defining C_{bw} and C_{9w} to be the mass fractions of the combustible gas and the ash vapor, respectively, at the interface and letting Z'_{bs} and Z'_{9s} be the mass fractions in the combustible matter and ash, respectively, comprising the coal at any given time, then:

$$\rho_{bw} = \rho_w C_{bw}$$

$$\rho_{9w} = \rho_w C_{9w} \tag{3-23}$$

$$\rho_{bs} = \rho_s Z'_{bs}$$

$$\rho_{9s} = \rho_s Z'_{9s}$$

and

$$(\rho v_o)_s = (\rho v_o)_w$$

with Fick's First Law $$\rho v = -D\rho \frac{dC}{dr} \tag{3-24}$$

$$(\rho_b \bar{V}_b)_w = -D\rho \left(\frac{dC_b}{dr}\right)_w \tag{3-25}$$

An equation like 3-25 can be written for each species. At the interface the net rate of production of combustibles and ash can be found by considering the mass balance. The combustible is transported by diffusion across the interface at the rate

$$\rho D \left(\frac{dC_b}{dr}\right)_w \tag{3-26}$$

At the same time the combustible component is transported away from the interface by normal convection at a rate given by

$$\rho v_o \; C_{bw} \tag{3-27}$$

and toward the interface at the rate

$$\rho v_o \; Z'_{bs} \tag{3-28}$$

Thus the net rate of production is simply the normalized relative mass flux of the ash or

$$F = - \frac{(\rho_g \bar{V}_g)_s}{\rho v_o} \tag{3-29}$$

F is defined positive in the -r direction at the surface S. Combining equations 3-26, 3-27, 3-28 and 3-29 we have

$$\rho D\left(\frac{dC_b}{dr}\right)_w = \rho v_o (C_{bw} - Z'_{bs} - F) \tag{3-30}$$

In a similar manner for the ash

$$\rho D\left(\frac{dC_g}{dr}\right)_w = \rho v_o (C_{gw} - Z'_{gs} + F) \tag{3-31}$$

Note that

$$Z'_{bs} + Z'_{gs} = 1 \tag{3-32}$$

since the coal is considered to consist of only two components, that is combustible material and ash. However, in the case of the mass fractions of the combustible gas and ash vapor at the interface their sum will not necessarily equal to one because other gaseous species will be present at the interface.

The overall conservation of energy between the interface W and the surface S can be stated as

Volatilization Energy = (Heat Transfer by Conduction)-
(Heat Transfer by Radiation)

(3-33)

The volatilization energy will be related to the latent heat of volatilization, i.e., the energy required to "drive off" the combustible and vaporize a portion of the ash of the particle. In this sense the latent heat, L, must be a weighted average of the latent heats of volatilization of the combustible and ash. Thus

$$\hat{L} = Z_{bs}L_b + Z_{gs}L_g \tag{3-34}$$

where

$$Z_{bs} = Z'_{bs} + F$$

$$Z_{gs} = Z'_{gs} - F \tag{3-35}$$

In other words the weighting factors Z_{bs} and Z_{gs} are the mass fractions of the combustible and ash vapor portion of the coal particle corrected for the relative mass flux of

the ash. Referring again to equation 3-33 the net energy gain of the particle is

$$\underbrace{\rho v_o \hat{L}}_{\text{Net energy for volatilization}} = \underbrace{\lambda \left(\frac{dT}{dr}\right)_w}_{\text{Conduction thru diffusion layer}} - \underbrace{q_r}_{\text{Radiation lost by particles}} \tag{3-36}$$

The boundary conditions at the gas stream and particle surface can be considered for $r \longrightarrow \infty$ and $r = R$. For the condition $r \longrightarrow \infty$ the boundary conditions are obvious

$$\begin{aligned} C_a &= C_{a\infty}, && \text{(Oxidant)} \\ C_b &= 0, && \text{(Fuel)} \\ C_g &= C_{g\infty}, && \text{(Ash Vapor)} \\ C_e &= C_{e\infty}, \text{ and} && \text{(Inert)} \\ T &= T_\infty. \end{aligned} \tag{3-37}$$

For $r = R$, i.e., the particle surface, the boundary conditions for the fuel and ash vapor are:

$$\rho D \frac{dC_b}{dr} = \rho v \left(C_{b_w} - Z'_{bs} - F\right) \tag{3-38}$$

$$\rho D \frac{dC_g}{dr} = \rho v \left(C_{g_w} - Z'_{gs} + F\right) \tag{3-39}$$

For the oxidant at $r = R$

$$C_a = \frac{dC_a}{dr} = 0 \tag{3-40}$$

which implies a flame sheet in the gas phase [37]. For the inerts

$$\rho D \frac{dC_e}{dr} = \rho v C_e \tag{3-41}$$

where

$$C_b = \frac{K_o}{3\bar{C}_o}\frac{R_u}{\hat{M}}\delta_s R_o \left(\frac{R}{R_o}\right)^{\hat{\beta}} Z'_{bs}\frac{\sqrt{T_s}}{P}\exp(-E_v/R_uT_s) + \tag{3-42}$$

$$+ \frac{K_{wo}}{\bar{C}_o}\frac{R_u}{\hat{M}}\rho_g\left(\frac{m_3 + m_7}{m_g}\right) Z'_{bs}\frac{\sqrt{T_s}}{P}\exp(-E_s/R_uT_s)$$

$$C_g = \frac{M_g}{\hat{M}}\frac{Z'_{gs}}{P}\exp(A_g - B_g/T_s). \tag{3-43}$$

The chemical source terms in equations 3-12 thru 3-16 and 3-18 are a function of species mass fractions, pressure and temperature. The pressure is assumed to be equal to the local freestream pressure and thus the conservation equations along with 3-36 and 3-41 are a self-consistent boundary value problem if ρv, v_o, Z'_{bs}, Z'_{gs} and F are known.

To render equations 3-38 thru 3-41 a self-consistent set of surface boundary conditions, four auxiliary equations are required. Equations 3-32, 3-42, and 3-43 are three of them. The fourth will be an equation relating Z'_{gs} to F and this will be done subsequently.

In the relationship for the mass fraction of the fuel, equation 3-9, this relation is obtained by using the expression for the saturation partial pressure of the combustibles along with the saturation pressure deduced for the CO_2, H_2O surface reaction via the equation of state. The relationship for the mass fraction of the ash vapor, equation 3-43, is deduced using the partial pressure that corresponds to the saturation pressure of S_iO_2 via the equation of state. The conservation equation 3-15 for the

inert species is completely decoupled from the rest of the equations and thus the inert species have no direct effect on the energetics of the problem as would be expected. The conservation of combustion product relationship, equation 3-16, gives the mass fraction of the combustibles from the solution of the other equations; therefore the present problem is reduced to being concerned with the conservation of oxidant, fuel, ash vapor, conservation of energy and the associated boundary conditions. Thus, the combustion rate and therefore the rate of generation of the combustion products as defined by the set of equations 3-1 can be determined.

A diffusion flame will be established if the gas phase reaction is sufficiently fast. With this in mind, it is convenient to eliminate the gas phase reaction terms between the conservation of oxidant, conservation of fuel, and conservation of energy relationships. This type of manipulation can be found in Williams [35] and will not be repeated here. However, it is accomplished by defining new variables

$$\sigma_a = \frac{dM_d}{aM_a} C_a + \frac{c_{pg}T}{\Delta\hat{h}_o}$$

$$\sigma_b = \frac{dM_d}{bM_b} C_b + \frac{c_{pg}T}{\Delta\hat{h}_o} \qquad (3\text{-}42a)$$

$$\gamma = \sigma_b - \sigma_a ,$$

where T is the diffusion layer gas temperature. Using the stoichiometric relation along with the conservation

equations for oxidant, fuel and energy they can be combined to produce the following:

$$\frac{d}{dr}(r^2\rho v\sigma_a) = \frac{d}{dr}(r^2\rho D\frac{d\sigma_a}{dr})$$

$$\frac{d}{dr}(r^2\rho v\sigma_b) = \frac{d}{dr}(r^2\rho D\frac{d\sigma_b}{dr}) \qquad (3\text{-}43a)$$

$$\frac{d}{dr}(r^2\rho v\gamma) = \frac{d}{dr}(r^2\rho D\frac{d\gamma}{dr})$$

In a one-dimensional spherically symmetric system the overall continuity equation can be written as:

$$\dot{m}' = 4\pi r^2\rho v_o = \text{constant} \qquad (3\text{-}44)$$

Using 3-44 with equations of the type given in 3-43a i.e.

$$r^2\rho v_o = \frac{\dot{m}'}{4\pi} \qquad (3\text{-}45)$$

then

$$\frac{d\sigma_a}{dr} = \frac{d}{dr}\left[\frac{4\pi r^2\rho D}{\dot{m}'}\frac{d\sigma_a}{dr}\right]$$

$$\frac{d\sigma_b}{dr} = \frac{d}{dr}\left[\frac{4\pi r^2\rho D}{\dot{m}'}\frac{d\sigma_b}{dr}\right] \qquad (3\text{-}46)$$

$$\frac{d\gamma}{dr} = \frac{d}{dr}\left[\frac{4\pi r^2\rho D}{\dot{m}'}\frac{d\gamma}{dr}\right]$$

Introducing the dimensionless variable

$$\zeta \equiv \dot{m}' \int_r^\infty (4\pi r^2\rho D)^{-1}\, dr \qquad (3\text{-}47)$$

then equation 3-46 reduces to

$$\frac{d\sigma_a}{d\zeta} = -\frac{d^2\sigma_a}{d\zeta^2}$$

$$\frac{d\sigma_b}{d\zeta} = -\frac{d^2\sigma_b}{d\zeta^2} \qquad (3\text{-}48)$$

$$\frac{d\gamma}{dr} = -\frac{d^2\gamma}{d\zeta^2}$$

The solution to this type of differential equation is

$$y = A + Be^{-\zeta}$$

thus the solutions for equation 3-48 are:

$$\sigma_a = k_1 + k_2 \exp(-\zeta)$$
$$\sigma_b = k_3 + k_4 \exp(-\zeta) \qquad (3\text{-}49)$$
$$\gamma = k_5 + k_6 \exp(-\zeta)$$

The constants K_1 through K_6 are constants of integration. In order to effect a closed form integration of equation 3-47 an average constant value of ρD is assumed. Next a set of boundary conditions are derived for σ_a, σ_b and γ which in turn correspond to the original boundary conditions given for the mass fractions of oxidant, fuel and temperature given in equations 3-37 through 3-41 with a view of the definitions given in equation 3-42. Application of these boundary conditions to equation 3-49 and subsequent manipulation of solutions gives the following:

$$\dot{m} = \overline{\rho D}\ \frac{3\rho m_s}{\delta_s R^2}\ \ln\ \frac{Z_{bs} + \frac{bM_b}{aM_a}\ \frac{m_1}{m_g}}{(Z_{bs} - C_b)} \qquad (3\text{-}50)$$

$$T_s = \frac{\Delta\hat{h}_o}{c_{pg}} \left\{ \frac{dM_d}{aM_a}\ \frac{m_1}{m_g} + \frac{c_{pg}T_g}{\Delta\hat{h}_o} - \left[\left(\frac{\dot{m}\delta_s}{3\rho m_s}\right)R\hat{L} + q_R\right] \right.$$

$$\left. \left[\exp\left(\frac{\dot{m}\delta_s R^2}{3\rho m_s \overline{\rho D}}\right) - 1\right] \Big/ \left[\frac{1}{L_e}\left(\frac{\dot{m}\delta_s}{3\rho m_s}\right)\Delta\hat{h}_o R\right] \right\} \qquad (3\text{-}51)$$

$$\frac{Z_{9s} - 1 - \frac{bM_b}{aM_a}\ \frac{m_1}{m_g}}{Z_{9s} - 1 + C_b} = \frac{Z_{9s} - \frac{m_9}{m_g}}{Z_{9s} - C_9} \qquad (3\text{-}52)$$

Keeping in mind that an ultimate global solution for the combustor flow is to be developed, these relationships have been expressed in terms of global combustor variables m_1, m_g, m_s, $\dot{m}$, and ρ. On examining equation 3-40, the mass fraction of the combustibles at the coal surface is defined in equation 3-43. This term will approach zero as the volatilization process within the coal particle nears completion. Equation 3-50 becomes the relationship which gives the combustion rate of the char by the diffusion limited surface reaction.

With this development in mind for the analysis of the combustion of a coal particle we now will consider the global behavior of the gas solid mixture.

In Figure 3-3 is shown a schematic of a constant area one dimensional flow of a chemically reacting mixture of gas and solid particles. The main velocity of the flow of the particle and the gases is assumed to be equal and with this assumption, the following conservation equations govern the flow:

$$\frac{d\rho u}{dx} = 0 \tag{3-53}$$

$$\rho u \frac{du}{dx} = - \frac{dP}{dx} \tag{3-54}$$

$$\rho u A \frac{dh}{dx} = -Q \tag{3-55}$$

As previously mentioned in the discussion of combustion chemistry, the species that are being considered consist of oxygen, carbon monoxide, carbon dioxide, nitrogen, nitrogen dioxide, nitric oxide, water, sulfur dioxide, ash, and hydrogen. In the following, these will be referred to by subscripts of 1 through 10 respectively; however, in the case of the solid particles, they will be denoted by the subscript s. Thus, in writing the species conservation equation the following relationships result:

$$\rho u \frac{dm_s}{dx} = -\dot{m} \tag{3-56}$$

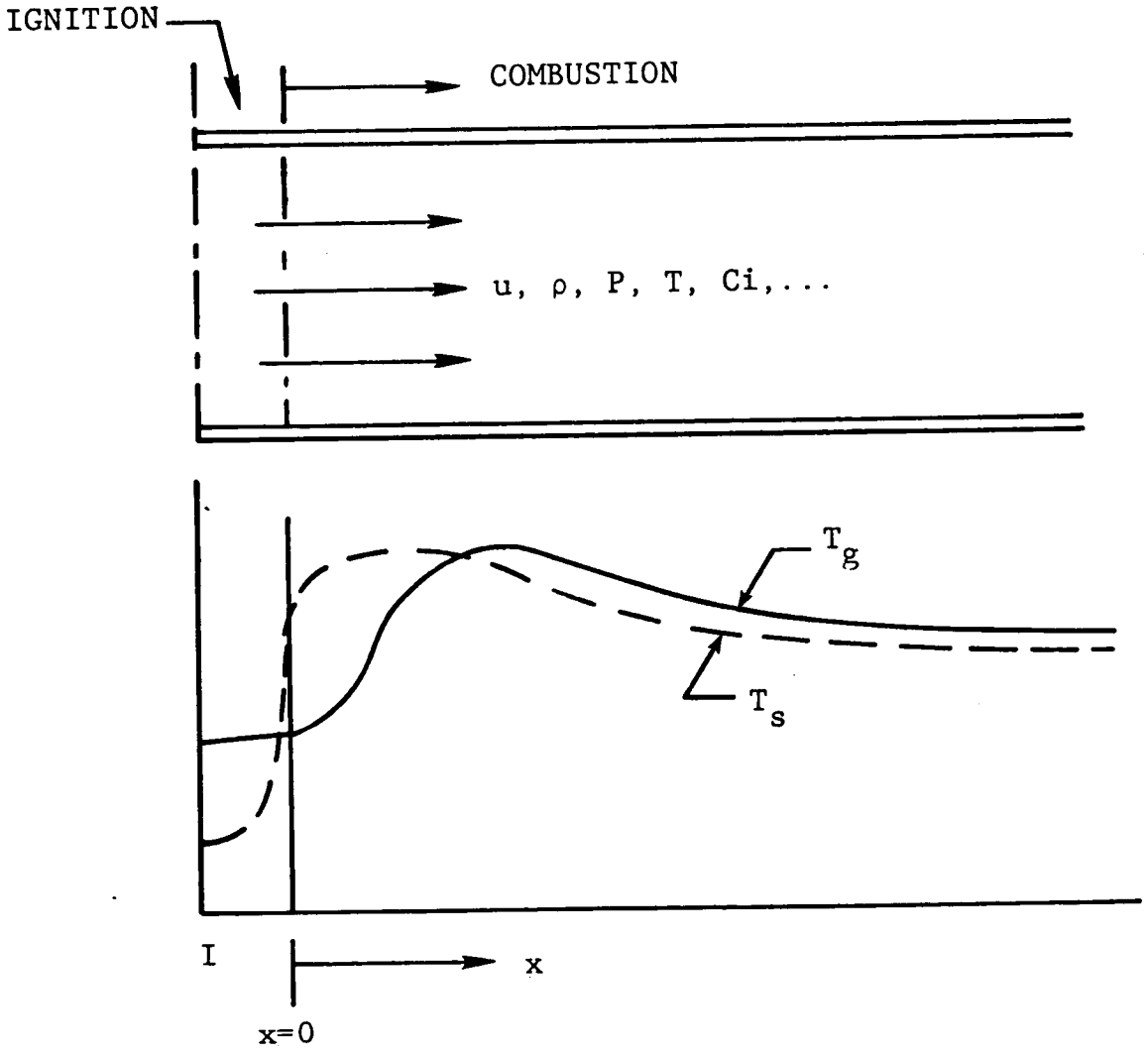

Figure 3-3. One-Dimensional Combustor Model [6]

$$\rho u \frac{dm_1}{dx} = -1/2\left(\frac{M_1}{M_3}\right)W_3 - \left(\frac{aM_1}{bM_b}\right)Z_v\, Z_{bs}\, \dot{m} + \left(\frac{M_1}{2M_{10}}\right)W_{10}, \tag{3-57}$$

$$\rho u \frac{dm_2}{dx} = -\left(\frac{M_2}{M_3}\right)W_3, \tag{3-58}$$

$$\rho u \frac{dm_3}{dx} = \left(\frac{M_3}{M_C}\right)Z_C\, Z_{bs}\, \dot{m} + W_3, \tag{3-59}$$

$$\rho u \frac{dm_4}{dx} = 1/2\left(\frac{M_4}{M_5}\right)W_5, \tag{3-60}$$

$$\rho u \frac{dm_5}{dx} = \left(\frac{M_5}{M_N}\right)Z_N\, Z_{bs}\, \dot{m} + W_5, \tag{3-61}$$

$$\rho u \frac{dm_6}{dx} = -2\left(\frac{M_6}{M_5}\right)W_5, \tag{3-62}$$

$$\rho u \frac{dm_7}{dx} = Z_{bs}\left[\left(\frac{M_7}{2M_H}\right)Z_H + Z_7\right]\dot{m} - \left(\frac{M_7}{M_{10}}\right)W_{10}, \tag{3-63}$$

$$\rho u \frac{dm_8}{dx} = \left(\frac{M_8}{M_S}\right)Z_S\, Z_{bs}\, \dot{m}, \tag{3-64}$$

$$\rho u \frac{dm_g}{dx} = \dot{m} Z_{gs} \tag{3-65}$$

$$\rho u \frac{dm_{10}}{dx} = W_{10} \tag{3-66}$$

$$\rho u \frac{dZ'_{gs}}{dx} = \frac{\dot{m}F}{m_s} \tag{3-66a}$$

The source terms for the species that occur on the right hand side of these equations have been constructed to satisfy the previously discussed chemical reactions. Note that a relationship (equation 3-66a) now exists between the mass fraction of the ash Z'_{gs} to the normalized relative mass flux, F.

The total enthalpy of the reaction mixture as given by Chung, [37] can be defined for equation 3-55 as:

$$\begin{aligned} h &= \sum_i m_i h_i + \frac{u^2}{2} \\ &= \sum_i m_i (c_{pi} T_i + h_i^\circ) + \frac{u^2}{2} \\ &= m_g c_{pg} T_g + m_s c_{ps} T_s + \frac{u^2}{2} + m_s(\Delta h^\circ - L) \\ &\quad + m_2 \Delta h_3 \frac{M_3}{M_2} + m_6 \Delta h_5 \frac{M_5}{2M_6} + m_{10} \Delta h_{10} - m_s Z'_{gs}(\Delta h^\circ - L + L_g) \end{aligned} \tag{3-67}$$

Assuming the gaseous mixture to obey the equation of state:

$$P = \rho_g \frac{R_u}{\hat{M}} T_g \tag{3-68}$$

where

$$\hat{M} = \frac{\sum_i (m_{gi})}{\sum_i (m_{gi}/M_i)}$$

The effect of combustion is reflected in the conservation equations for the combustor through the mass fraction of the solid species, m_s, in the mass rate of generation of total gaseous species per unit volume, $\dot{m}$, and the particle surface temperature T_s. Equation 3-55 governs the mass fraction of the solid species m_s; $\dot{m}$ and T_s are given by equations 3-50 and 3-51 respectively.

At this point, there are 21 equations (equations 3-55 thru 3-68 and 3-50 thru 3-51) and there are 28 unknown functions. Seven additional relationships are required and these become equations 3-32, 3-34 and 3-34 (two equations) as well as the following relationships for the mass fractions and the equation governing the particle radius.

$$m_s + m_g = 1 \tag{3-69}$$

$$m_g = \rho_g/\rho \tag{3-70}$$

$$\rho u \frac{d(\rho n R)}{dx} = -\frac{\dot{m}}{3m_s} \tag{3-71}$$

The gas phase reaction terms, that is the chemical source terms, W, and the heat transfer, Q, are functions of the 28 variables that we have previously discussed. Thus, a self-consistant set of 28 equations and as many unknown functions are now obtained. It should be pointed out that

detailed consideration does not have to be given to the chemical source terms since the gas phase reactions are considered to take place at such a rate that the gas phase mixture is in a state of chemical equilibrium. Thus these terms will be eliminated between the governing equations with the aid of the appropriate equilibrium relationship.

For the high temperatures that are involved in the present work, the predominant mode of heat transfer will be by radiation. However, cases could develop such that the convective heat transport through the wall boundary layer will not be negligible. In reality, both solid particles and gaseous species interchange in heat with the combustor wall.

Much work has been carried out on the radiative transport properties of combustion gas products and one such relationship has been developed by Heywood and Womack [38] for cylindrical combustors of diameter D_c given as follows:

$$Q_{Rg} = 4.77 \times 10^{-5} \left(\frac{A_w}{V_c} \right) \left[\varepsilon_g \left(\frac{T_g}{100} \right)^4 - \varepsilon_w \left(\frac{T_w}{100} \right)^4 \right]$$

with

$$\varepsilon_g = 1.53 \times 10^{-5} T_g \sqrt{D_c} \qquad (3\text{-}72)$$

where the temperatures are in °R, D_c, A_w, and V_c, are in ft., $ft.^2$, and $ft.^3$ respectively. Q_{Rg} is then the radiative

loss in Btu per ft.^{3}-sec of the gas. This relationship is valid when the combustion products do not contain particles.

In a combustor, such as that employed in the present work, the solid particles play a dominant role in the radiative scattering and transport. With solid particle dominant radiation a one dimensional analysis can only be made with the assumption that the net radiative heat loss to the combustor wall of width Dx at x is equally shared by all particles contained in the mixture volume of $Dc^2\ dx/4$ at x. With this in mind the following relationships can be written:

$$Q_{Rs} = 4.77 \times 10^{-5}\ \hat{\varepsilon}_s \left(\frac{A_w}{V_c}\right)\left[\left(\frac{T_s}{100}\right)^4 - \left(\frac{T_w}{100}\right)^4\right]$$

$$q_R = \frac{Q_{Rs}}{N_s A_s} = 1.59 \times 10^{-5}\ R\left(\frac{\delta_s}{\rho_s}\right)\left(\frac{A_w}{V_c}\right)\ \hat{\varepsilon}_s\left[\left(\frac{T_w}{100}\right)^4 - \left(\frac{T_w}{100}\right)^4\right] \qquad (3\text{-}73)$$

where $\hat{\varepsilon}_s = \varepsilon_s \varepsilon_w$

In the above equations temperatures and lengths are in degrees Rankine and feet respectively, Q_{Rs} and q_R are in Btu per ft.^{3}-sec and Btu per ft^2-sec respectively. The calculations can be made for either q_R or Q_{Rs} and these may be substituted in equation 3-55 for Q depending on the particle density in the combustor. The code, as developed, is able to accept either case.

Considering again the conservation equations, the gas phase chemical reaction rates will be eliminated by manipulation, employing the appropriate equilibrium relationship.

With this in mind equations 3-53 thru 3-67 and 3-71 will be transformed into a simpler set of equations and through appropriate manipulation and combining of these 16 equations the following set results:

$$\frac{dm_{130}}{dx} = \left(1/2\,\frac{M_1}{M_C}\,Z_C - \frac{aM_a}{bM_b}\,Z_v\right) Z_{bs}\,\dot{m}\ , \tag{3-74}$$

$$\frac{dm_{120}}{dx} = \frac{M_2}{M_3}\left(\frac{aM_a}{bM_b}\right) Z_v Z_{bs}\,\dot{m}, \tag{3-75}$$

$$\frac{dm_{45}}{dx} = 1/2\left(\frac{M_4}{M_N}\right) Z_N Z_{bs}\,\dot{m}\ , \tag{3-76}$$

$$\frac{dm_{46}}{dx} = 0\ , \tag{3-77}$$

$$\frac{dm_{70}}{dx} = \left(\frac{M_7}{2M_H}\,Z_H + Z_7\right) Z_{bs}\,\dot{m}\ , \tag{3-78}$$

$$\frac{dm_{sR}}{dx} = 0\ , \tag{3-79}$$

$$\frac{dm_8}{dx} = \left(\frac{M_8}{M_S} \right) Z_S Z_{bs} \dot{m} \ , \tag{3-80}$$

$$m_9 = m_{so}(Z'9_s)_o - m_s Z'9_s , \tag{3-81}$$

$$m_{130} = m_1 + 1/2 \frac{M_1}{M_3} m_3 - \frac{M_1}{2M_{10}} m_{10} , \tag{3-82}$$

$$m_{120} = - \frac{M_2}{M_3} m_1 + 1/2 \frac{M_1}{M_3} m_2 + \frac{M_1 M_2}{2M_3 M_{10}} m_{10} , \tag{3-83}$$

$$m_{45} = -m_4 + 1/2 \frac{M_4}{M_5} m_5 \ , \tag{3-84}$$

$$m_{46} = 2\left(\frac{M_6}{M_5} \right) m_4 + 1/2\left(\frac{M_4}{M_5} \right) m_6 \ , \tag{3-85}$$

$$m_{70} = m_7 + \left(\frac{M_7}{M_{10}} \right) m_{10} \ , \text{ and} \tag{3-86}$$

$$m_{sR} = \ell n \ (m_s^{1/3}/R). \tag{3-87}$$

The equations with the gas phase reaction terms produce three equilibrium relationships in the limit of an infinitely fast reaction rate. They describe the equilibria of the equations and they are:

$$\frac{m_2}{m_3}\left(\frac{m_1}{m_g}\right)^{1/2} = \frac{1}{(P)^{1/2}}\left(\frac{M_2}{M_3}\right)\left(\frac{M_1}{\hat{M}}\right)^{1/2} K_1, \tag{3-88}$$

$$\frac{(m_6)^2}{m_5(m_4 m_g)^{1/2}} = \frac{1}{(P)^{1/2}} \frac{M_6^2}{M_5(\hat{M}M_4)^{1/2}} K_2 \text{ , and} \tag{3-89}$$

$$\frac{m_7}{m_{10}}\left(\frac{m_g}{m_1}\right)^{1/2} = (P)^{1/2} \frac{M_7}{M_{10}}\left(\frac{\hat{M}}{M_1}\right)^{1/2}\left(\frac{K_3}{K_1}\right), \tag{3-90}$$

where

$$K_1 = \exp\left(10.463 - \frac{6.14 \times 10^4}{T_g}\right),$$

$$K_2 = \exp\left(10.169 - \frac{3.20 \times 10^4}{T_g}\right), \text{ and} \tag{3-91}$$

$$K_3 = \exp\left(2.946 - \frac{5.346 \times 10^3}{T_g}\right).$$

In equations 3-88 thru 3-91 T_g and P are in degrees Rankine and atmosphere respectively and equations 3-91 are valid in the temperature range of interests, i.e., 3000 to 6000 degrees R. The remaining equations are 3-53 thru 3-56 and they are reproduced here for completeness.

$$\frac{d\rho u}{dx} = 0 \tag{3-92}$$

$$\rho u \frac{du}{dx} = - \frac{dP}{dx} \tag{3-93}$$

$$\rho u A \frac{dh}{dx} = -Q \tag{3-94}$$

$$\rho u \frac{dm_s}{dx} = -\dot{m} \tag{3-95}$$

$$\rho u \frac{dZ'_{9s}}{dx} = \frac{\dot{m}F}{\dot{m}_s} \tag{3-96}$$

These equations can be solved by numerical integration.

At this point, of the 16 equations, equations 3-53 thru 3-67 and 3-75 have been replaced by an equal number of equations, that is by 3-74 thru 3-81, 3-88 thru 3-90 and 3-92 thru 3-96. These equations along with the 12 auxillary equations 3-67 thru 3-76, 3-32, 3-34, 3-35 and 3-50 thru 3-52, constitute a complete set of 28 equations defining the 28 unknown functions. However, before they can be solved, a set of initial conditions must be specified for equations 3-74 thru 3-80 and equations 3-92 thru 3-96. The initial conditions for 3-74 thru 3-80 are obtained from those of the

chemical species such as m_1, m_2, etc. at X = 0 via equations 3-82 thru 3-87.

As previously stated the ignition period is not taken to be quasi-steady state because of the thermal shock involved in the the heating of the coal particles and the ignition solution is analyzed separately. The composition of the coal presented by the ultimate analysis is transformed to an oxygen and ash free basis in the following manner. Let Z''_i be the mass fraction of the i_{th} constituent of the coal by the ultimate analysis. The oxygen and ash free basis mass fractions Z_i are given by:

$$Z_i = \frac{Z''_i}{1 - Z''_{ash}} \quad \text{for } i = C, N, \text{ and } S,$$

$$Z_H = \frac{Z''_H - (1/8)Z''_O}{1 - Z''_{ash}}, \qquad (3\text{-}97)$$

$$Z_7 = \frac{(9/8)Z''_O}{1 - Z''_{ash}},$$

$$Z_O = 0,$$

$$Z_v = Z_C + Z_H + Z_N + Z_S = 1 - Z_7. \qquad (3\text{-}98)$$

The net heating value of the coal must also be on an ash free basis hence:

$$\Delta h^\circ - L = \frac{HV}{1 - Z''_{ash}} \quad ,$$

and

$$\Delta \hat{h}_o = \Delta h^\circ \left(\frac{bM_b}{dM_d} \right) . \qquad (3\text{-}99)$$

HV is the lower heating value of the coal.

The conversion of the chemical species specified in equation 3-1 has been assumed to take place at the diffusion flame according to the one step simple reaction as previously presented. Thus the conservation of mass at the diffusion flame requires that the average molecular weight of the gasifying fuel can be evaluated by the following equation:

$$M_b = \left(\frac{aM_a}{b} \right) Z_v \left[Z_C \frac{M_3}{M_C} + Z_N \frac{M_5}{M_N} + Z_H \frac{M_7}{2M_H} + Z_S \frac{M_8}{M_S} + Z_7 - 1 \right]^{-1} \qquad (3\text{-}100)$$

After the coal properties have been transformed to the appropriate basis, the 12 initial conditions for equations 3-74 thru 3-80 and 3-92 thru 3-96 are obtained from the following relationships using equations 3-81 thru 3-87. The point at X = 0 denotes the end of the ignition process, then these relationships have been derived to satisfy the chemistry and mass conservation requirements as previously set forth at X = 0.

$$m_s = \frac{\hat{F}_b(1 - \Delta m'_s)}{\hat{F}} \quad , \tag{3-101}$$

$$m_1 = \frac{\hat{F}_o - \Delta m'_s \hat{F}_b\left(\frac{aM_a}{bM_b}\right)Z_v}{\hat{F}} \quad , \tag{3-102}$$

$$m_2 = 0 \quad , \tag{3-103}$$

$$m_3 = m_{sI}(\Delta m'_s)\, Z_C\left(\frac{M_3}{M_C}\right) \quad , \tag{3-104}$$

$$m_4 = \frac{(.767)\hat{F}_{air}}{\hat{F}} \quad , \tag{3-105}$$

$$m_5 = m_{sI}(\Delta m'_s)\, Z_N \frac{M_5}{M_N} \quad , \tag{3-106}$$

$$m_6 = 0 \quad , \tag{3-107}$$

$$m_7 = m_{sI}(\Delta m'_s)\left[Z_H \frac{M_7}{2M_H} + Z_7\right] \quad , \tag{3-108}$$

$$m_8 = m_{sI}(\Delta m'_s)\, Z_S \frac{M_8}{M_S} \quad , \tag{3-109}$$

$$m_9 = 0 \quad , \tag{3-110}$$

$$m_{10} = 0, \text{ and} \tag{3-111}$$

$$Z'_{9so} = \frac{m_{sI}}{m_{so}} Z''_{ash}, \tag{3-112}$$

where

$$\Delta m'_s = \frac{c_{ps}(T_{so} - T_{sI})}{c_{ps}T_{so} + (\Delta h^\circ - L)}, \text{ and} \tag{3-113}$$

$$\hat{F} = \rho u A. \tag{3-114}$$

With the above 12 equations 3-101 through 3-112, the initial pressure is specified, ρu is already specified through F which is given by equation 3-114 and the enthalpy, h, is implicitly specified from equations 3-101 thru 3-112 thru the definition which is equation 3-114.

The particle surface temperature at X = 0, i.e., T_{so} which appears in equation 3-113 must be consistant with that given by the combustion solution in equation 3-51. The determination of the initial conditions requires an interactive solution over T_{so}, i.e., the initial particle temperature.

At this point, the analytical solution has been formulated. In the devolatilization relationship (equation 3-5) the pre-exponential factor, K_o, activation energy, E_v and the factor $\hat{\beta}$ must be determined from existing experimental results. Available values vary greatly as shown in Chapter 2. The values for K_o amd E_v were chosen by Chung from reference 39. The factor $\hat{\beta}$ was determined

by Chung from analysis of data given in reference 40. The experiments in references 39 and 40 were chosen because the experimental conditions were for heating rates and final temperature approaching those that would be expected in a high temperature coal combustor. The values determined by Chung were

Activation Energy, $E_V = 5.9 \times 10^7$ ft-lb/lb-mole

Pre-exponential factor, $K_o = 10^{11}$/min

$\hat{\beta}$ Factor = 11/3

These are the values that were used in the analysis of the experimental data in this work.

In Chapter 2 the activation energy and pre-exponential factor were chosen such that the analytical solutions were forced to fit the experimental results. In the present work values were chosen based on other experiments and were not adjusted to fit the data.

The results of the solution of the model will be discussed in Chapter 5. A sample print-out of the solution is given in the Appendix.

CHAPTER 4

EXPERIMENTAL APPARATUS AND PROCEDURE

The experimental work reported here was performed using a pulverized coal combustor shown schematically in Figure 4-1. The combustor consists of an oxidant preheater shown in Figure 4-2 and a water cooled cylindrical coal combustor shell (variable length) that had a diameter of 14 inches. The preheated oxidant injection velocity and spatial distribution was varied by changing injection schemes. Oxidant was injected coaxially with the coal jet as well as through a multiport injector shown schematically in Figure 4-3. The assembly of the multiport injector in the combustor is shown in Figure 4-4.

Combustor Configurations

The three fundamental combustor configurations employed in the tests are depicted in Figure 4-5. In configuration (a) the basic feature is that of coaxial oxidant injection with no recirculation. In configuration (b) the primary feature is coaxial oxidant injection with recirculation. In configuration (c) the oxidant is injected through a multiport oxidant injection plate with strong recirculation.

Data used in this work were collected from tests that were performed using the three MHD flow train configurations shown in Figures 4-6, 4-7, and 4-8. During these experiments, data were taken for coal flow rates over the range of

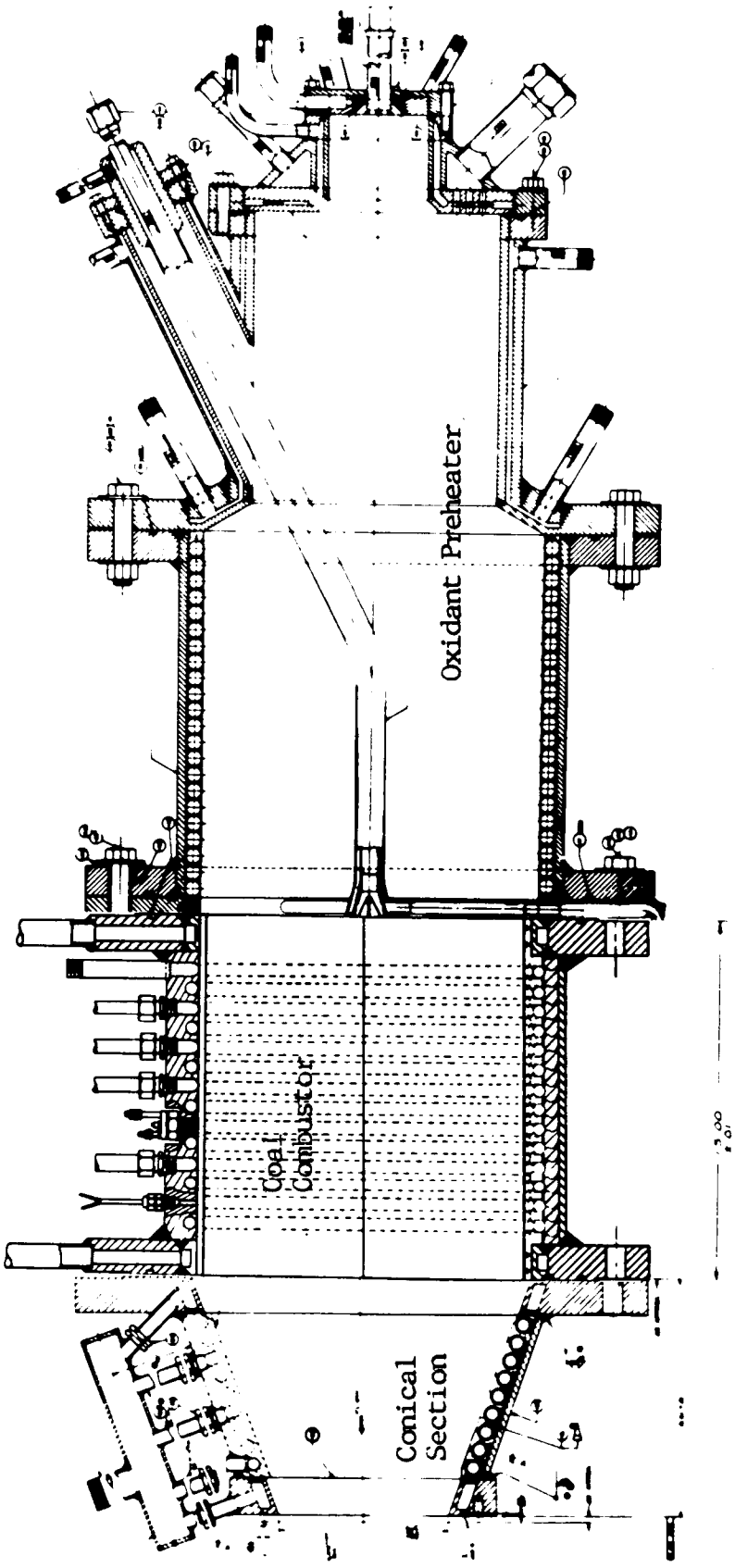

Figure 4-1. Oxidant Preheater/Coal Combustor Assembly.

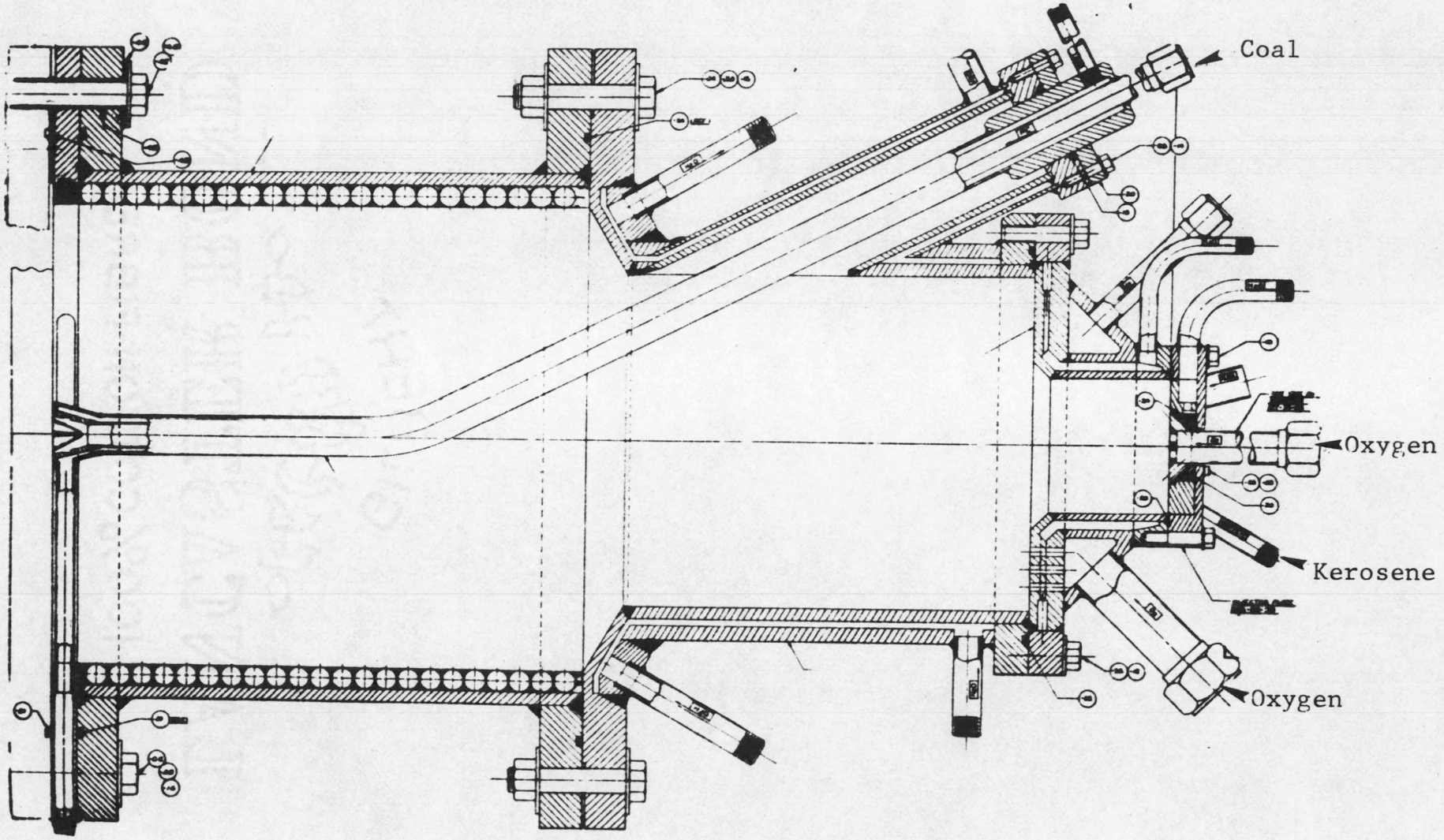

Figure 4-2. Oxidant Preheater

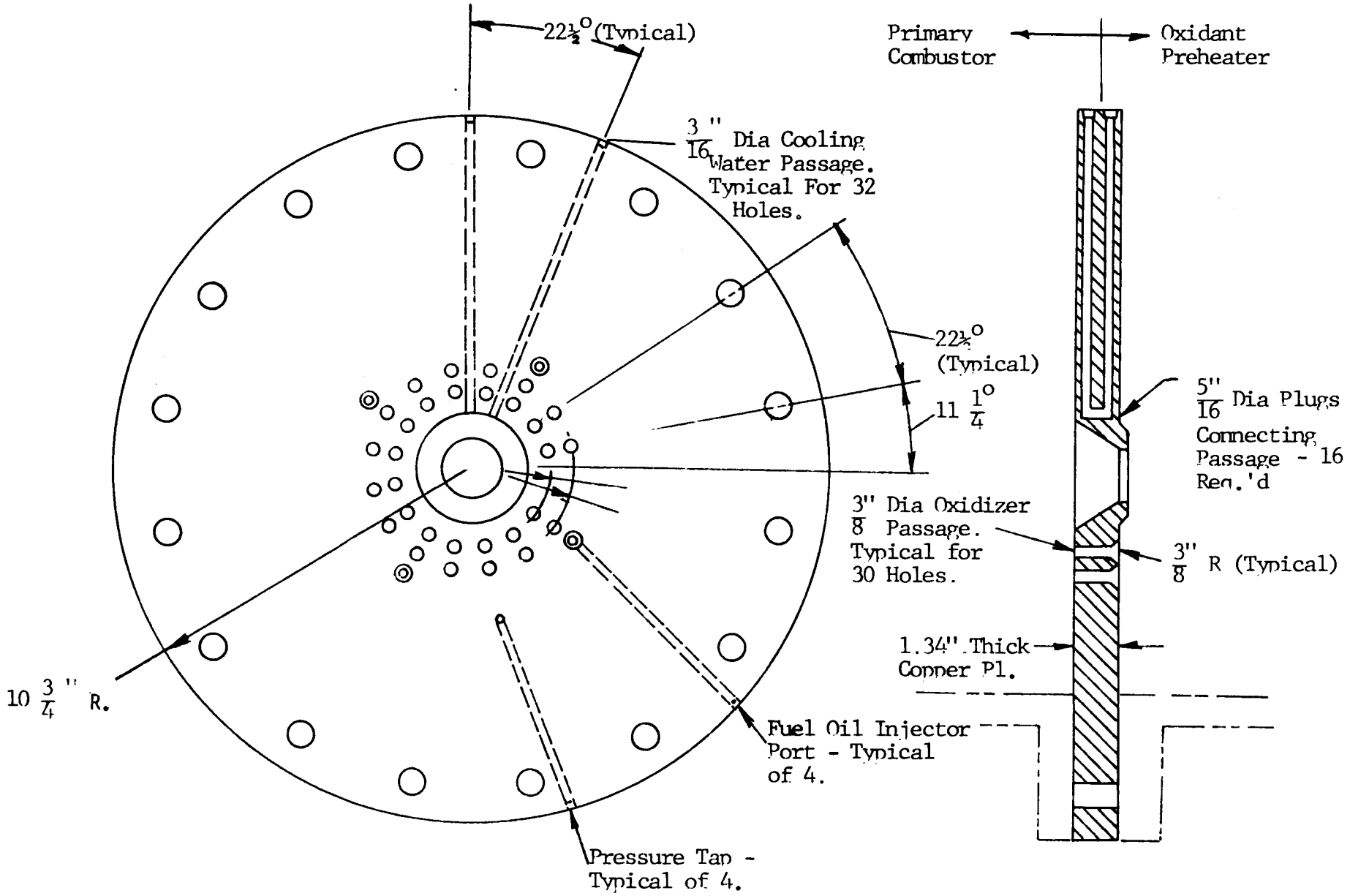

Figure 4-3. Multiport Oxidant Injector

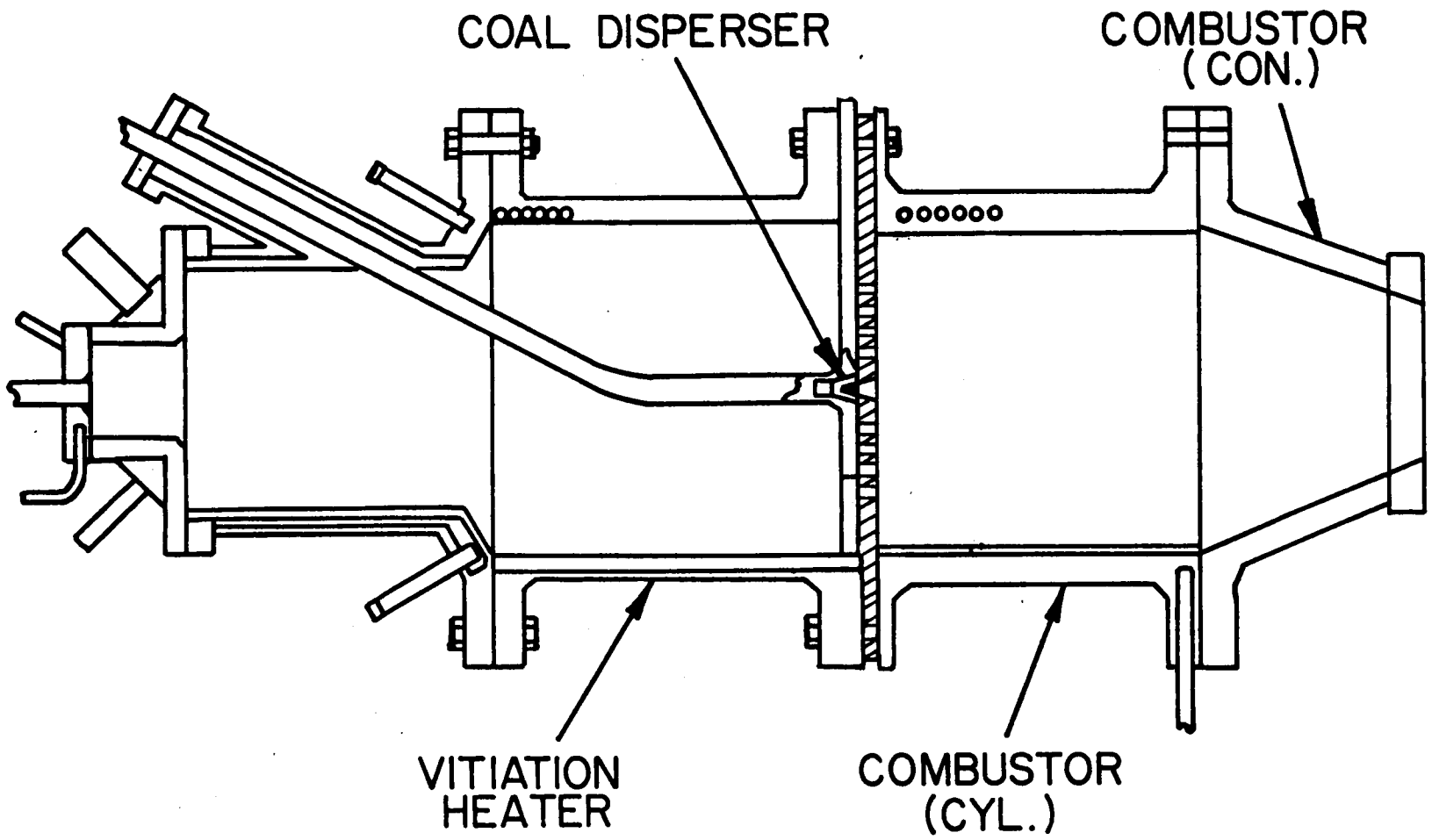

Figure 4-4. Oxidant Preheater/Coal Combustor with Water-Cooled Injector Plate

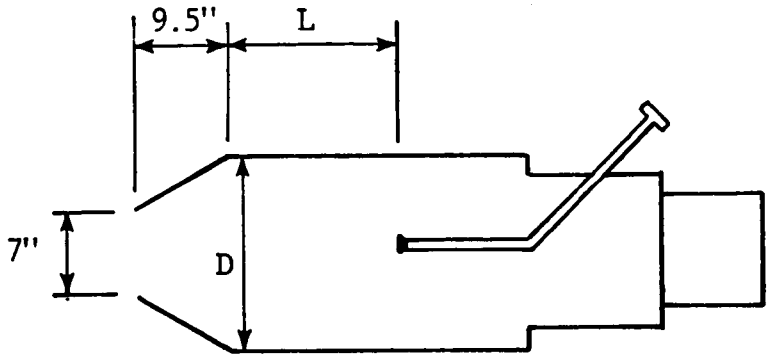

L (in)	D (in)
15	14
27	14

(a) Coaxial Oxidant Injection, No recirculation

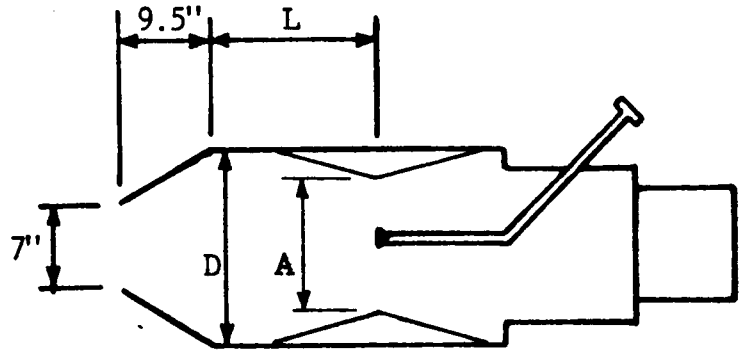

L (in)	D (in)	A (in)
15	14	6.5
15	14	8.5
27	14	6.5

(b) Coaxial Oxidant Injection, with recirculation

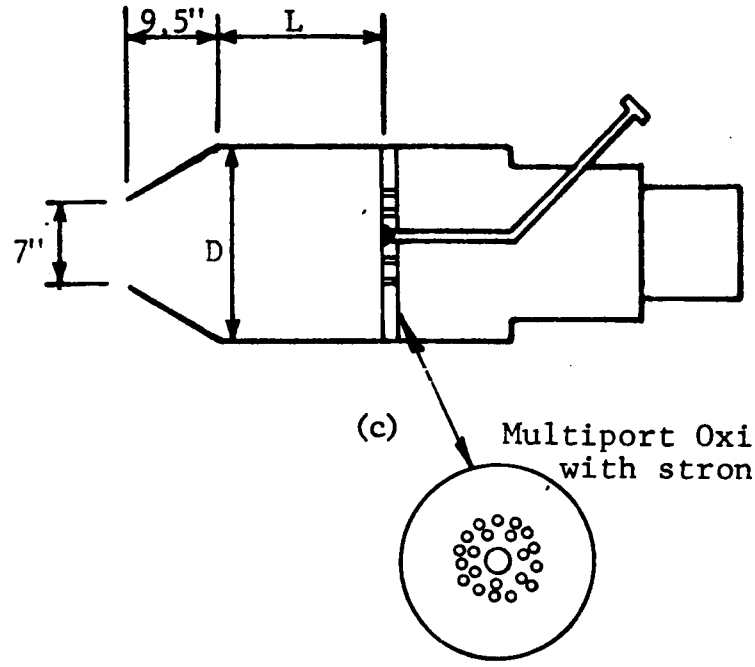

L (in)	D (in)
15	14
60	14

(c) Multiport Oxidant Injection with strong recirculation

Figure 4-5. Coal Combustor Configurations

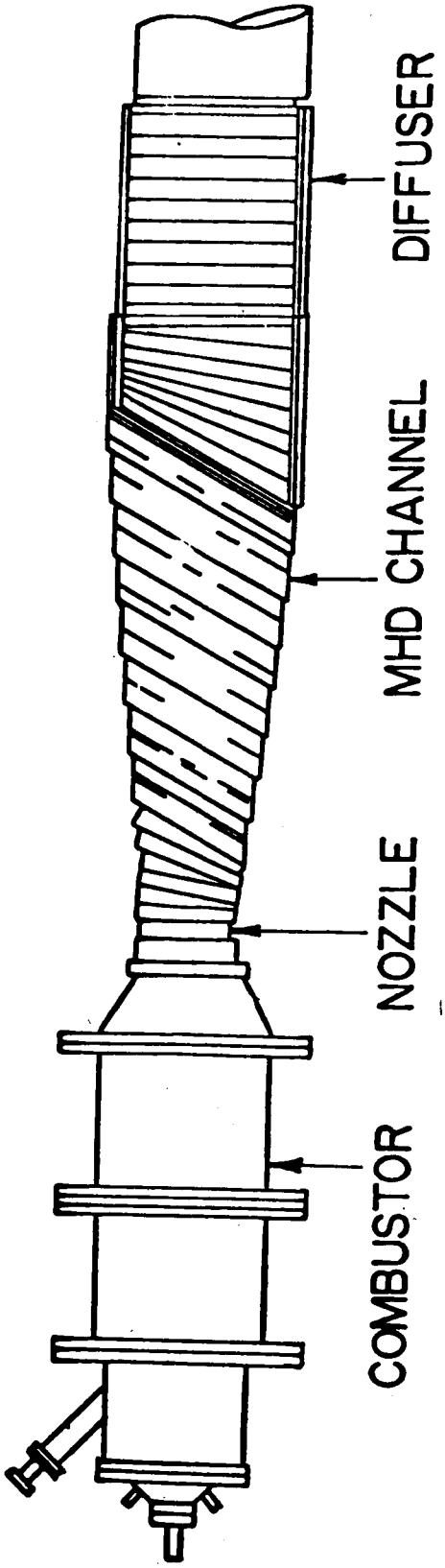

Figure 4-6. Coal Combustor with MHD Generator.

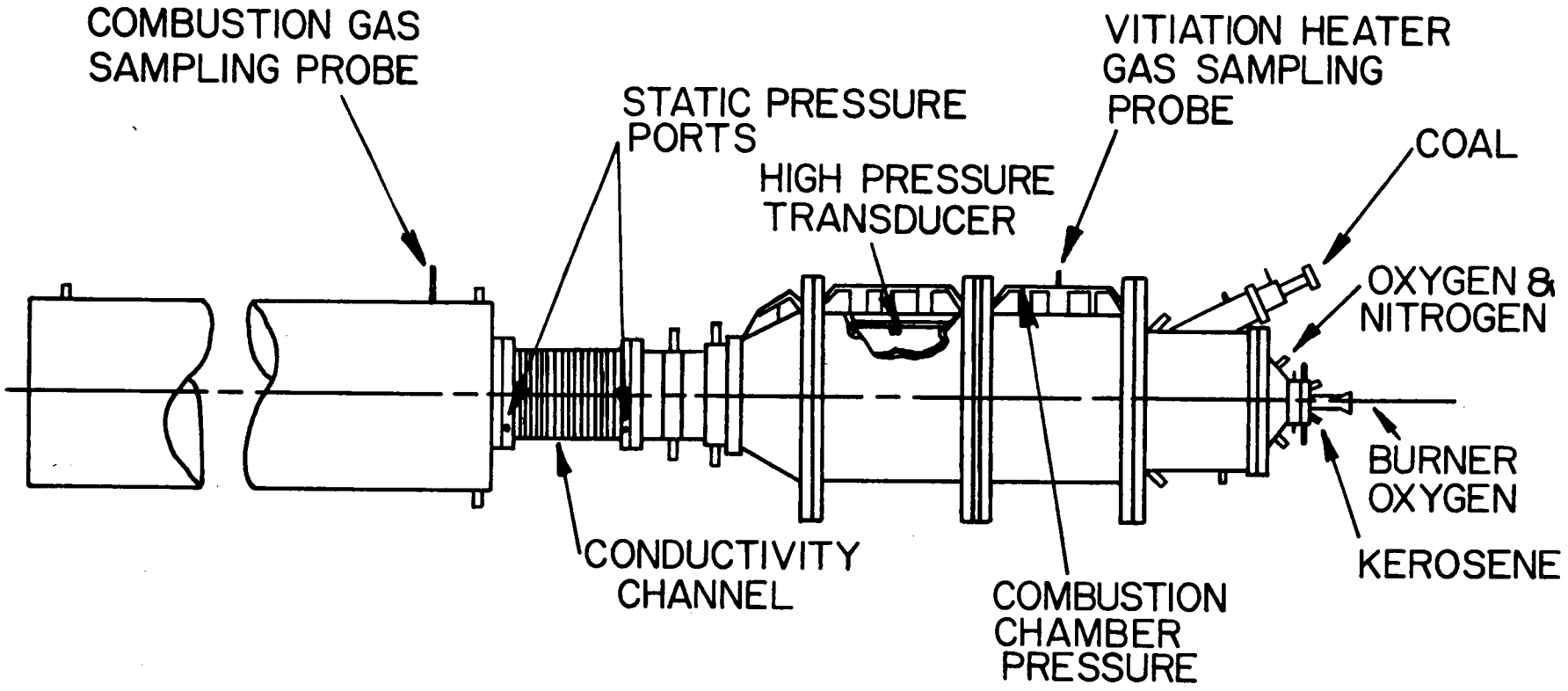

Figure 4-7. Coal Combustor with Conductivity Channel

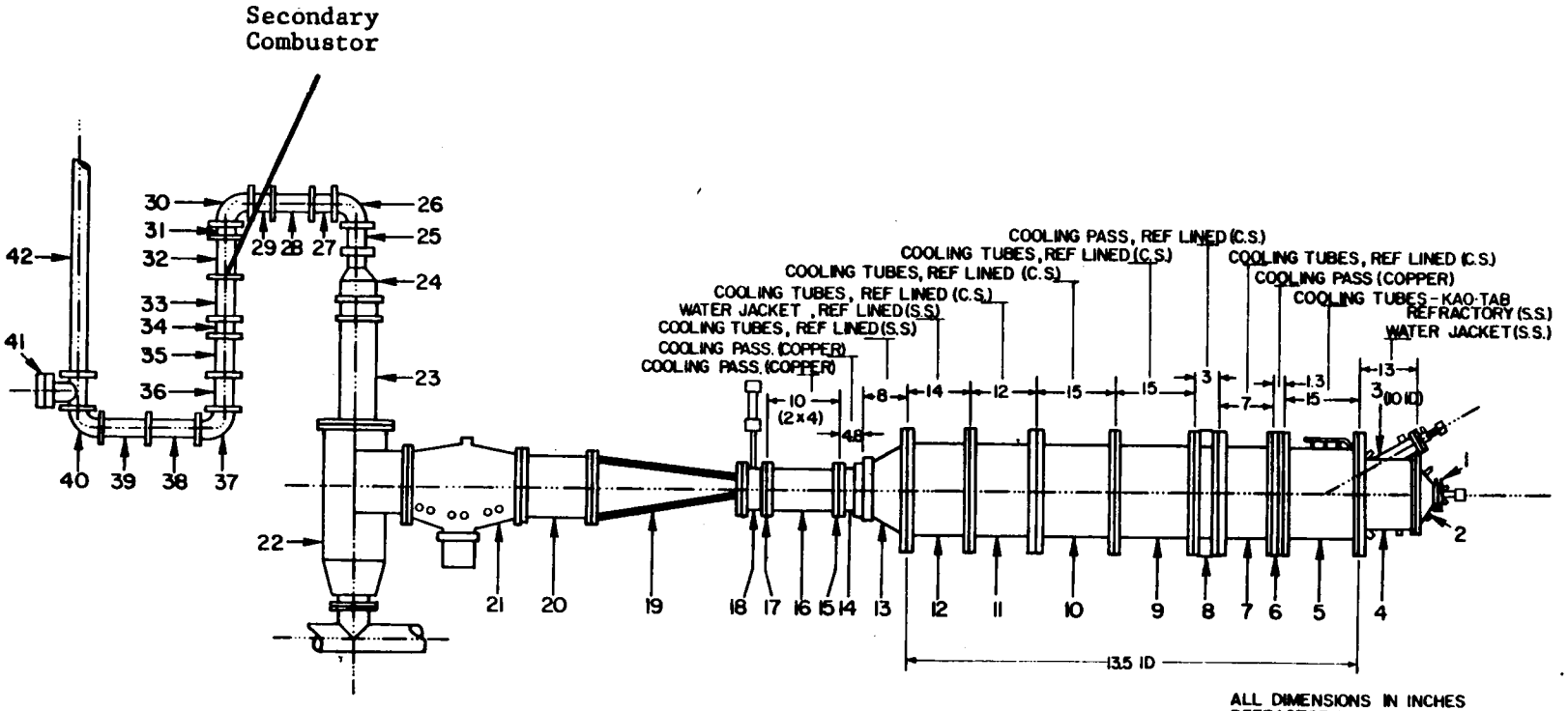

SCHEMATIC OF TEST SET UP

ALL DIMENSIONS IN INCHES
REFRACTORY: CARBORUNDUM 11 LI-
SILICON CARBIDE
MATERIALS ARE GIVEN IN PARENTHESIS

0.5 lbs/sec to 1 lb/sec. Combustion pressure was varied from approximately 2 to 5 atmospheres.

The flow train depicted in Figure 4-6 consisted of the oxidant preheater/coal combustor with a sonic nozzle on the discharge feeding into an MHD generator channel. In this configuration the combustor performance was evaluated using an MHD generator for diagnostics, i.e., combustor performance was related to power produced by the MHD generator. In the flow train shown in Figure 4-7, the combustor installation was the same as that in Figure 4-6; however, the conductivity channel was installed to measure the plasma conductivity exiting the combustor. The flow train depicted in Figure 4-8 consisted of the oxidant preheater/coal combustor with the coal combustor portion of the assembly being much longer. In this configuration the combustion gases pass through a nozzle into a conductivity channel and through a device that is used to throttle the flow to increase the combustor pressure. The coal flows in Figures 4-6 and 4-7 were nominally 1 lb/sec while in Figure 4-8 the flows were nominally 0.5 lbs/sec.

For the purposes of this report, major sources of data in all three flow train configurations consisted of the gas analysis taken near the combustor discharge, heat transfer data that was taken from the combustor as well as slag and particle size analysis. Data were taken to examine the effects of mixing and residence time on combustor performance. Combustor residence time was changed by either

holding the flow rate constant and increasing the combustor pressure by throttling or by physically increasing the combustor volume. Effects of mixing were evaluated by changing the method of oxidant injection into the coal combustor.

Coal Characteristics

In all of the experiments the coal was fed into the combustion chamber under highly dense phase conditions with coal injection densities of approximately 23 pounds per cubic foot. The coal was fed into the combustor using nitrogen as a carrier gas with a ratio of coal to nitrogen of 100:1 by weight. The coal used in each test was Illinois #6, 70% through 200 mesh, with a nominal size of 50 microns. A typical fuel analysis is shown in Table 4-1 and a typical sieve analysis is shown in Table 4-2.

Gas Analysis

The high temperature, dense particle populations found in oxygen blown coal combustors make water cooled sampling probes the only reliable method of measuring the gas phase composition with any accuracy. The gas analysis stream used in this work is an extraction method with continuous monitoring of species of interest through dedicated instrumentation. The sample conditioning system is shown in Figure 4-9. In this system a sample is drawn by a teflon diaphragm pump through a heated filter and sample line to a sample conditioner. The sample conditioner consists of a refri-

TABLE 4-1

TYPICAL FUEL ANALYSIS

COMPONENT	%	Variance
Moisture	3.0	± 1.0
Ash	12.5	± 2.5
Sulfur	3.9	± 0.2
Carbon	66.0	± 3.0
Hydrogen	4.9	± 0.2
Nitrogen	1.2	± 0.1
Oxygen	8.5	(by difference)
BTU/# (HHV)	12,100	± 150
Volatile Matter	38.9	(proximate analysis)
Fixed Carbon	61.1	(DAF Basis)

Ash Analysis	(percent of ash)	Variance
SiO_2	53.	± 3.0
Al_2O_3	14.	± 2.0
Fe_2O_3	21.	± 2.5
CaO	3.9	± 0.5
K_2O	2.3	± 0.3
Na_2O	0.3	± 0.1
TiO_2	0.9	± 0.1
MgO	0.9	± 0.1
SO_3	4.0	± 0.5

TABLE 4-2

TYPICAL SIEVE ANALYSIS

AFTER PULVERIZATION

% in Sieve	Sieve Size
2.0 percent on 100	150 micron
8.3 percent on 140	105 micron
13.3 percent on 200	75 micron
10.3 percent on 270	53 micron
14.6 percent on 325	45 micron
51.5 percent pass 325	45 micron
100.0 TOTAL	

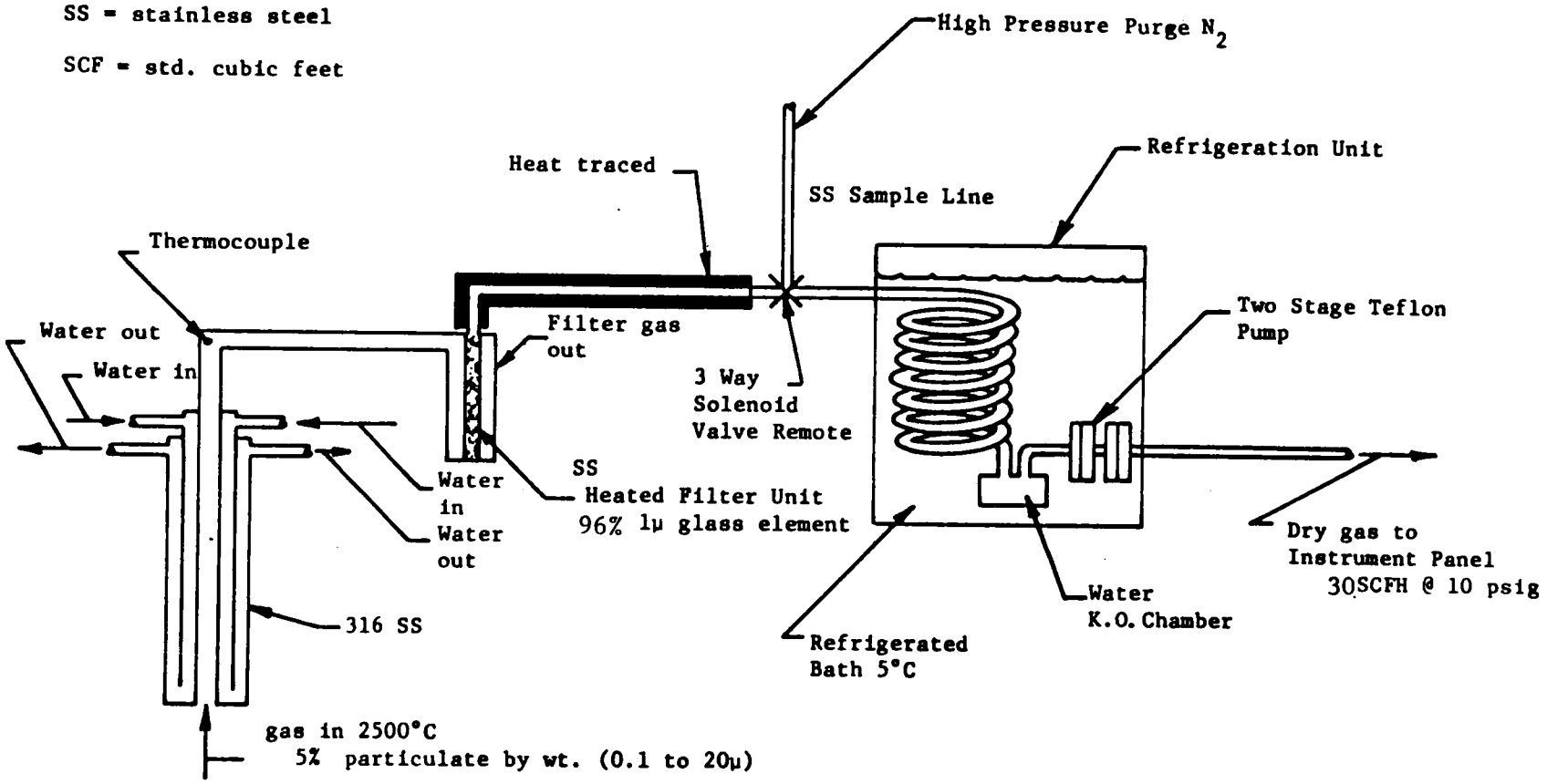

Figure 4-9. Sample Probe and Sample Handling System.

geration bath of ethylene glycol. The water is condensed from the gas stream at 5°C and rejected from the system. The dry gas is then pumped to the gas analysis instrumentation. The following gases were continuously monitored:

CO_2	infrared method	0-100 pct, ± 1 pct
CO	infrared method	0-30 pct, ± 0.3 pct
CO	infrared method	0-2000 ppm ± 20 ppm
H_2S	amperometric method	0-10,000 ppm ± 1000 ppm
SO_2	pulsed fluorescence method	0-5000 ppm ± 50 ppm
NO	chemiluminescent method	0-25 pct, ± 0.25 pct
O_2	fuel cell ZrO_2	0-25 pct, ± 0.25 pct

An additional capability was an on-line chromatograph which updates every two minutes for H_2, N_2, O_2, CH_4 and other fixed gases. The gas analysis system has a switching device allowing different locations to be analyzed for gas composition. As indicated, carbon dioxide and carbon monoxide are analyzed using an infrared method. The infrared instruments are non-dispersive IR units from Infrared Industries, Santa Barbara, California. Infrared is the most accepted method for CO and CO_2 analysis [44]. Pulsed fluorescence is used for measuring SO_2 concentration and this method has become most accepted in recent years. Chemiluminescence analysis is used for NO_x measurement. Hydrogen sulfide is measured using the amperometric method and this is the general method that is used when analyzing this gas [44]. The oxygen content was measured using an oxygen specific fuel

cell oxygen analyzer. This instrument is accurate but has a slow response time compared to other methods available. However, it is widely used in the utility industry and elsewhere for monitoring and controlling combustion processes.

The gas chromatograph is a Beckman GC 725 and has been modified to be an online chromatograph with automatic sampling sequence. A thermal conductivity detector provides a universal type of sensor for components in concentration ranges above 0.5%. A molecular sieve-column is used for H_2, N_2, O_2, CH_4, and CO in a 4 minute analysis time. Calibration standards from Union Carbide are used to obtain response factors for the instrument.

In all cases calibration standard gases from Union Carbide were used to check the accuracy of the instruments.

An analog digital converter interfaces the typical instrument output of 0 to 100 millivolts with the UTSI data acquisition system, which has a scan rate of more than 200 data points in 0.5 seconds. This provided more than adequate response to the instruments and sampling time involved.

The difficulty with this measurement is that gases in a high temperature equilibrium state when the samples are taken are changed due to the decrease in temperature after passing through the water cooled probe and sample conditioning system. However, it is felt that since the total carbon in the feed coal is being measured and compared with the carbon content of the combustion gases the inaccuracies

introduced are taken into account.

Heat Transfer

The heat transfer to the combustor was determined by measuring the cooling water flow rate through each cooling circuit and then measuring the cooling water inlet and outlet temperatures using thermocouples. Calculation of the heat carried away by the cooling water in a particular segment allowed the heat flux distribution to be determined.

Particulate and Slag Measurements

Particulate size distribution was measured using a cascade impactor. The cascade impactor is a Brink impactor modified by the Babcock & Wilcox Company. Details of the impactor are given in Reference 41.

Slag and particle depositions were analyzed using optical microscopy, scanning electron microscopy, and energy dispersive x-ray technique. These methods were used to determine the mineral composition of slag deposited within the flow train as well as to evaluate particle sizes and particle composition.

In addition to these diagnostic measurements, in a few of the experiments, MHD generator power was measured. These measurements were made to evaluate the combustor performance in terms of MHD requirements. No details of these measurements are given here; however, the operation of these devices is well documented in the literature [48].

In addition, the input stream variables were measured using conventional methods. These consisted of measuring the oxygen and nitrogen flow rates using orifice plates and pressure drop transducers. The coal flow was measured using change in coal hopper weight as well as a Micro-Motion flow meter. Details of the operation of the Micro-Motion flow meter are given in Reference 42.

CHAPTER 5

EXPERIMENTAL RESULTS AND COMPARISON WITH THEORY

In Chapter 4 it was pointed out that the experimental data were taken in three flow train configurations represented by Figures 4-6, 4-7 and 4-8 (Pages 100,101,102). To facilitate discussion of the experimental data within this chapter we will refer subsequently to each of these configurations as FT1, FT2, and FT3. The flow train referred to as FT1 consisted of the coal combustor using a preheated oxidant, with the combustion gas exhausting through a sonic nozzle into an MHD generator through an exhaust duct to the atmosphere. Within this experimental configuration, primary diagnostic techniques consisted of gas sampling downstream of the diffuser (on the order of 1 ms from combustor discharge), generator power production, heat loss measurements from the combustor and flow train and combustion chamber pressure. Analyses were also made of slag deposits within the flow train.

In the flow train referred to as FT2 the experimental setup consisted of an oxidant preheater, with the coal-fired combustor discharging through a sonic nozzle into a conductivity channel and then into the exhaust. For the purposes of this work, the primary measurement techniques were combustion gas sampling just downstream of the conductivity channel (on the order of 1 ms from combustor discharge), heat loss measurements within the combustor and flow train,

combustion chamber pressure and slag analysis.

The configuration referred to as FT3 consisted of the coal combustor with an expanded volume in conjunction with an oxidant preheater. The discharge gases of the combustor passed through a nozzle into a conductivity channel and through a throttling valve used to vary combustor pressure. Beyond the throttling valve the combustion products flowed through the balance of the downstream components. In the FT3 configuration the primary experimental data were obtained using a sampling probe downstream of the coal injector, heat transfer measurements in the flow train and combustor, the combustion chamber pressure, slag analysis and particle size measurements. In all three cases the input flows were monitored as well as the other facility parameters that are required to operate each flow train.

In Figure 4-5, (Page 99), three fundamental oxidizer injection schemes are described. To facilitate discussion of the experimental data, the configuration depicted in 13a will be referred to as the NR (no recirculation) oxidizer injection scheme. In this configuration the basic flow pattern is one without recirculation. The oxidizer is injected into the combustion chamber with velocities on the order of 30 ft/second. The oxidizer injection scheme depicted in 13b will be referred to as the MR (moderate recirculation) configuration. This configuration allowed for the increase of the coaxial oxidizer velocity and created recirculation zones within the coal combustor. In this configuration the

oxidizer velocity was on the order of 75-150 ft/second. The injection scheme depicted in Figure 13c will be referred to as the SR (strong recirculation) configuration. The basic feature of this injection method was that high velocity parallel jets of oxidizer entered the combustion chamber through orifices producing a region of strong recirculation over the first few inches of the coal combustor. In this configuration the oxidizer velocities were on the order of 800 feet/second.

In summary, the experimental flow train configurations will be referred to as FT1, FT2, and FT3 and will be as presented in Chapter 4. The oxidizer injection schemes will be referred to as NR, MR, and SR.

The three oxidizer injection schemes generated significantly different recirculating patterns within the coal combustor. Variable combustor volumes were used with the different injection schemes at constant combustor pressure to investigate the effects of residence time on the combustion of pulverized coal. In addition, in configuration FT3 the effects of residence time were studied by increasing the combustion pressure by throttling the discharge flow.

Coal particle heating rates for these tests were on the order of 10^5 degrees K per second while final combustor temperatures were in excess of 2800° K. No provisions were made in these tests for measurement of the combustor temperature; however, from generator performance and electrical conductivity measurements, it is well known that for combustion

conditions such as those described here the final temperatures will be near 3000°K.

The data summarized in Table 5-1 are presented in three major groups defined by the oxidizer injection scheme, i.e., NR, MR, and SR. The primary data were obtained from heat transfer measurements and combustion gas sampling with particle size measurement and slag analysis as secondary techniques. These data will be discussed for each fundamental configuration.

Experimental Heat Transfer Measurements, Coaxial Oxidant Injection

Heat transfer measurements made at the various axial locations of the combustor were indicative of the gas temperature at a given section. In deducing the progress of combustion within the chamber, variations in heat flux can be used to evaluate its progression. The heat flux was determined by evaluating the heat absorbed by the cooling water circulating through the cooling tubes at a particular location within the combustor. Under the harsh environment of the MHD coal combustor, conventional diagnostic techniques are not applicable. The indirect measurement of average heat flux distribution offers a simple means of monitoring the rate of heat release in the combustion process.

Figures 5-1 through 5-3 are representative heat flux distributions obtained for the first four cases listed in Table 5-1. Figure 5-1 and 5-2 are heat flux distributions obtained for combustion residence times of 24 and 21 milli-

TABLE 5-1

TEST SUMMARY

Test No.	Exp. Conf.	O_x Inj.	Tot Mass Flow	Thermal Input	Comb. Press	Stoic Ratio	Coal Flow	O_2 Flow	N_2 Flow	Fuel Oil	Seed Flow	N_2/O_2 Ratio	O_x Inlet Temp.	$\%O_2$ Oxidant	Oxidant Inj. Vel.	Comb. Vol.	Plug Flow Res. Time	Exp. Carbon Conversion	Cal. Carbon Conversion	Generator Power Output
-	-	-	$\frac{lbm}{sec}$	MW	PSIA	ϕ	$\frac{lbm}{sec}$	$\frac{lbm}{sec}$	$\frac{lbm}{sec}$	$\frac{lbm}{sec}$	$\frac{lbm}{sec}$	-	°K	%	$\frac{Ft}{Sec}$	IN^3	$\frac{10^{-3}}{Sec}$	%	%	KW
36-13	FT1	NR	4.06	16.0	75	0.86	1.1	2.29	0.46	0.095	0.11	0.200	1560	67.3	30	3172	21	92	-	23
36-20	FT1	NR	3.71	13.8	73	0.95	0.93	2.22	0.37	0.093	0.10	0.167	1600	69.3	28	5019	37	98	-	28
36-21	FT1	NR	3.49	13.4	71	0.96	0.9	2.12	0.37	0.093	0.10	0.175	1650	68.1	27	5019	39	98	-	25
31-10	FT2	NR	3.60	13.5	75	0.96	0.9	2.1	0.4	0.10	0.10	0.190	1740	66.0	28	3172	24	93	-	-
36-16	FT1	MR	3.79	14.5	76	0.92	0.97	2.22	0.39	0.103	0.11	0.176	1725	67.2	77	2778	16	84	-	25
36-18	FT1	MR	3.83	14.1	73	0.96	0.93	2.26	0.43	0.11	0.10	0.190	1770	65.6	138	2778	16	86	-	26
36-19	FT1	MR	3.68	13.7	72	0.96	0.93	2.20	0.353	0.092	0.10	0.160	1610	69.7	130	4625	30	97	-	27
3902	FT1	SR	3.41	12.2	72	0.93	0.81	1.98	0.444	0.090	0.09	0.222	1650	64.8	1230	3172	25(17)	100	(100)	40
4302	FT3	SR	1.84	7.3	66	0.82	0.49	0.99	0.31	0.05	0.06	0.313	1685	59.3	661	1540*	13.3	93	90	-
4302	FT3	SR	1.84	7.3	52	0.82	0.49	0.99	0.31	0.05	0.06	0.313	1685	59.3	661	1540*	10.5	87	86	-
4303	FT3	SR	1.93	7.4	40	0.74	0.505	0.92	0.4	0.047	0.055	0.435	1587	53.0	670	1540*	8	83	80	-
4304	FT3	SR	2.08	7.3	73	0.95	0.51	1.12	0.41	0.04	0.051	0.366	1267	60.0	769	1540*	13	94	92	-
4304	FT3	SR	2.025	6.75	42	0.98	0.449	1.062	0.417	0.047	0.05	0.393	1450	57.0	747	1540*	8	82	84	-
4304	FT3	SR	1.959	9.2	46	1.07	0.410	1.046	0.424	0.046	0.033	0.405	1452	56.0	743	1540*	9	88	86	-
4304	FT3	SR	2.008	6.8	56	0.99	0.497	1.048	0.419	0.044	0.05	0.400	1397	57.0	740	1540*	15	98	96	-
4304	FT3	SR	1.828	5.2	75	1.20	0.346	0.984	0.418	0.040	0.04	0.425	1354	56.0	706	1540*	16	99	100	-
4305	FT3	SR	2.122	7.6	44	0.88	0.519	1.088	0.410	0.048	0.057	0.377	1469	57.0	757	1540*	8	84	82	-
4305	FT3	SR	2.125	7.5	53	0.89	0.516	1.084	0.421	0.046	0.058	0.388	1418	57.0	760	1540*	9.6	87	85	-
4305	FT3	SR	2.147	7.7	48	0.87	0.527	1.096	0.418	0.047	0.059	0.381	1435	58.0	765	1540*	8.6	88	84	-
4305	FT3	SR	2.113	7.4	57	0.91	0.506	1.086	0.420	0.045	0.056	0.387	1395	58.0	760	1540*	10.4	89	87	-
4305	FT3	SR	2.071	7.0	65	0.97	0.475	1.085	0.416	0.043	0.052	0.383	1352	58.0	756	1540*	12.1	94	92	-

*Volume of Combustor to Gas Sampling Point

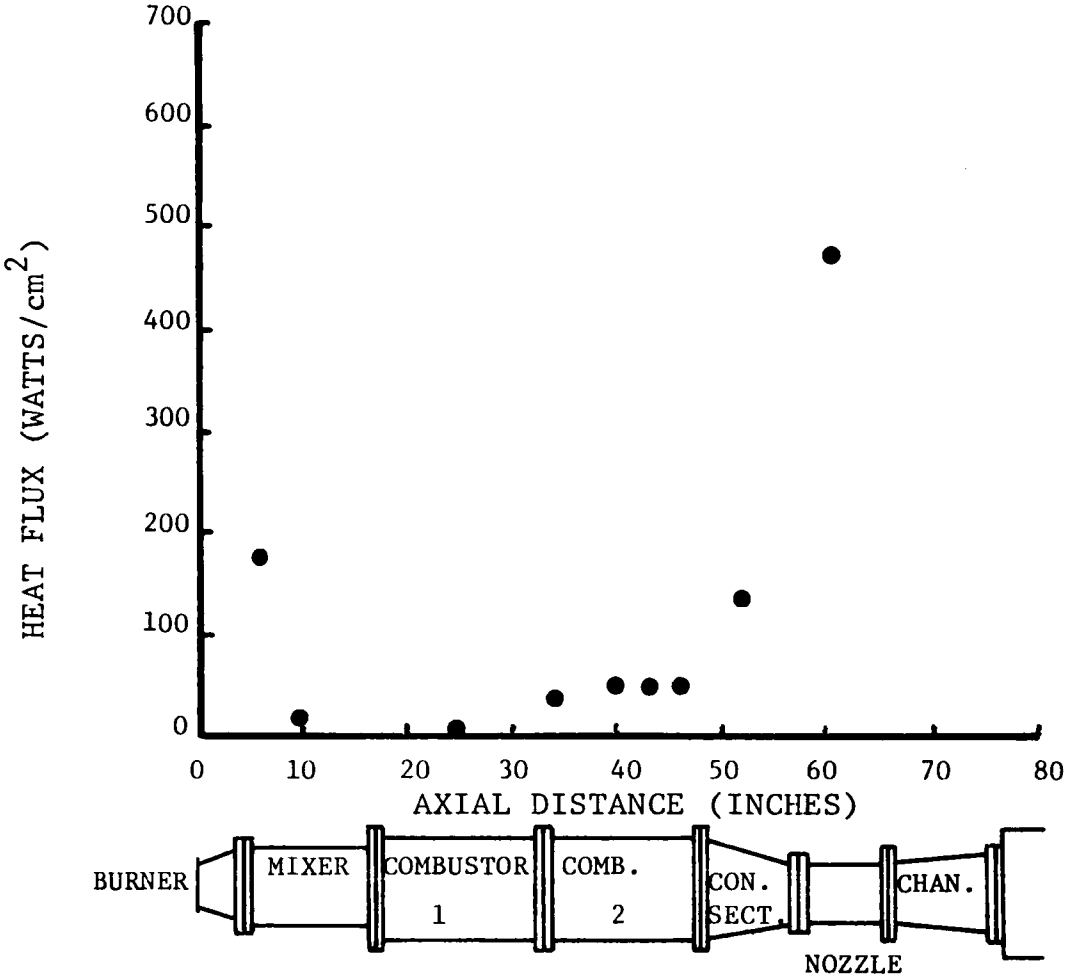

Figure 5-1. Heat Flux Distribution Through Nozzle

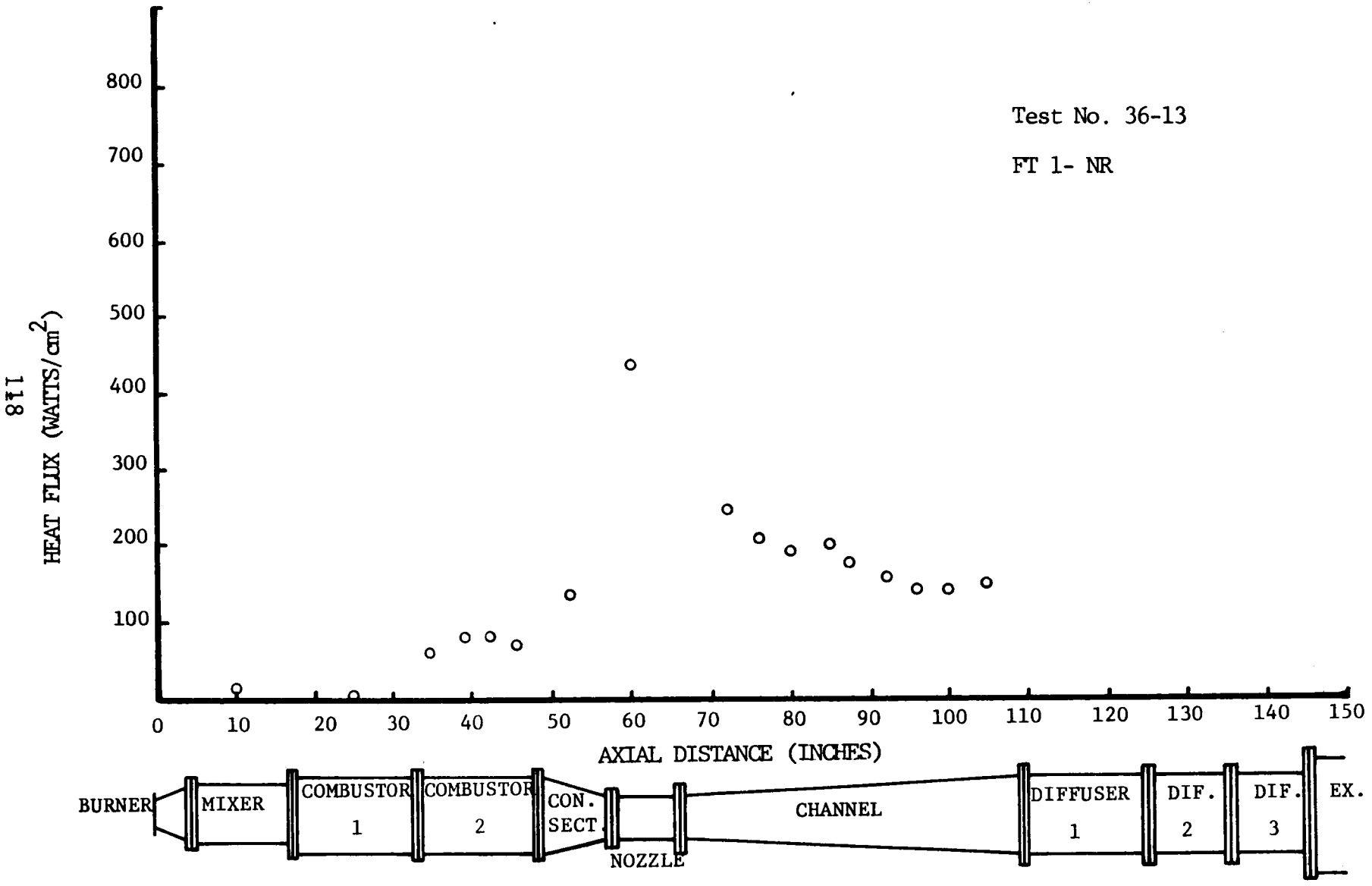

Figure 5-2. Heat Flux Distribution Through Diffuser

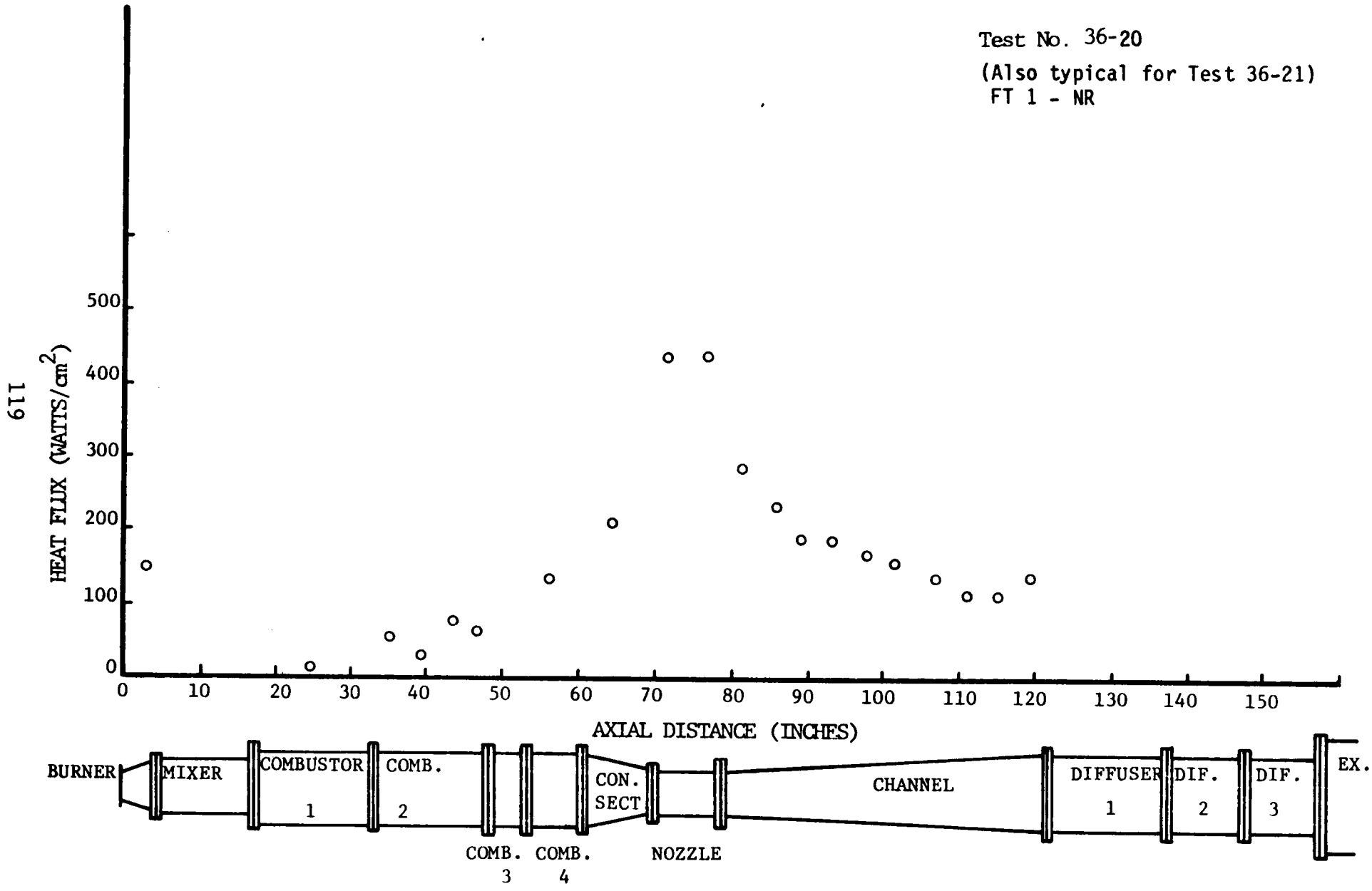

Figure 5-3. Heat Flux Distribution, Test No. 36-20.

seconds respectively. For both of these cases there is no significant difference in the heat flux distributions. Figure 5-3 is a heat flux distribution obtained for a combustor residence time of 39 milliseconds. Comparing these data to that in Figure 5-1 the increased heat release with the added combustion residence time is indicated by the increase in the heat flux near the discharge end of the combustion chamber. In the case of combustion residence times of 21 and 24 milliseconds, the carbon conversion efficiency was 92 and 93% respectively. The carbon conversion efficiency was 98% for combustion residence times of 37 and 39 milliseconds. The effect of the increase of combustion residence time is to increase the carbon conversion. In the NR oxidizer injection scheme the mixing zone is quite long and consequently a long time must be given for the oxidant to mix with coal and to lead to the subsequent heat release.

Figures 5-4, 5-5 and 5-6 are representative heat flux distributions for the MR oxidizer injection scheme with various combustion residence times. Figures 5-4 and 5-5 are the heat flux distributions for a combustion residence time of 16 milliseconds with different oxidant velocities. In these cases the heat fluxes within the coal combustion chamber remained very low with low carbon conversion efficiencies. Figure 5-6 is a heat flux distribution for a combustion residence time of 30 milliseconds. The heat fluxes for this configuration show an increase in the portion of the combustor that was added to increase residence time.

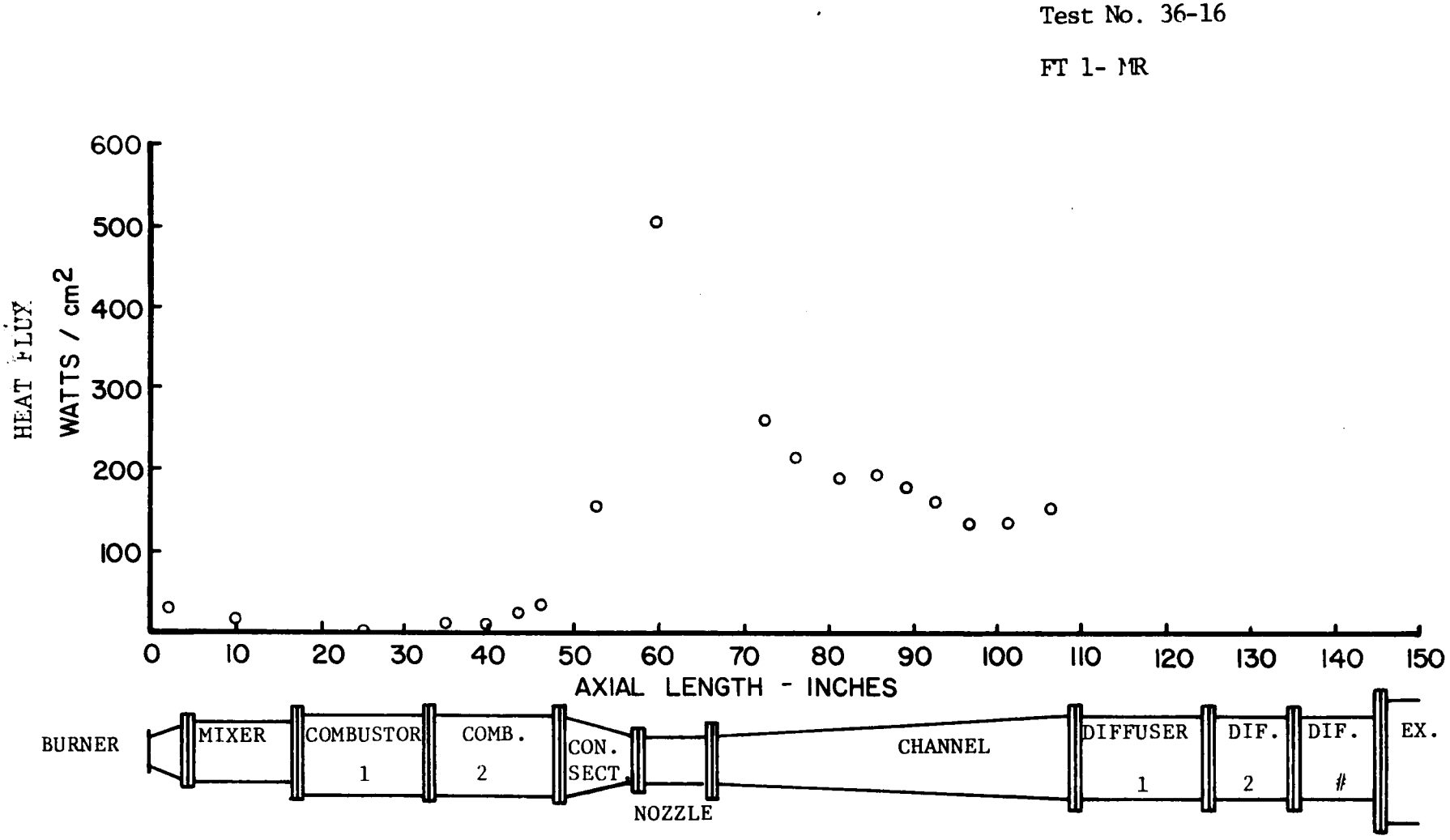

Figure 5-4. Heat Flux Distribution, Test No. 36-16.

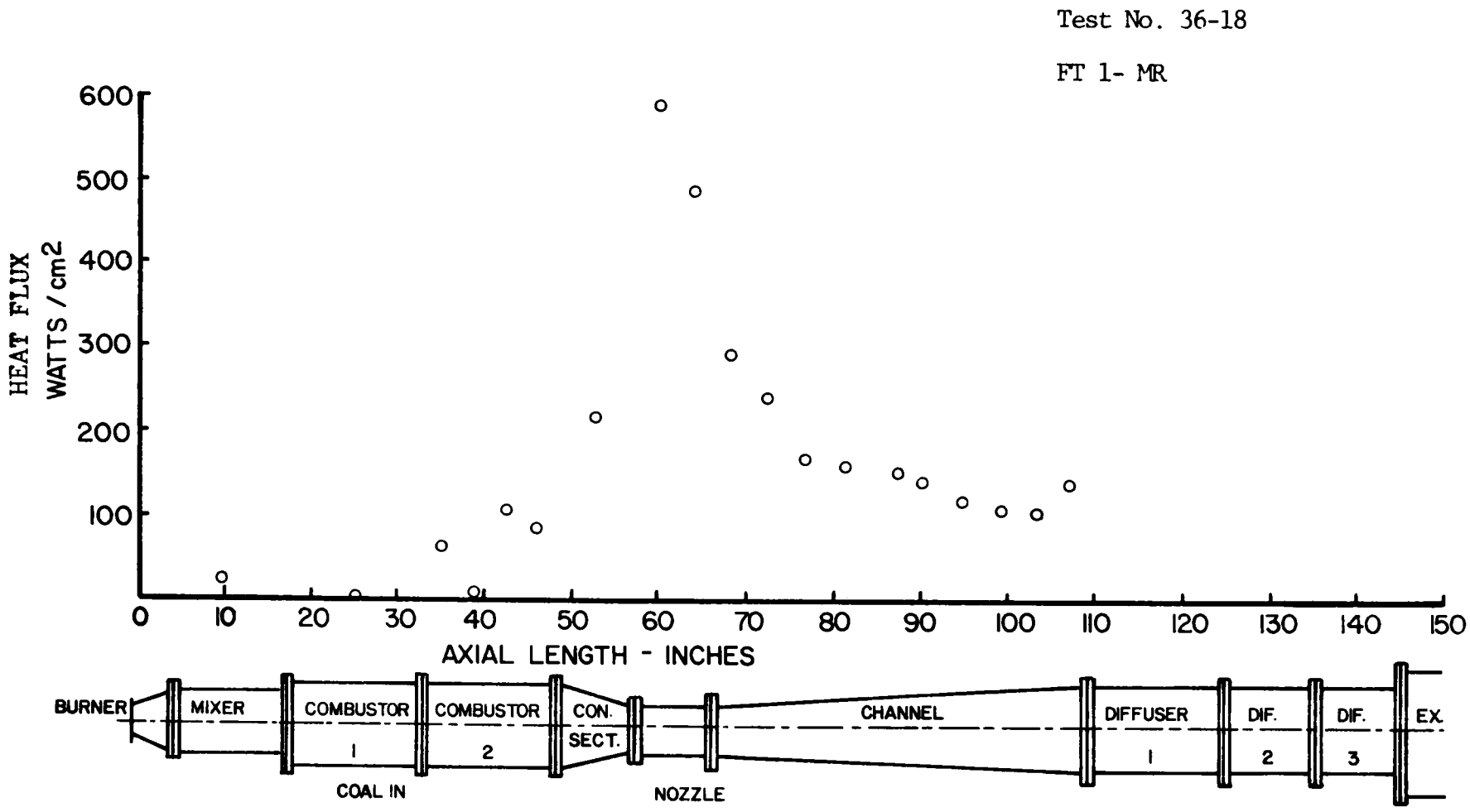

Figure 5-5. Heat Flux Distribution, Test No. 36-18.

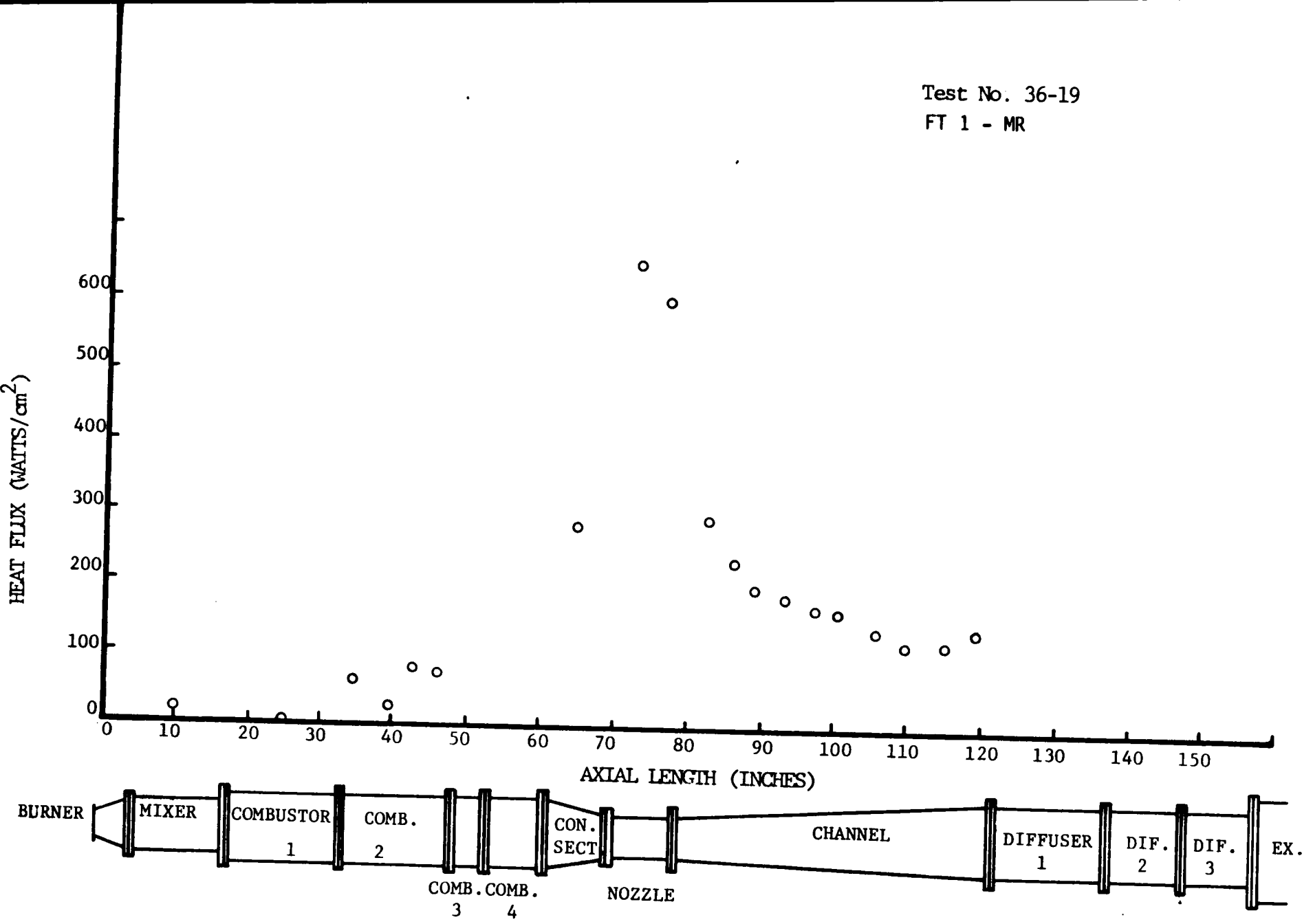

Figure 5-6. Heat Flux Distribution, Test No. 36-19.

In this particular scheme the carbon conversion was 84 and 86% for a residence time of 16 milliseconds and was 97% for a residence time of 30 milliseconds. A significant result on comparing this data to that collected with the NR configuration is that for the same carbon conversion efficiencies the residence time has been decreased by approximately 9 milliseconds by increasing the injection velocity of the oxidizer. This points out the importance of mixing on the pulverized coal combustion process. It is important to reiterate the strong dependence of the MHD process on temperature (nearly exponential); therefore a minimum volume combustor must be developed for MHD application.

Carbon Conversion for Coaxial Oxidant Injection

Stickler [43] has conducted experiments at the AVCO Everett Research Laboratory with a coal combustor very similar to the NR and MR configurations used here. The coal combustor at AVCO features a coaxial injection of preheated oxidizer (1700°K) with an oxygen concentration of approximately 40%. Injection velocities of 32 to 147 ft per second were typical of his experiments. These values are near the range of those that were used in this work for the coaxial oxidant injection schemes. The coal used by Stickler in these experiments was a Pittsburgh Seam HVA bituminous that is very similar to Illinois #6. In Figure 5-7 carbon utilization as a function of residence time is shown. The present results as superimposed upon those presented by Stickler

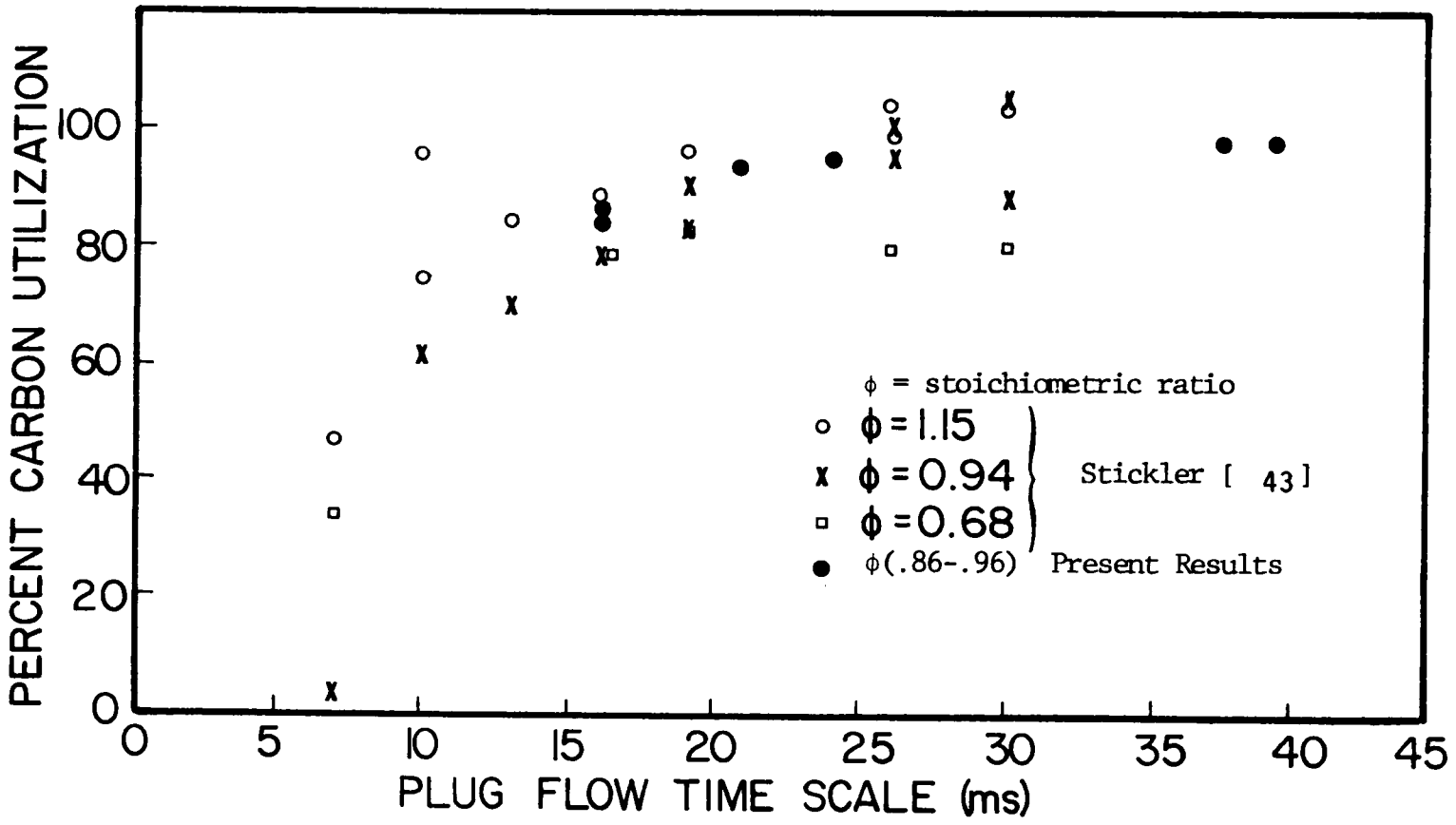

Figure 5-7. Carbon utilization dependance on plug flow residence time.

show very good agreement between the two sets of experimental data. Stickler's results along with the present results indicate that for coaxial oxidant injection, high carbon utilization can only be achieved by having long residence times. He pointed out that the type of behavior exhibited in Figures 5-7 would not be characteristic of all coals. Stickler's study included lignites which showed similar behavior; however, at residence times less than 20 milliseconds the carbon utilization was normally less than 50%.

Experimental Heat Transfer, Multiport Oxidant Injection

Figure 5-8 is a typical heat flux distribution obtained for the SR oxidizer injection scheme. This heat flux distribution shows a very rapid heat release near the coal combustor exit. These high heat release rates are due to the rapid mixing that occurred due to the "flame holder" action of the oxidizer injection plate. Figure 5-9 presents a comparison of heat flux distributions for the two fundamental schemes discussed i.e., the coaxial injection scheme (NR, MR) and the multiport injection scheme (SR). In the case of the multiport oxidizer injection the heat release rate is almost one and one-half as great. The results show that heat release rate is strongly dependent on the rate of mixing between the coal particles and the oxidant.

Experimental Carbon Conversion Summary

Figure 5-10 is a summary of carbon conversion as a func-

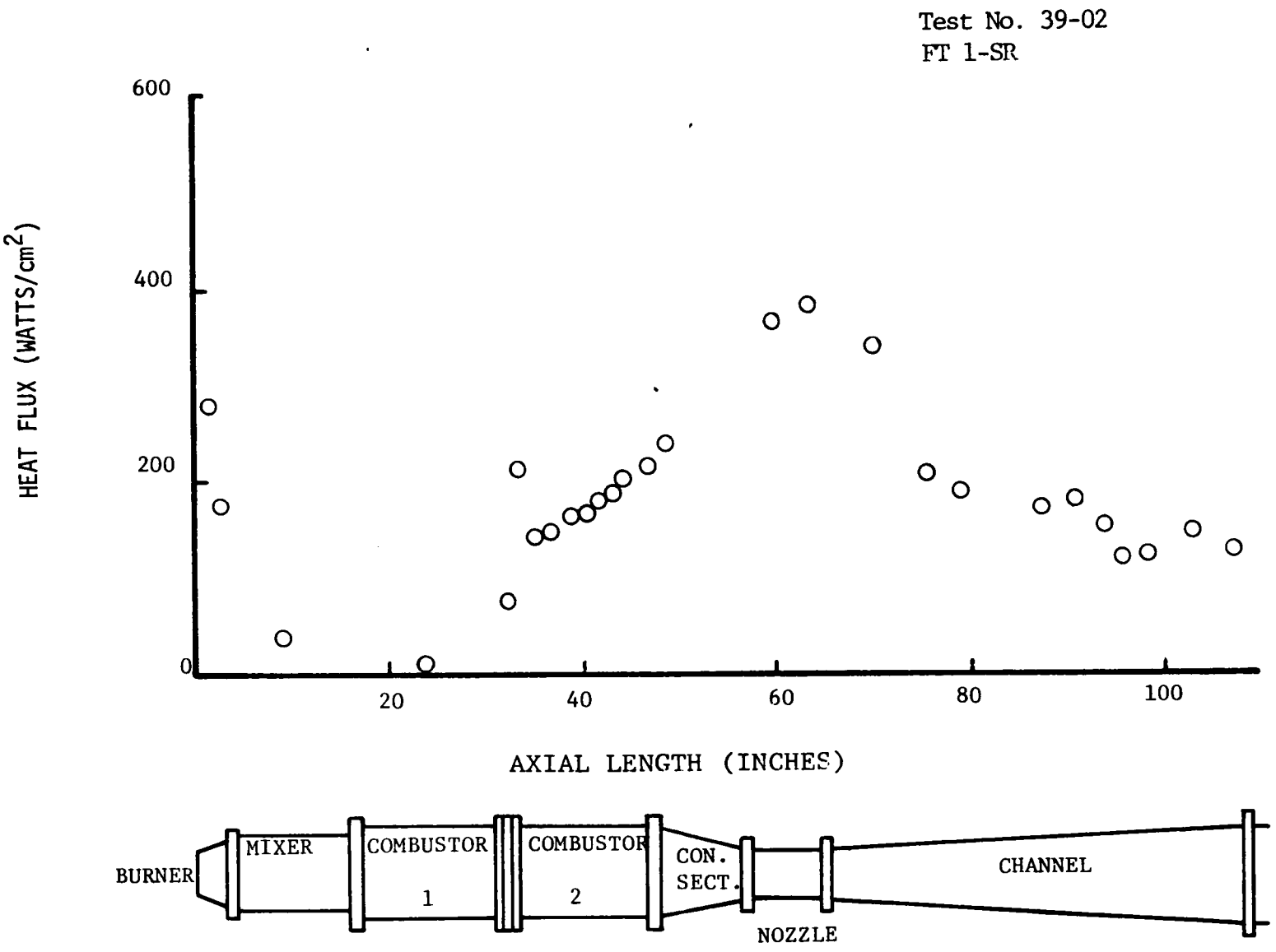

Figure 5-8. Heat Flux Distribution, Test No. 39-02.

Configuration No.	Condition
1	Ambient Temperature pure oxygen
2, 2a	Preheated oxidant, coaxial and multiport injection
3	Preheated oxidant, coaxial with increased combustor volume.

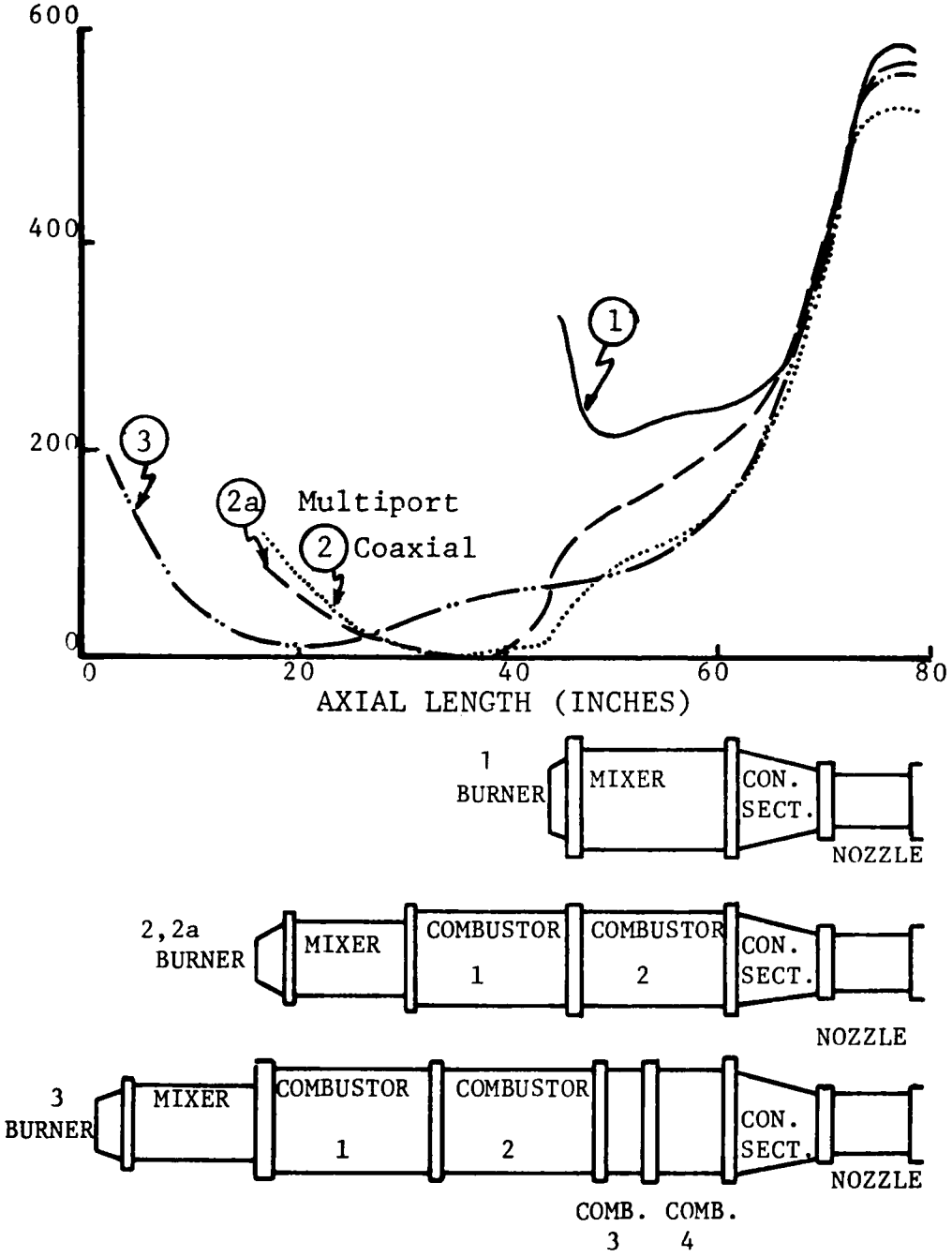

Figure 5-9. Composite Heat Flux Distribution

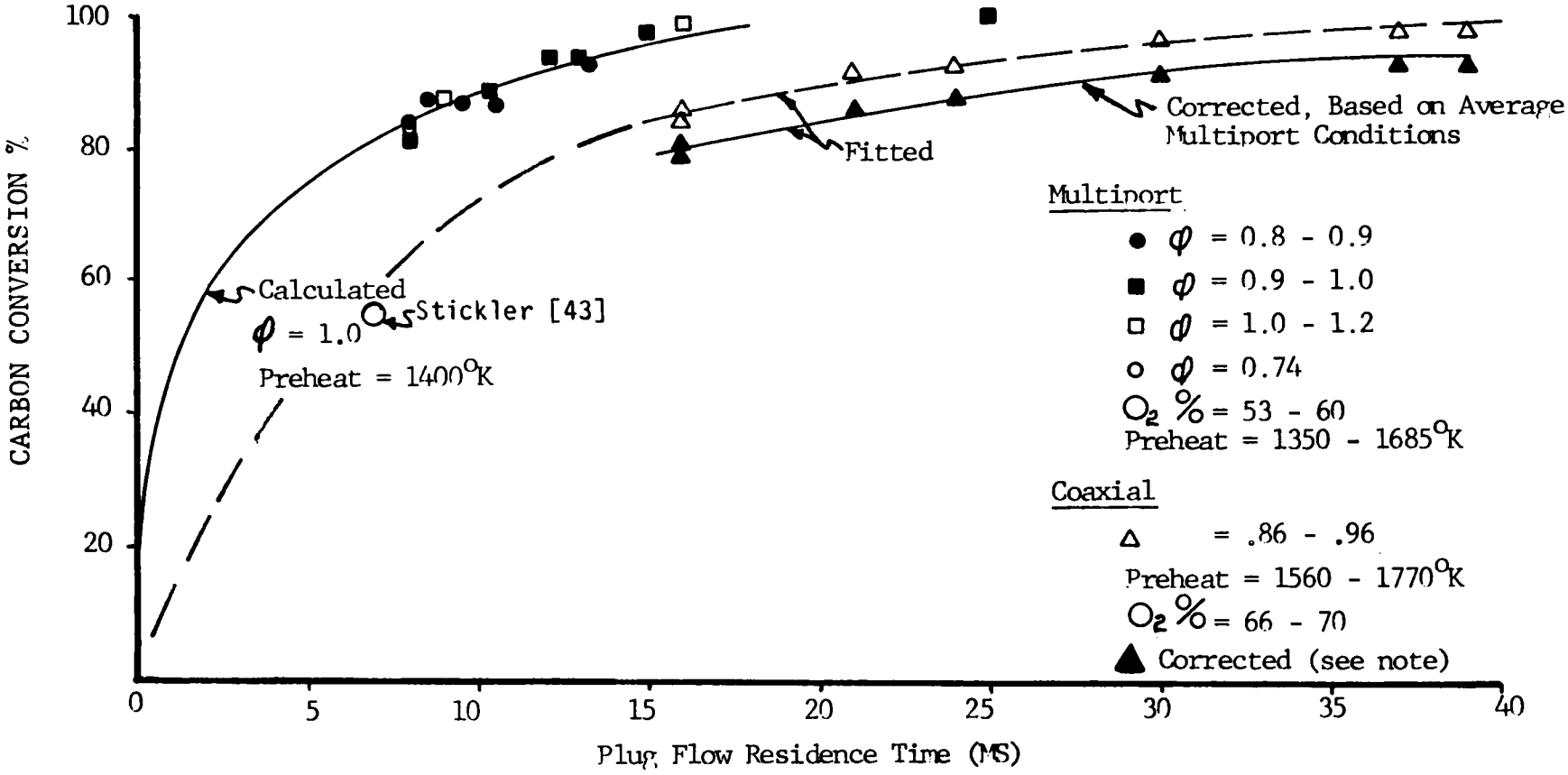

Figure 5-10. Carbon Conversion as a Function of Residence Time

tion of residence time for the cases studied. Two significant results can be concluded by examining the data:

1) For a given residence time the total carbon conversion is significantly increased with increase in mixing.

2) The rate of carbon conversion is increased dramatically with increase in mixing.

The calculated carbon conversion is also shown in Figure 5-10. The calculation agrees very well with the multiport oxidizer injection case (which will be discussed later). This might be expected since the theoretical model assumed perfect mixing. The agreement between predicted and the experimental values for the SR case also indicates the good mixing obtained in this injection scheme. Proceeding in time, the slope of the calculated carbon conversion versus time decreases. This is explained by noting that as devolatilization proceeds, the "bound" carbon consists of molecules with higher activation energies and thus the rate of conversion decreases in time. As the slope becomes nearly linear (range over which these experiments were conducted) the difference in carbon conversion rate can be examined. In both cases the near linear behavior occurs above 80% carbon conversion. It must be kept in mind that the experimental conditions were not identical and a comparison of pertinent average conditions is as follows:

Parameter	Multiport	Coaxial
Stoichiometry	0.93	0.95
Preheat	1470°K	1665°K
% O_2 in oxidizer	57.9%	67.6%

As shown, the coaxial case had higher average oxidant preheat and oxygen concentration with a slightly higher average stoichiometric ratio. The effect of all three parameters is to increase the rate of carbon conversion.

A quantitative comparison of the carbon conversion is difficult due to the differences in test conditions. However, a comparison can be made if the effects of preheat, O_2 concentration and stoichiometric ratio are examined parametrically. Based on a parametric evaluation, the values for the coaxial case were adjusted to the average conditions of the multiport case as shown also on Figure 5-10. Comparing the carbon conversion at the "same" conditions, it is shown that the increase in mixing increased the carbon conversion by approximately 22.5% at 16 ms. If the slopes are taken to be linear for carbon conversions in excess of 80%, then the carbon conversion rate of the multiport case is found to increase by a factor of 2.43 over the coaxial case.

Qualitatively the effect of increase in mixing is to increase the oxygen concentration at the coal particle surface thereby increasing the diffusion of oxygen. With the increase in diffusion the volatile release rate is increased.

The experimental results indicate that for the conditions of these experiments, the rate of carbon conversion is mixing rather than kinetically dependent.

This conclusion is supported by both heat transfer and gas analysis. The implication is that there is a strong relationship between rate of mixing and rate of carbon conversion. The coupling of mixing through diffusion, which depends on the concentration of oxygen at the particle surface, affects the rate of carbon conversion. At present there does not exist a model to calculate numerically the flow field and mixing rates for the multiport injection configuration. However the experimental results indicate the rate dependent effect of mixing and thus emphasize the importance of combustor aerodynamics on the combustion of pulverized coal.

Comparison of Theoretical and Experimental Results

The experimental data were compared to calculated carbon conversion efficiencies and heat loss using the combustion model described in Chapter 3. The combustion model used is one-dimensional; therefore, no two-dimensional effects such as mixing are considered. Within this context it was impossible for the theoretical model to distinguish the behavior of the NR and MR oxidizer injection coal combustors. However, the comparison between the theoretical values and the calculated values in the case of the SR oxidizer injection scheme is good. Typical results for this comparison are shown in Figures 5-11 through 5-14. Figure 5-11 is a comparison of experimentally determined heat loss for the SR oxidizer injection combustor with heat loss

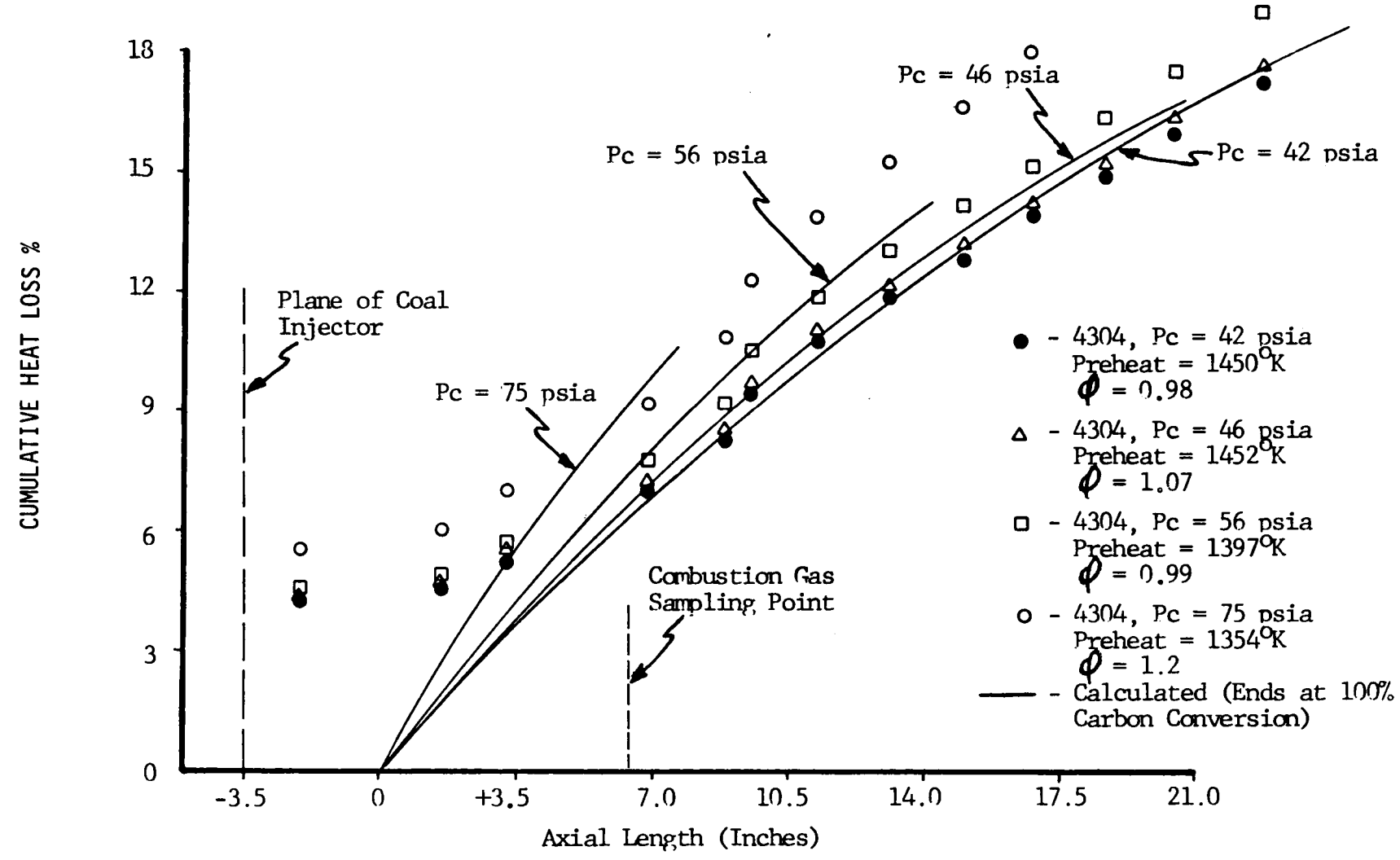

Figure 5-11. Cumulative Heat Loss

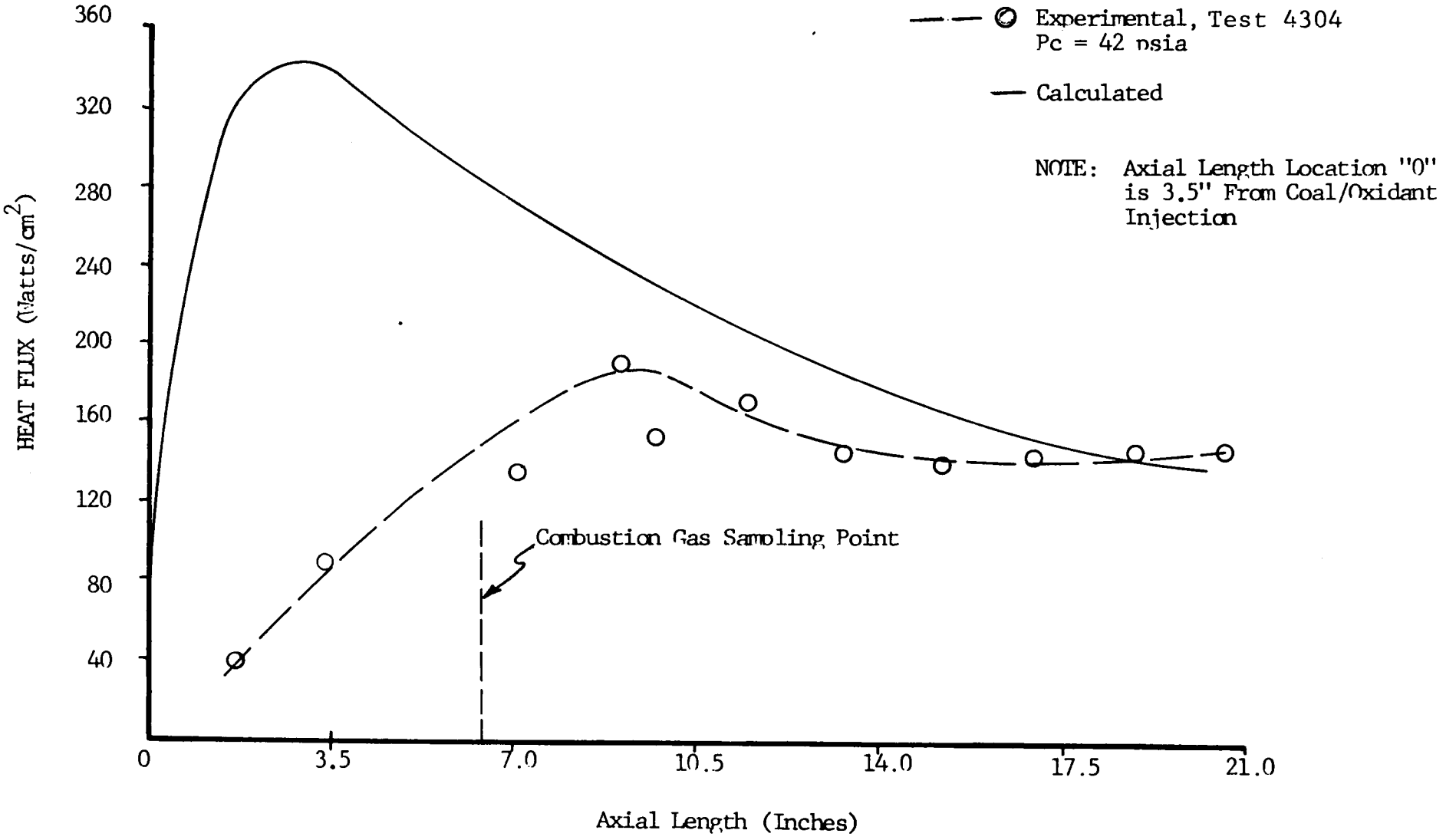

Figure 5-12. Comparison of Experimental And Calculated Heat Flux Distribution

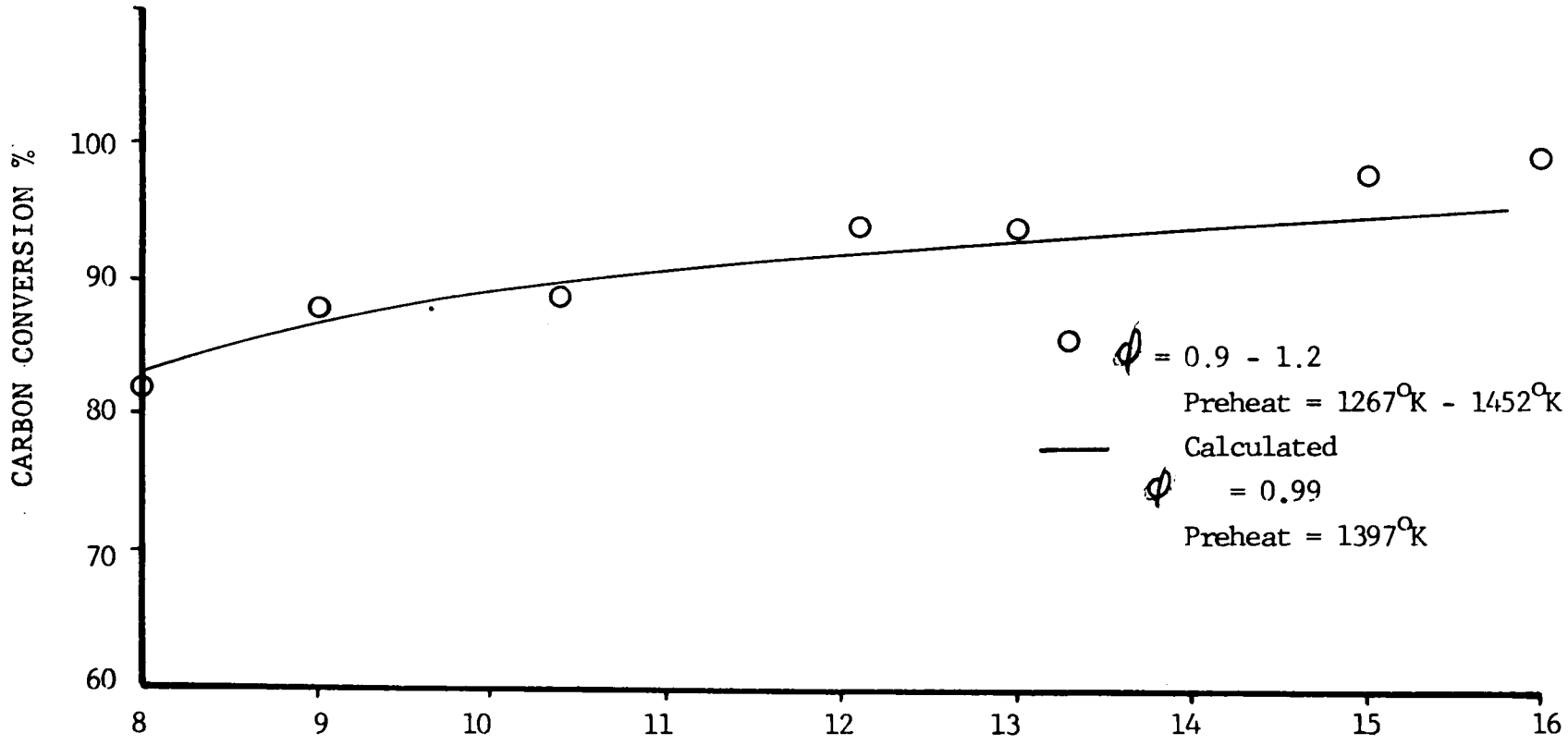

Figure 5-13. Comparison of Theoretical and Experimental Carbon Conversion

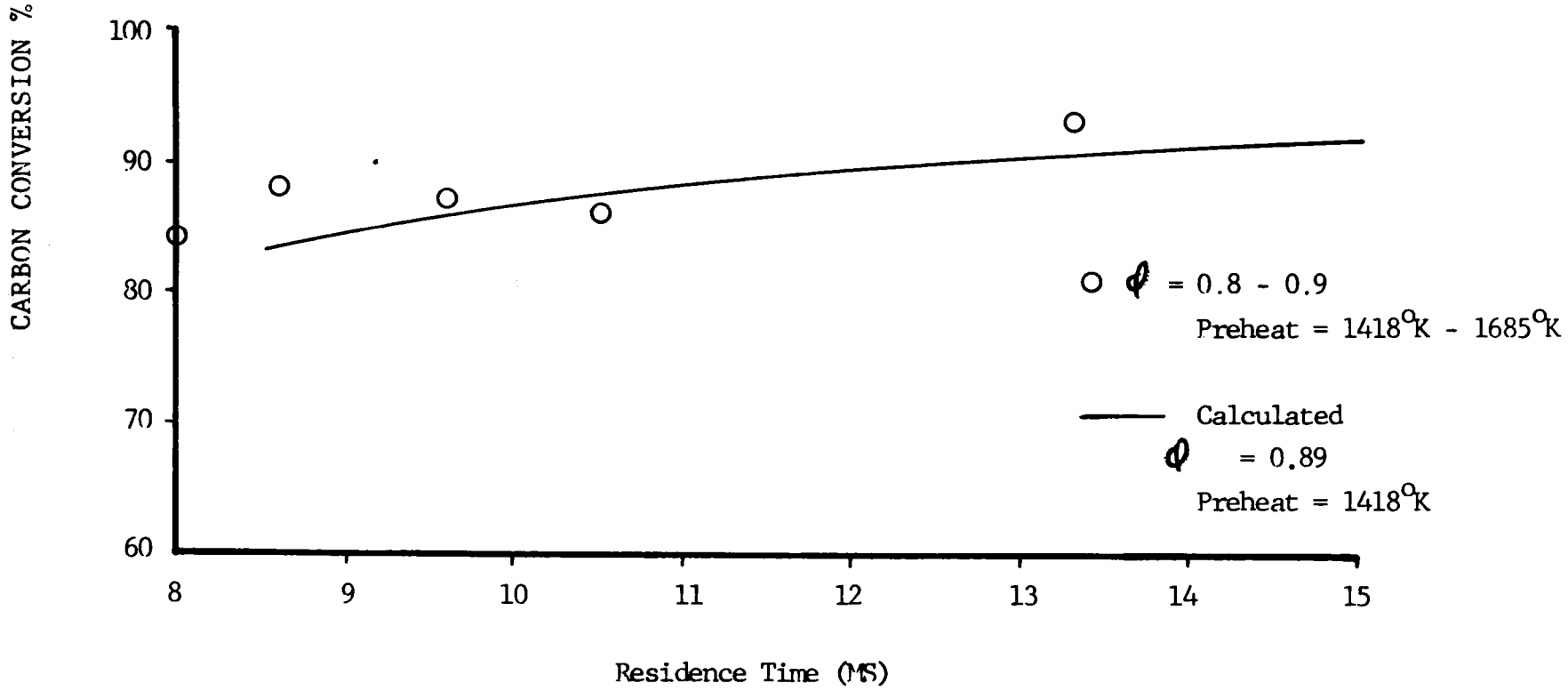

Figure 5-14. Comparison of Theoretical and Experimental Carbon Conversion, Fuel-Rich.

calculated from the theoretical model. The characteristic shape of the calculated heat loss is very near to that measured for the coal combustor. Figure 5-11 shows the heat loss measurements for four combustor conditions. The comparison between the calculated values and the experimental values is good in all four cases provided that the calculated values are shifted three and one-half inches from the coal/oxidant injection point. Recalling that the model assumes complete mixing it becomes necessary to adjust the calculated values by a "pseudo mixing length". Within the initial portion of the combustor, mixing as well as ignition must occur and the model assumes both to happen instantaneously. At the point 0 in Figure 5-11 the experimental heat loss has a value of four to six percent. This is the loss that occurs in the oxidant preheater and injection plate. The model cannot predict these losses and therefore a direct comparison of heat flux will not be valid.

The radiation model presented in Chapter 3 is very simplified in that it assumes the radiative heat sink is uniformly distributed in the radial direction. This is obviously not true in the real case. The calculated maximum heat flux is much higher than the measured heat flux and peaks much earlier as shown on Figure 5-12. The consequence of this comparison is that the calculated gas and particle temperature in the initial portion of the combustor is not correct. However, when the calculated heat flux approaches the measured value then the calculated temperatures will be near the actual temperature.

Figures 5-13 and 5-14 are comparisons between experimental and calculated carbon conversions for the SR oxidant injection cases. Excellent agreements are found for both near stoichiometric conditions (Fig. 5-3) and slightly fuel rich (Fig. 5-4).

In summary the model predicts quite accurately the cumulative heat loss and carbon conversion provided that an adjustment is made for the "pseudo mixing length". This agreement gives confidence in the calculation of global parameters such as gas temperature, particle temperature, velocity, gas composition, etc. provided that the coal/oxidant injection is such that rapid mixing occurs.

Parametric Study

Figures 5-15 through 5-19 are the results of a parametric study of the effects of stoichiometry, oxidant preheat, and oxidant composition on carbon conversion. The trends shown in Figure 5-15, 5-16, 5-17 and 5-18 compare favorably with experimental data that have been gathered by researchers [43] as to the general behavior of various types of coals. For increases in stoichiometry and preheat temperature, carbon conversion rate will increase. For a given residence time and oxidant mixture, the carbon conversion is not a strong function of preheat temperature. However, as shown in Figure 5-16 carbon conversion is strongly affected by the oxygen concentration in the preheated oxidant. Figure 5-17 shows the carbon conversion as function of residence time at

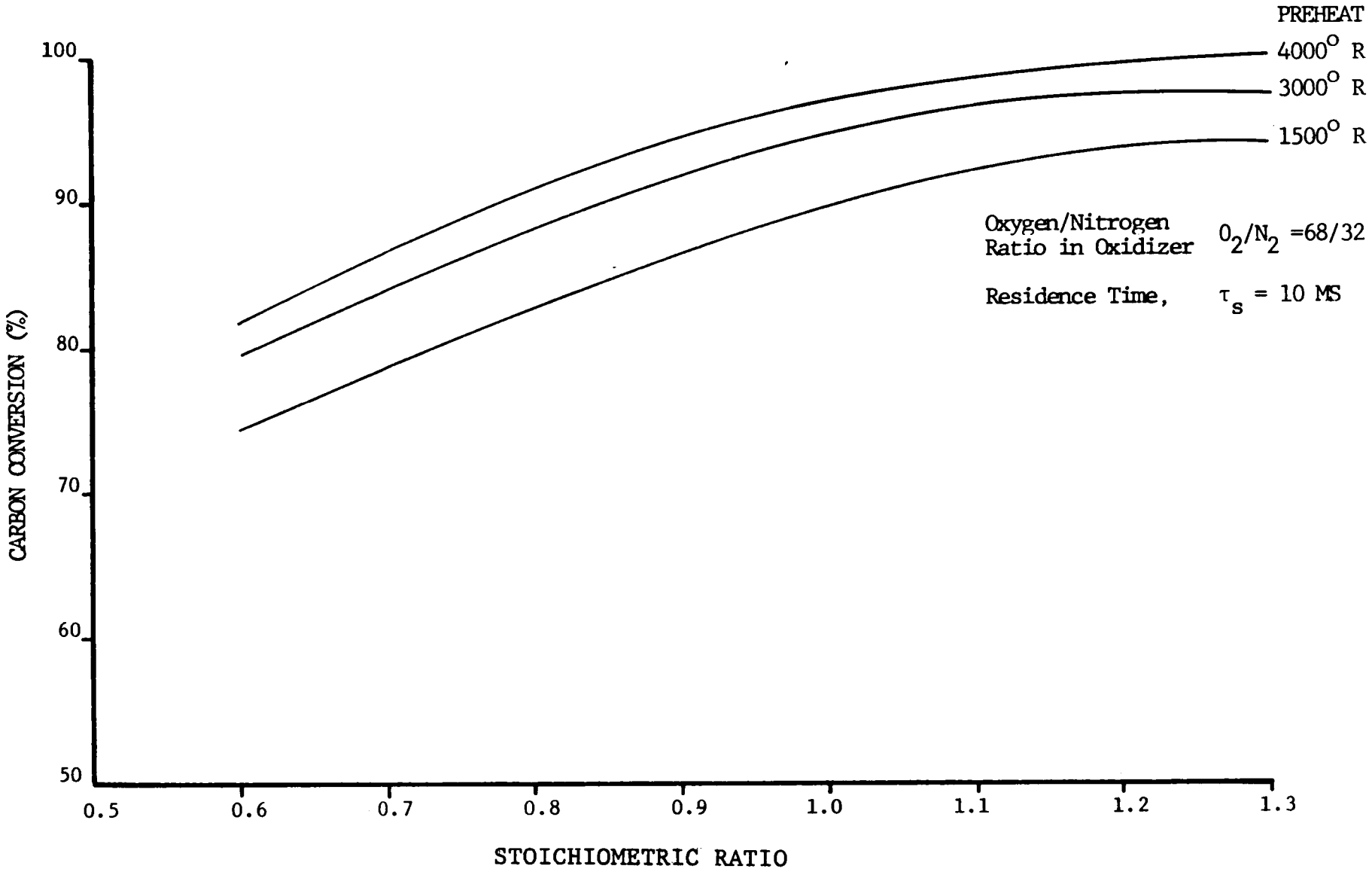

Figure 5-15. Carbon Conversion Dependence on Preheat and Stoichiometric Ratio

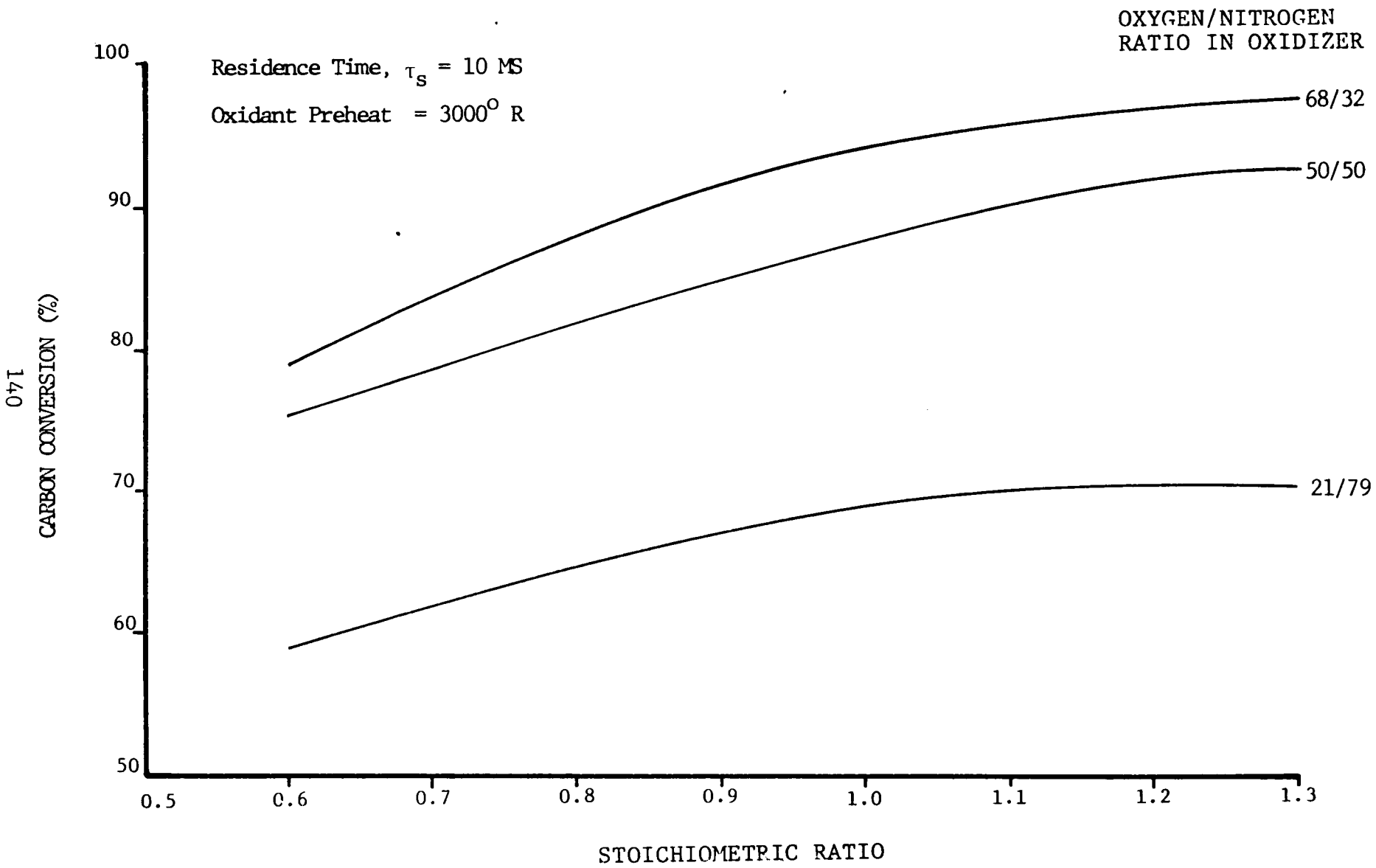

Figure 5-16. Carbon Conversion Dependence on Oxygen Concentration and Stoichiometric Ratio

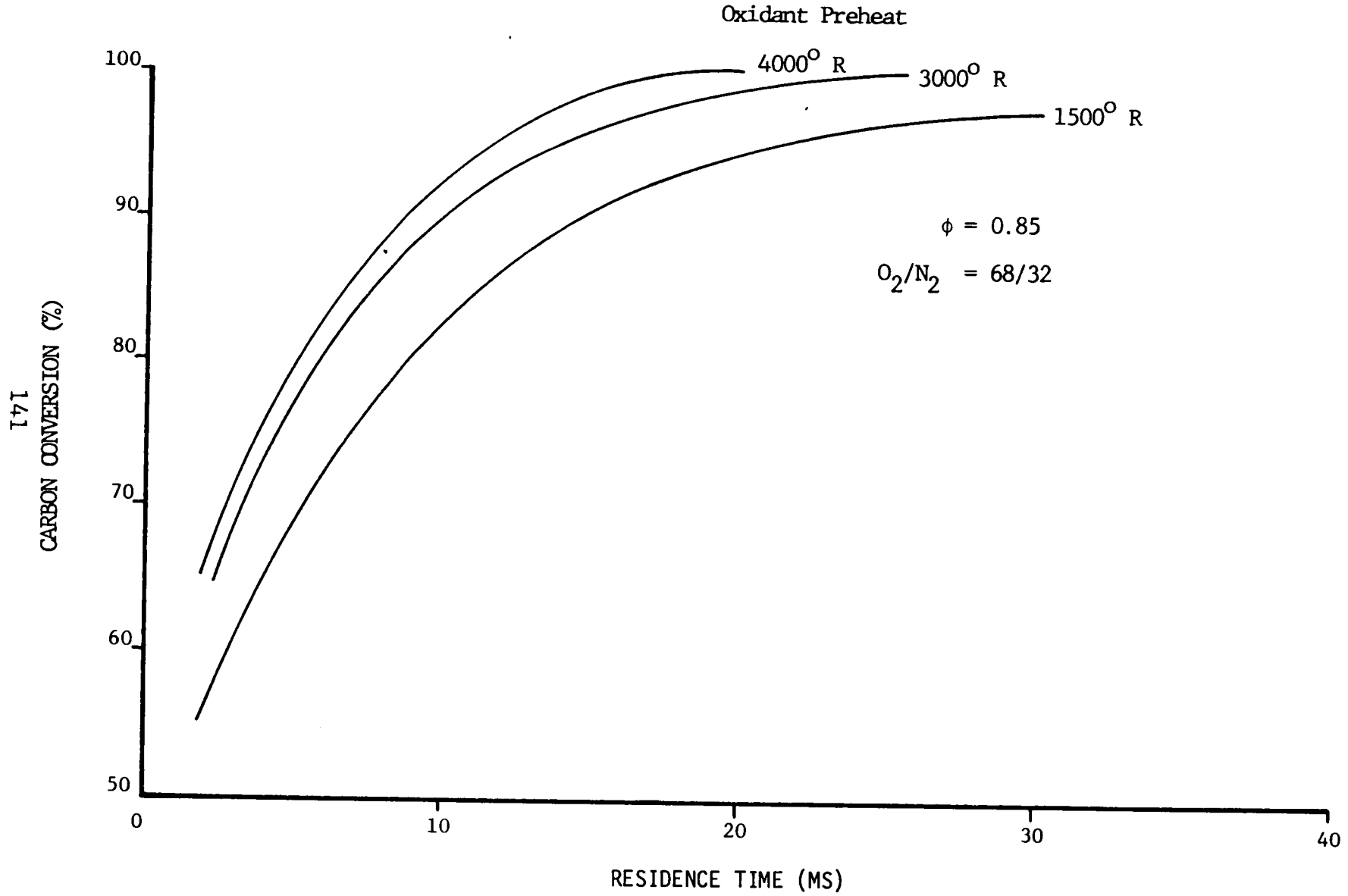

Figure 5-17. Carbon Conversion Dependance on Residence Time and Oxidant Preheat

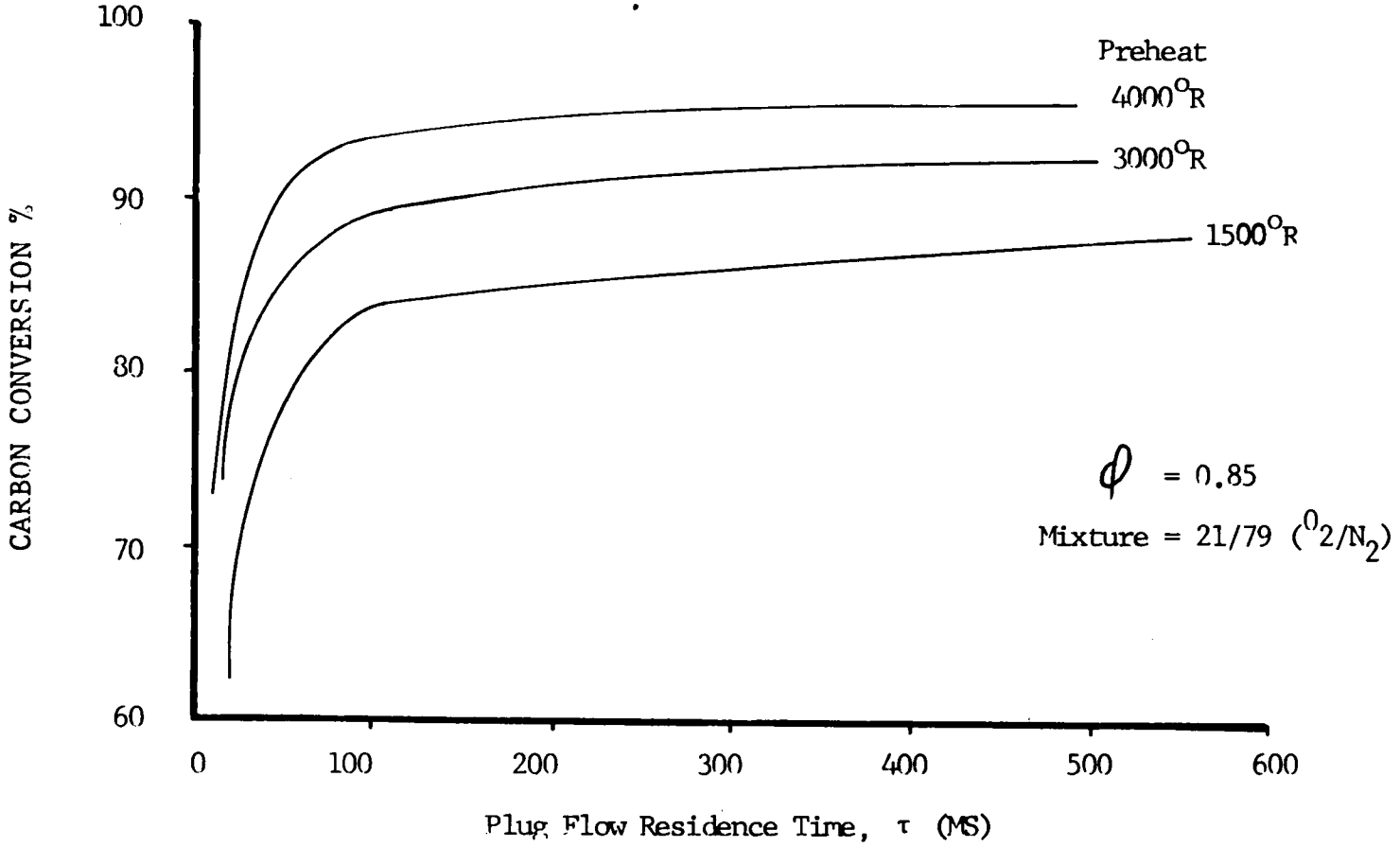

Figure 5-18. Carbon Conversion as a Function of Residence Time

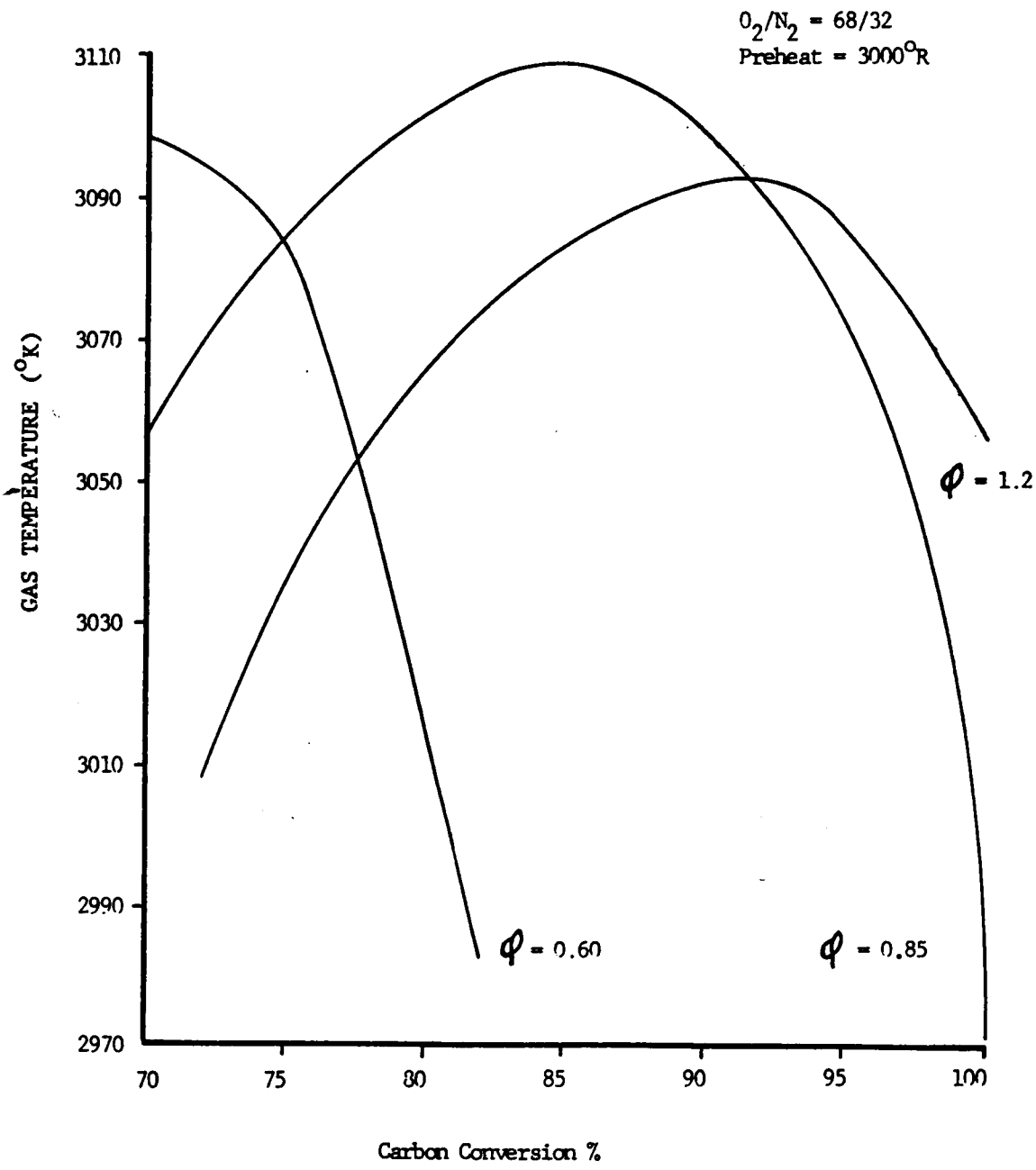

Figure 5-19. Gas temperature as a function of carbon conversion.

a given stoichiometry for various oxidant preheat temperatures. As the preheat temperature is increased the carbon conversion increases at the same residence time; however, the asymptotic behavior should be noted. Figure 5-18 shows carbon conversion as a function of residence time and preheat for a mixture ratio near air. The required residence times for total carbon conversion becomes much greater than 500 ms as would be expected.

Figure 5-19 shows the gas temperature as a function of carbon conversion efficiency and stoichiometry. The data presented are for an oxygen concentration of 68% and preheat temperature of 3000°R. These conditions are near those that are the subject of this experimental work. Figure 5-19 shows that the maximum gas temperature is attained before carbon burn-out. In the case of coal-fired MHD combustors the objective is to obtain a high gas temperature and carbon utilization becomes of secondary importance. Therefore, in the case of MHD combustors, optimum power generation should be sub-stoichiometric with a residence time such that the carbon conversion is at a level where maximum gas temperatures can be achieved. At the same time, heat loss must be minimized which leads to the utilization of a minimum volume combustor.

The experimental results indicate that for high carbon utilization the carbon conversion process is strongly dependent on the rate of mixing between the coal and oxidant. Experimental data for the cases in which mixing was not rapid showed that to achieve high carbon utilization, it was

necessary to increase the combustion residence time significantly. In the case of MHD combustors this is not a desirable feature because of the increase in heat loss with combustor volume.

Free Carbon

Particulate sampling was performed using the modified Brink's impactor as previously described. Particle size measurements [44] ranged from 0.2 microns to 2 microns and are shown in Figure 5-20. Analysis of the particles showed that K_2SO_4 was the dominant specie with some fly ash. Upon examination using the ASTM method [45], no carbon was found. Based on these experiments the conclusion was that no submicron carbon particles were present in the exhaust flow at the experimental conditions encountered here.

After each run the slag deposits within the combustor and flow train were sampled. Analyses were made for BTU and carbon percentage by the ASTM method. These tests show no carbon was present in the slag. These results were verified by the ASTM method with low loss on ignition (less than 1/2 percent) and the BTU value of the sample being zero. Ash deposits collected on the gas sample probe also were analyzed and no carbon was found in these slag deposits.

The results of the particle size measurements and slag analyses indicate that under the conditions for these experiments, no free carbon was present.

Particulate sampling and slag analysis are direct methods of determining the presence of free carbon but in

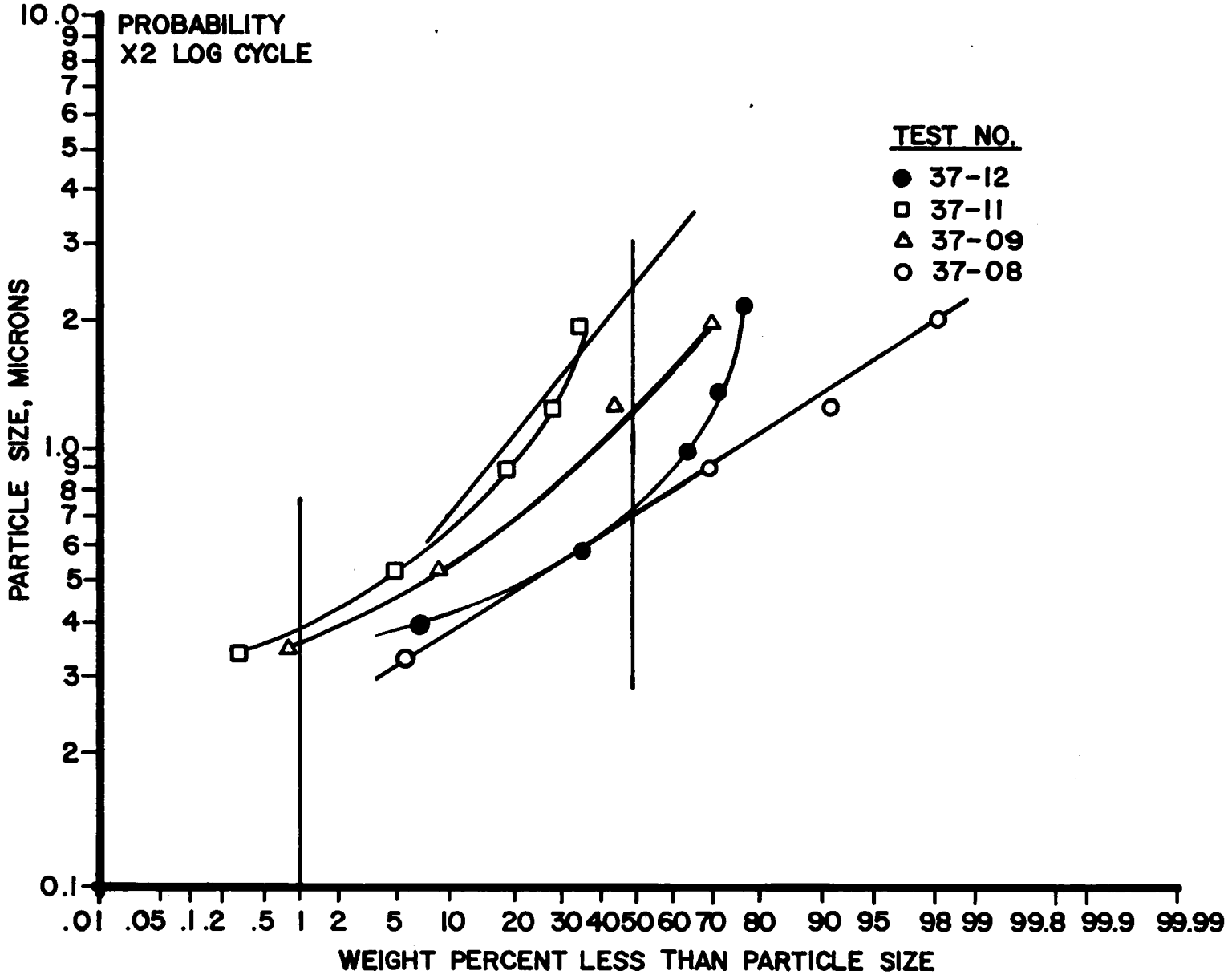

Figure 5-20. Size Distribution of Fly Ash [44].

configuration FT3 an indirect method is available. In Figure 4-8 (Page 102) a secondary combustor is shown. The purpose of the secondary combustor is to provide an oxygen rich combustion zone to complete the combustion reaction (the primary combustor is nominally sub-stoichiometric). The secondary combustor is designed to complete the combustion of hydrogen and carbon monoxide while producing nitrogen oxide below EPA limits.

The performance of the secondary combustor is evaluated by taking combustion gas samples before and after the combustor. The combustion gases entering the secondary combustor contain primarily CO, H_2, CO_2, N_2 and H_2O. After the combustion reaction in the secondary combustor no CO is found and the carbon balance before and after is in agreement. This would not be the case if free carbon was burned in the secondary combustor, i. e. the downstream total carbon would be greater than that determined from the upstream gas sample. As previously reported [46] no free carbon has been observed in the combustion gases of the primary combustor. This method is indirect, but does support the conclusion of no free carbon based on particle and slag analysis.

The conclusions reached are that under the conditions of these experiments, total carbon burn-out occurs in the combustor and no free carbon exists in the exhaust flow. These results are confirmed by the particle and ash analysis results as well as observed performance of the secondary combustor.

CHAPTER 6

SUMMARY, CONCLUSIONS AND RECOMMENDATIONS

Summary

The work described here was part of a coal-fired MHD combustor development program. Satisfactory MHD combustor performance requires high combustion gas temperature (approximately 2800°K) and which in turn dictates a design with minimum heat loss. A minimum heat loss design will have a low surface to volume ratio. The high temperature requirement implies high heat release rates and thus short combustor residence times. Heat release rates in an MHD combustor will be of the order of 10^6 BTU/sec while in conventional pulverized coal combustors the heat release rates are on the order of 10^3 BTU/sec.

To attain low heat loss and short residence times, it becomes necessary to design the combustor with a high rate of mixing between the fuel and oxidant. This requirement was met with the multiport oxidant injection plate designed as part of this project.

Diagnostics in an MHD combustor are very difficult due to the high temperature and particle densities. The only alternative was to use the heat flux distribution in the combustor in a qualitative sense to determine increases in heat release rates. When coupled to the gas analysis this proved to be adequate in evaluating changes in combustor performance with variations in oxidant velocity and distri-

bution and residence time.

The experimental results showed strong coupling between mixing rate and heat release rate (i.e. carbon conversion). In conditions such as those encountered in a pulverized coal MHD combustor, increasing mixing rate increases the oxidant diffusion rate relative to the kinetic reaction rate.

These experimental results establish the basis for the design of coal-fired MHD combustors and when compared to the theoretical model impacts present devolatilization theory. Present one-step, first order reaction models will not predict high rate devolatilization. However, the results of the present work show that a formulation in which the rate of devolatilization is dependent on the instantaneous coal particle mass will predict the experimental results. In Chapter 2 a review of present work in this area was presented and the general trend towards increasing complexity of analytical models was observed. However, the results presented here demonstrate the applicability of a one-step,first-order reaction model provided that a high rate of mixing occurs. Together, the experimental results and the theoretical model support the conclusion that diffusion rate increases with increase in mixing rate.

The parametric study showed that maximum combustion gas temperature is attained with carbon conversion on the order of 85% at a stoichiometry of 0.85, oxidant preheat temperature of 3000°R and oxygen concentration in the oxidant

of 68%. In a pulverized coal MHD combustor, where maximum gas temperatures are desired, carbon conversion should be less than 100%. The optimum carbon conversion would depend on stoichiometry, oxidant preheat temperature and oxygen concentration in the oxidant.

It has been speculated that at coal-fired MHD combustor conditions, operated sub-stoichiometrically, free carbon will exist in the form of soot. During these experiments no free carbon was found using presently available methods for determination. This conclusion was reached by both direct and indirect methods. In the case of coal-fired MHD flow trains, this conclusion impacts the design of the secondary combustor in that it should be designed to convert CO to CO_2 rather than to convert carbon to CO_2.

Conclusions

Based on the results of this work the following conclusions can be reached:

1. At the experimental conditions investigated in the present work, the combustion process becomes dominated by the mixing rate of the oxidant and fuel. Rapid mixing will increase volatile yield rate; however, there is a finite rate at which the reaction will occur based on mass transfer to the particles.

2. With high oxidant preheat temperature and oxygen concentration, pulverized coal can be totally oxidized in residence times less than 25 milliseconds provided that the rate of mixing of the oxidant and fuel is rapid.

3. Since efficient MHD combustors require high temperatures with low heat loss, it is desirable that the combustors be designed such that rapid

mixing occurs between the oxidizer and fuel. The residence time should be reduced so as to maximize peak temperature (rather than carbon conversion). Under these conditions the maximum gas temperature will be reached with minimum heat loss.

4. For a bituminous coal at high heating rates (approximately 10^5 degrees C per second), high final temperatures (approximately 3000°K) and substoichiometric conditions, total devolatilization occurs rapidly; i.e., the carbon content of the coal particles is converted to carbon monoxide and carbon dioxide and no free carbon is found to exist in combustion products.

5. The theoretical one-dimensional model described in this work will predict the observed experimental behavior provided that the mixing of the oxidizer and fuel is very rapid. The model is limited in its applicability because an estimate of the mixing length is required. As indicated, it will not accurately predict combustion behavior for cases such as coaxial injection of the oxidizer and fuel.

6. Rapid devolatilization can be modeled by single rate equation if volatile yield is taken as a function of the coal particle mass rather than a discrete fraction of the initial coal particle mass.

7. Based on the model, volatile yield rate increases with the following:

   a. Combustion pressure

   b. O_2 partial pressure in oxidant

   c. Oxidant temperature

   d. Stoichiometry in the reacting flow

   e. Residence time

8. Based on studies using the theoretical model, in conditions where high temperatures are important, such as in MHD combustors, the carbon utilization should be limited to about 85% at substoichiometric conditions because peak gas temperatures occurs somewhat before complete carbon conversion.

9. The theoretical model can be used to study oxygen blown gasifiers and could be used to aid design of these systems. The model does consider the carbon surface gasification reaction which would be important in coal gasifiers.

10. Gas analysis is a reliable way of measuring carbon conversion in conditions such as those described in this work. Because of high ash vaporization it is doubtful that the ash tracer method of anaylsis will reliably predict carbon conversion.

Recommendations

The following recommendations are made for further work:

1. The model could be improved by introducing aerodynamic effects such that the initial mixing region could be described theoretically.

2. A further improvement could be made by introducing a statistical distribution of coal particle size.

3. Further experimental work should be done in the area of reducing the carbon utilization to achieve maximum temperatures such as those required for MHD combustors.

4. In the case of MHD combustors where carbon utilization is not of primary importance, the effects of unburned carbon on conductivity are unknown and need to be investigated.

5. Experimental studies should be performed to determine the effect of oxidant preheat temperature on volatile yield in combustion systems.

REFERENCES

REFERENCES

1. Vulis, L.A, "Thermal Regimes of Combustion." McGraw Hill, New York, 1961.

2. Field, M.S., D.W. Gill, B.B. Morgan, and P.G.W. Hawksley "Combustion of Pulverized Fuel," British Coal Utilization Research Association, Leatherhead, Surrey, England 1967.

3. Essenhigh, R.H. and J.B. Howard, "Combustion Phenomena in Coal Dusts and the Two-Component Hypothesis of Coal Combustion ," Pennsylvania State Studies No. 31, Pennsylvania State University, 1971.

4. Anthony, D.B. and J.B. Howard, "Coal Devolatilization and Hydrogasification ," AIChE J. 22, 1976.

5. Howard, J.B., W.A. Peters, and E.M. Suuberg, Product Composition and Kinetics of Lignite Pyrolysis in "Symposium of Coal Gasification Kinetics American Chemical Society Preprints, Vol. 22, American Chemical Society, Washington, D.C., 1977.

6. Chung, P.M. and R.S. Smith, "An Analysis of a High Temperature Coal Combustor According to a One-Dimensional Flow Model," Argonne National Laboratory Report, Report No. ANL/MHD-77-2, 1977.

7. Chauvin, F. and R. Loison, "Pyrolyse Rapide de Charbon," Chim. Ind. (Paris) 91, pp. 269-275, 1964.

8. Anthony, D.B., H.C. Hottel, J.B. Howard, and H.P. Meissner, "Rapid Devolatilization of Pulverized Coal," in Fifteenth Symposium (International) on Combustion. The Combustion Institute, Pittsburgh, Pennsylvania, 1975.

9. Gannon, R., D. Stickler, S. Ubhayakar, C. VonRosenberg, Jr., "Rapid Devolatilization of Pulverized Coal in Hot Combustion Gases ," Proc. 16th Symposium (International on Combustion), MIT, Cambridge, August, 1976.

10. Essenhigh, R.H. and J.B. Howard, "Mechanism of Solid-Particle Combustion with Simultaneous Gas-Phase Volatiles Combustion ," in Eleventh Symposium (International) on Combustion, pp. 399-408, The Combustion Institute, Pittsburgh, Pennsylvania., 1967.

11. Horton, M.D., and L.D. Smoot, "Propagation of Laminar, Pulverized Coal-Air Flames," in Sixteenth Symposium (International) on Combustion, pp. 375-387, The Combustion Institute.

12. Gannon, R.E., H. Kobayashi, and D.B. Stickler, "Modeling of Coal in Eastern States Section," The Combustion Institute, Silver Springs, MD, 1975.

13. Howard, J.B., W.A. Peters, and E.M. Suuberg, "Product Composition and Kinetics of Lignite Pyrolysis," 173rd National Meeting, Am. Chem. Soc. Div. Fuel Chem., New Orleans, LA, March 20-25, 1977.

14. Ubhayakar, S.K., "The Behavior of Coals in Pyrolysis Under Conditions of Rapid Heating," Lecture Notes, Penn State University, University Park, Pennsylvania, 1977.

15. Coates, R.L. and J.N. Glassett, High Rate, High Temperature Pyrolysis of Coal, Final Technical Report to Bituminous Coal Research, Inc. Brigham Young University, Provo, Utah, 1974.

16. Howard, J.B., A.S. Padia, A.F. Sarofim, "The Behavior of Ash in Pulverized Coal under Simulated Combustion Conditions in Central States Section," The Combustion Institute, New York, New York, April, 1976.

17. Cogoli, J.G., Essenhigh, R.H., and D. Gray, "Problems in Pulverized Coal and Char Combustion," in Coal Gasification, p. 72, Advances in Chemistry Series, No. 131, Am. Chem. Soc., Washington, D.C., 1974.

18. Kobayashi, H., "Kinetics of Rapid Devolatization of Pulverized Coal," Sc. D. Thesis, Department of Mechanical Engineering, M.I.T., Cambridge, 1976.

19. Heffington, W.M., G.E. Parks, S.S. Penner, and K.G.P. Sulzman, "Oxidation Rates in the Post-Induction Period for Methane Over a Wide Range of Equivalence Ratios," Western States Section Meeting of the Combustion Institute, University of California, San Diego, October 18-20, 1976.

20. Bertling, H. and W. Peters, "Kinetics of the Rapid Degasification of Coals," Fuel, 44, 317, 1965.

21. Howard, J.B., H. Kobayashi, and A.F. Sarofim, "Coal Devolatilization at High Temperatures," Sixteenth Symposium (International) on Combustion, M.I.T., Cambridge, August 15-21, 1976.

22. Badzioch, S., P.G.W. Hawksley, and C.W. Peter, "Kinetics of Thermal Decomposition of Pulverized Coal Particles," Ind. Eng. Chem. Process Design and Develop., 9, 1970.

23. Bachelor, J.D., H.F. Johnstone, and H.N. Stone, "Low Temperature Carbonization Rates in a Fluidized Bed," Ind. Eng. Chem., Vol.46, pp. 274, 1954.

24. Pitt, G.J., "The Kinetics of the Evolution of Volatile Products From Coal," Fuel, Vol.44, pp. 267, 1962.

25. Essenhigh, R.H., N. Nsakala, and P.L. Walker, Jr., "Characteristics of Chars Produced by Pyrolysis Following Rapid Heating of Pulverized Coal," 173rd National Meeting, Am. Chem. Soc. Div. Fuel Chem., New Orleans, LA, March 20-25, 1977.

26. Gray, M.D., and G.M. Kimber, "Rapid Devolatilization of Small Coal Particles," Combus. Flame, Vol.11, pp.360 1967.

27. Fitgerald, D., and D.W. Van Krevelen, "Chemical Structure and Properties of Coal XXI-The Kinetics of Coal Carbonization," Fuel, Vol.38, pp. 17, 1959.

28. Johnson, J.L., "Kinetics of Coal Gasification in Hydrogen During Initial Reaction Stages," Joint U.S. -U.S.S.R. Symposium on Coal Gasification/Liquefaction, Moscow, U.S.S.R., October 12-13, 1976.

29. Reidelbach H. and M. Summerfield, "Kinetic Model for Coal Pyrolysis Optimization," 169th National Meeting, Am. Chem. Soc. Div. Fuel Chem., 20, No. 1, Philadelphia, Pennsylvania, April 6-11, 1975.

30. Gannon, R.E., H. Kobayashi, and D.B. Stickler, "Rapid Devolatilization Modeling of Coal," Eastern States Section, Fall Meeting of the Combustion Institute, Applied Physics Laboratory, Maryland, November 12-13, 1974.

31. Gannon, R.E., D.B. Stickler, and S.K. Ubhayakar, "Modeling of Pulverized Coal Entrained-Bed Gasifiers," Fuel, Vol. 56, pp. 281, 1977.

32. Gannon, R.E., D.B. Stickler, and S.K. Ubhayakar, C.W. VonRosenberg, Jr., "Diagnostics for Thermal Cracking of Coal Volatiles in Entrained-Bed Gasifiers," Western States Section Meeting of the Combustion Institute, University of California, San Diego, CA, October 18-20, 1976.

33. Louis, J.F., et. al, "Open Cycle Coal Fired MHD Power Generation," Final Report for the Period 21, May, 1971, 31, May, 1975, Department of Aeronautics and Astronautics, MIT, prepared for ERDA Fossil Energy Contract No. E (49-18)-1209, Vol. I and II.

34. Spaulding, D.B., "Some Fundamentals of Combustion," Gas Turbine Series, Vol.2, Butterworth Scientific Publications, London, England, 1955.

35. Williams, F.A., Combustion Theory, Addison Wesley, London, England, 1965.

36. Ahluwalia, R., "Asymptotic Multiple Reaction Ignition Theory of Solid Fuel," Ph.D. Dissertation, University of Illinois at Chicago Circle, Department of Energy Engineering, 1977.

37. Chung, P.M., "Chemically Reacting Nonequilibrium Boundary Layers," Advances in Heat Transfer, Vol. II, Chapter 2, Academic Press, New York, New York, 1965.

38. Heywood, J.B., and G.J. Womack, "Open Cycle MHD Power Generation." Pergamon Press, Oxford, Great Britain, 1969.

39. Juntgen, H., and K. VanHeek, "Gas Release from Coal as a Function of the Rate of Heating," Fuel, Vol. 47, 103, 1968.

40. Essenhigh, R.H., and J.B. Howard, "Pyrolysis of Coal Particles in Pulverized Fuel Flames," I & EC Process Design and Development, Vol. 6, pp. 74, 1967.

41. Downs, W., and S.S. Strom, "New Particle Size Measuring Probe-Applications to Aerosal Collection and Emissions Evolution," Transaction ASME, Journal of Engineering for Power, 1972.

42. Baucum, W. E., "Evaluation of Coriolis Mass Flow Meter for Pulverized Coal Flows," DOE Topical Report No. FE-10815-45, 1979.

43. Stickler, D.B., et. al, "Progress in Coal Combustion Research at AERL," 18th Symposium Engineering Aspects of Magnetohydrodynamics, Butte, Montana, 1979.

44. Lanier, J., et. al, "Secondary Combustor Performance," Quarterly Technical Progress Report, July-September, 1978, DOE Report No. FE-1760-35.

45. ASTM Method D3178-73, Handbook of ASTM Standards, Part 26, 1979.

46. Attig, R., P. Kulesza, and J. Lanier, "Secondary Combustor Evaluation," DOE Report No. FE-1760-41, 1979.

47. Arora, B.S., "A Mathematical Model of a Pulverized Coal Fired Combustion Chamber." PhD Dissertation, University of Tennessee, 1976.

48. Wu, Y. C. L, "Performance Theory of Diagonal Conducting Wall MHD Generators," AIAA Journal, Vol. 14, No. 10, pp. 1362-1368, Oct. 1976

49. Mentser, M. H., O'Donnel, J., Ergin, S., and Friedell, R.A., "Rapid Thermal Decomposition of Bituminous Coals," Coal Gasification, Advances in Chemistry Series, No. 131, pp. 1-7, American Chemical Society, Washington, D. C. (1974).

APPENDIX

```
          CASE PAK 1      TEST 43   59802  4000 K
 A=1.
 B=1.
 D=1.
 BETA=12.0
 CC=1.761E+10
 CCa=2.5E+06
 CD=1.125
 COAL_CONSUMED_CRIT=99.99
 CPG=0.50
 CPS=0.50
 DELTA_H3=2766.
 DELTA_H5=1372.0
 DELTA_H10=51606.
 DELTA_S=65.
 ERR=.000001
 ESKU=45000.
 EVRU=38140.
 Ea=.8
 ESW=.77
 FLOW_AIR=0.96
 FLOW_COKE_02=1.39
 FLOW_COAL=1.00
 HHV=10890.
 KKK=0
 L=2520.
 Lu=730.
 Le=1.
 MW(1)=32.
 MW(2)=28.
 MW(3)=44.
 MW(4)=28.
 MW(5)=46.
 MW(6)=30.
 MW(7)=16.
 MW(8)=64.
 MW(9)=44.
 MW(10)=2.
 MW(11)=1.
 MW(12)=32.
 MW(13)=32.
 MW(14)=12.
 MW(15)=14.
 PC_ASH=22.50
 PRESSURE(1)=10384.
 PRINT_CONSTANTS='NO'
 QRATIO=1.0
 QR%=1.0
 RADIUS(1)=.000082
 RHOD_AVE=0.0001U149
 R_UNIV=1544.
 SEC_PAGE='YES'
 T_GAS(1)=3000.
 T_SOLID2=500.
 T_WALL=2800.
 UNITS='METRIC'
 ZC=.5940
 ZN=.0108
 ZH=0.0441
 ZH2O=.0270
```

```
 ZS=.0351
 ZOX=.0640
 IPR=4
 PR(1)=.1
 DPR(1)=.01
 PR(2)=0.7
 DPR(2)=.05
 PR(3)=5.
 DPR(3)=.20
 PR(4)=999.
 DPR(4)=1.
 JOT=3
 XC4(1)=.3
 DXT(1)=.0005
 XC4(2)=1.
 DXT(2)=.005
 XC4(3)=2.
 DXT(3)=.01
 DXT(4)=.050;


 I   CERTAIN DEFINITIONS FROM 2ND OUTPUT PAGE
 I   ------- ----------- ---- --- ------ ----
 I       VAPOR PRESSURE
 I         FUEL1 = COMBUSTIBLE VAPORIZED DUE TO PARTICLE HEATING
 I         FUEL2 = COMBUSTIBLE VAPORIZED DUE TO CHEMICAL SURFACE REACTION WITH CO_2 AND H_2O
 I       FF = DEVIATION FROM PROPORTIONAL VOLITILIZATION OF ASH & FUEL REMAINING IN COAL
 I - - - - - - - - - - - - - - - - - - - - - - - - - - - - - - - - - -


 STOICHIOMETRIC OXYGEN TO FUEL RATIO =  1.9016
 ACTUAL OXYGEN TO FUEL RATIO =  1.6137
 STOICHIOMETRIC OXYGEN RATIO =  0.8477
```

POSITION METERS	TIME (M. SEC.)	PRESSURE KILO PA.	VELOCITY M/SEC	DENSITY KG/M_3	GAS TEMP. K	SOLID TEMP.-K	PART RAD MICRONS	M DOT KG/(S-M_3)	% COAL BURNED	% ASH VAPORIZED	AVE M.W.	ENTHALPY J/GRAM
0.0000	0.00	506.76	10.296	1.54925	1666.67	277.78	24.99360	0.0000	0.0000	0.0000	30.6290	9531.71
0.0000	0.00	506.76	10.621	1.54649	1666.67	2547.10	23.86739	143.2578	16.6664	0.0000	31.3242	9531.59
0.0007	0.01	506.76	10.640	1.52348	1668.74	2552.23	23.82701	142.0722	17.2250	0.0441	31.3214	9531.45
0.0003	0.03	506.76	10.841	1.49980	1713.65	2557.36	23.78728	139.1724	17.7702	0.0891	31.3429	9531.32
0.0005	0.04	506.75	10.971	1.49960	1737.67	2562.99	23.74824	136.2377	18.3036	0.1349	31.3638	9531.32
0.0030	0.25	506.71	13.487	1.21999	2075.36	2845.05	23.10848	101.8413	25.9491	1.0476	31.6574	9528.80
0.0061	0.46	506.68	15.529	1.05959	2355.02	2724.64	22.60911	81.5923	32.7904	2.5106	31.8824	9525.24
0.0091	0.65	506.66	17.048	0.98527	2548.98	2790.84	22.12450	69.4591	38.2444	4.4638	31.9802	9521.05
0.0122	0.84	506.64	18.198	0.90419	2619.27	2846.34	21.68585	61.3808	42.7305	6.5525	31.9758	9516.30
0.0152	0.96	506.62	19.103	0.86136	2709.97	2893.30	21.27760	55.5830	46.5196	9.9900	31.9146	9511.05
0.0183	1.14	506.61	19.837	0.82947	2834.73	2933.37	20.89048	51.1733	49.7506	13.5581	31.8315	9505.37
0.0213	1.29	506.60	20.430	0.80481	2886.48	2966.74	20.51809	47.6407	52.5260	17.6094	31.7458	9499.31
0.0244	1.44	506.59	20.973	0.78457	2916.45	2997.48	20.15855	44.6855	54.9238	22.0731	31.6660	9492.92
0.0274	1.58	506.58	21.422	0.76810	2940.44	3023.28	19.80782	42.0914	57.0001	26.8616	31.5974	9486.23
0.0305	1.72	506.56	21.814	0.75430	2960.47	3045.85	19.46531	39.7229	58.8242	31.8782	31.5399	9479.28
0.0457	2.40	506.55	23.208	0.70099	3029.59	3128.84	17.87859	29.0988	65.2451	57.0871	31.4779	9441.54
0.0610	3.04	506.54	24.064	0.68377	3056.41	3178.14	16.55847	19.5812	69.3054	76.4873	31.3003	9400.17
0.0762	3.67	506.53	24.647	0.66760	3072.99	3207.39	15.57310	12.4276	72.4065	87.5324	31.2159	9356.45
0.0914	4.28	506.52	25.078	0.65612	3085.13	3213.68	14.86810	8.2533	75.0261	92.4597	31.1133	9311.64
0.1067	4.88	506.52	25.407	0.64704	3094.41	3204.12	14.33144	5.1558	77.3145	94.3474	31.0088	9266.88
0.1219	5.48	506.51	25.681	0.64072	3101.00	3187.19	13.88094	5.0513	79.3383	95.0325	30.9116	9222.83
0.1372	6.07	506.51	25.909	0.63508	3105.48	3167.70	13.47629	4.3714	81.1432	95.2817	30.8252	9179.76
0.1524	6.65	506.51	26.101	0.63041	3108.24	3147.57	13.09980	3.8846	82.7652	95.3726	30.7494	9137.73
0.1676	7.24	506.50	26.264	0.62651	3109.65	3127.53	12.74329	3.5005	84.2329	95.4039	30.6831	9096.75
0.1829	7.81	506.50	26.402	0.62324	3109.85	3101.85	12.40260	3.1805	85.5653	95.4120	30.6251	9056.81
0.1981	8.39	506.50	26.519	0.62049	3109.38	3088.63	12.07478	2.9055	86.7826	95.4114	30.5742	9017.85
0.2438	10.11	506.50	26.770	0.61465	3103.72	3033.82	11.15416	2.2614	89.8653	95.4043	30.4563	8906.60
0.3048	12.37	506.49	26.941	0.61075	3094.14	2988.74	10.03826	1.8852	92.9709	95.4341	30.3581	8770.13
0.3658	14.63	506.49	26.988	0.60976	3073.48	2904.09	9.00762	1.2470	95.2564	95.5329	30.3071	8645.58
0.4267	16.89	506.49	26.950	0.61056	3054.70	2848.90	8.04360	0.9399	96.9456	95.7062	30.2875	8531.57
0.4877	19.16	506.49	26.857	0.61267	3035.34	2791.00	7.12495	0.7081	98.1850	95.9556	30.2915	8427.07
0.5486	21.44	506.50	26.778	0.61502	3015.84	2735.61	6.23615	0.5247	99.0758	96.2789	30.3122	8331.36
0.6096	23.72	506.50	26.577	0.61911	2996.74	2634.73	5.36326	0.3873	99.6913	96.6719	30.3451	8243.98
0.6553	25.45	506.50	26.457	0.62194	2983.48	2633.60	4.71187	0.3005	100.0047	97.0060	30.3784	8183.83

POSITION FEET	TIME (M. SEC.)	PRESSURE LB/FT_2	VELOCITY FT/SEC	DENSITY LB/FT_3	GAS TEMP. R	SOLID TEMP.-R	PARTICLE RADIUS-FT	M DOT LB/(S-FT_3)	% COAL BURNED	% ASH VAPORIZED	AVE M.W.	ENTHALPY BTU/LB
0.0000	0.00	10584.0	33.780	0.096716	3000.00	500.00	0.0000820	0.00000	0.0000	0.0000	30.6290	4262.84
0.0000	0.00	10584.0	34.840	0.096544	3000.00	4564.78	0.0000783	8.94327	16.6684	0.0000	31.3242	4262.78
0.0005	0.01	10584.0	34.908	0.095107	3039.73	4594.01	0.0000782	8.86926	17.2250	0.0441	31.3214	4262.73
0.0010	0.03	10583.9	35.035	0.093626	3084.57	4603.80	0.0000780	8.88823	17.7702	0.0891	31.3429	4262.67
0.0015	0.04	10583.9	35.995	0.093629	3128.17	4613.39	0.0000779	8.50502	18.3036	0.1349	31.3638	4262.67
0.0100	0.25	10583.0	44.250	0.076101	3735.64	4761.09	0.0000760	6.35773	25.9491	1.0476	31.6574	4261.54
0.0200	0.46	10582.3	50.949	0.066148	4239.03	4904.36	0.0000742	5.09363	32.7904	2.5106	31.8824	4259.94
0.0300	0.65	10581.8	55.927	0.060200	4586.48	5021.51	0.0000726	4.41618	38.2344	4.4638	31.9802	4258.07
0.0400	0.82	10581.4	59.705	0.056448	4822.69	5123.41	0.0000711	3.83187	42.7305	6.9525	31.9758	4255.95
0.0500	0.98	10581.1	62.672	0.053774	4985.95	5207.95	0.0000698	3.46993	46.5198	9.9900	31.9146	4253.60
0.0600	1.14	10580.8	65.083	0.051782	5102.51	5280.07	0.0000685	3.19464	49.7506	13.5581	31.8315	4251.06
0.0700	1.29	10580.6	67.094	0.050230	5188.48	5341.99	0.0000674	2.97448	52.5260	17.6094	31.7458	4248.35
0.0800	1.44	10580.4	68.808	0.048979	5253.20	5395.46	0.0000661	2.78962	54.9238	22.0731	31.6660	4245.49
0.0900	1.58	10580.3	70.283	0.047951	5303.60	5441.90	0.0000650	2.62768	57.0061	26.8616	31.5974	4242.50
0.1000	1.72	10580.2	71.569	0.047089	5343.24	5482.53	0.0000639	2.47982	58.8242	31.8782	31.5399	4239.39
0.1500	2.40	10579.7	76.143	0.044401	5453.48	5626.48	0.0000587	1.81658	65.2451	57.0871	31.3779	4222.51
0.2000	3.04	10579.4	78.952	0.042686	5501.54	5720.66	0.0000543	1.22241	69.3054	76.4873	31.3003	4204.01
0.2500	3.67	10579.2	80.864	0.041677	5531.39	5773.31	0.0000511	0.77583	72.4065	87.5324	31.2159	4184.46
0.3000	4.28	10579.0	82.278	0.040960	5553.23	5784.62	0.0000488	0.51524	75.0261	92.4597	31.1133	4164.42
0.3500	4.88	10578.9	83.350	0.040411	5569.74	5767.41	0.0000470	0.38429	77.3145	94.3474	31.0088	4144.40
0.4000	5.48	10578.8	84.256	0.039999	5581.80	5736.94	0.0000455	0.31534	79.3383	95.0325	30.9116	4124.70
0.4500	6.07	10578.7	85.004	0.039647	5589.86	5701.86	0.0000442	0.27269	81.1432	95.2817	30.8252	4105.44
0.5000	6.65	10578.7	85.634	0.039355	5594.83	5665.63	0.0000430	0.24251	82.7652	95.3726	30.7494	4086.64
0.5500	7.24	10578.6	86.167	0.039114	5597.48	5629.56	0.0000418	0.21853	84.2320	95.4039	30.6831	4068.32
0.6000	7.81	10578.6	86.620	0.038901	5591.92	5594.14	0.0000407	0.19855	85.5653	95.4120	30.6251	4050.45
0.6500	8.39	10578.5	87.003	0.038736	5596.88	5559.53	0.0000396	0.18139	86.7826	95.4114	30.5742	4033.03
0.8000	10.11	10578.4	87.830	0.038371	5586.70	5460.88	0.0000366	0.14118	89.8653	95.4043	30.4563	3983.27
1.0000	12.37	10578.4	88.391	0.038128	5582.90	5340.12	0.0000329	0.10395	92.9709	95.4143	30.3581	3922.24
1.2000	14.63	10578.4	88.535	0.038066	5532.27	5228.99	0.0000296	0.07785	95.2564	95.5329	30.3071	3866.54
1.4000	16.89	10578.4	88.418	0.038116	5498.47	5124.42	0.0000264	0.05868	96.9456	95.7062	30.2875	3815.55
1.6000	19.16	10578.4	88.114	0.038247	5463.62	5023.79	0.0000234	0.04421	98.1850	95.9556	30.2915	3768.82
1.8000	21.44	10578.5	87.691	0.038432	5428.54	4924.99	0.0000205	0.03301	99.0758	96.2789	30.3122	3726.01
2.0000	23.72	10578.5	87.194	0.038651	5394.11	4821.72	0.0000176	0.02418	99.6913	96.6719	30.3453	3686.93
2.1500	25.45	10578.6	86.800	0.038826	5370.27	4740.48	0.0000155	0.01876	100.0047	97.0060	30.3784	3660.03

POSITION	M.F. SOLID	M.F. O_2	M.F. CO	M.F. CO_2	M.F. N_2	M.F. NO_2	M.F. NO	M.F. H_2O	M.F. SO_2	M.F. ASH	M.F. H_2
0.0000	0.2985075	0.4816955	0.0000000	0.0000000	0.2197970	0.0000000	0.0000000	0.0000000	0.0000000	0.0000000	0.0000000
0.0000	0.2599462	0.3855368	0.0000000	0.1083696	0.2197970	0.0017656	0.0000000	0.0210918	0.0034929	0.0000000	0.0000000
0.0005	0.2566291	0.3823275	0.0000020	0.1119648	0.2192561	0.0000474	0.0023181	0.0217958	0.0036095	0.0000296	0.0000000
0.0010	0.2573374	0.3791823	0.0000027	0.1155298	0.2192375	0.0000441	0.0023978	0.0224857	0.0037238	0.0000598	0.0000000
0.0015	0.2560726	0.3761059	0.0000038	0.1189950	0.2192192	0.0000403	0.0024764	0.0231606	0.0038356	0.0000906	0.0000000
0.0100	0.2377724	0.3521152	0.0001862	0.1484150	0.2189646	0.0000136	0.0035675	0.0328227	0.0054377	0.0007036	0.0000014
0.0200	0.2209627	0.2936219	0.0017538	0.2104308	0.2187423	0.0000078	0.0045203	0.0413916	0.0068713	0.0016862	0.0000112
0.0300	0.2070566	0.2650318	0.0063138	0.2386590	0.2185662	0.0000060	0.0052749	0.0480441	0.0080121	0.0029981	0.0000374
0.0400	0.1949837	0.2438048	0.0137239	0.2582459	0.2184210	0.0000053	0.0058970	0.0533551	0.0089543	0.0046696	0.0000794
0.0500	0.1841774	0.2273033	0.0226228	0.2688974	0.2182988	0.0000050	0.0064209	0.0576851	0.0097483	0.0067097	0.0001311
0.0600	0.1743066	0.2143797	0.0316452	0.2734104	0.2181946	0.0000049	0.0068674	0.0612728	0.0104253	0.0091062	0.0001867
0.0700	0.1651649	0.2038930	0.0407305	0.2774921	0.2181051	0.0000049	0.0072509	0.0642817	0.0110069	0.0118272	0.0002426
0.0800	0.1566197	0.1952204	0.0496019	0.2800834	0.2180278	0.0000049	0.0075822	0.0668282	0.0115094	0.0148252	0.0002969
0.0900	0.1485864	0.1878891	0.0584820	0.2816666	0.2179607	0.0000050	0.0078698	0.0690055	0.0119457	0.0180414	0.0003476
0.1000	0.1410110	0.1816194	0.0672039	0.2831240	0.2179021	0.0000050	0.0081209	0.0708811	0.0123267	0.0214107	0.0003948
0.1500	0.1092253	0.1600326	0.0676719	0.2864199	0.2176952	0.0000054	0.0090076	0.0773487	0.0136722	0.0383421	0.0005790
0.2000	0.0868019	0.1465272	0.1042488	0.2883403	0.2175644	0.0000057	0.0095682	0.0814420	0.0145231	0.0513741	0.0007061
0.2500	0.0742095	0.1383085	0.1152313	0.2896714	0.2174645	0.0000060	0.0099963	0.0843390	0.0151729	0.0587904	0.0008091
0.3000	0.0628398	0.1278321	0.1255503	0.2904879	0.2173802	0.0000062	0.0103579	0.0868222	0.0157219	0.0620998	0.0009015
0.3500	0.0562779	0.1204656	0.1345963	0.2911552	0.2173064	0.0000065	0.0106739	0.0889651	0.0162016	0.0633677	0.0009853
0.4000	0.0511359	0.1135598	0.1425780	0.2917704	0.2172413	0.0000067	0.0109532	0.0908417	0.0166257	0.0638278	0.0010613
0.4500	0.0467929	0.1081146	0.1496111	0.2924631	0.2171831	0.0000069	0.0112023	0.0925084	0.0170039	0.0639952	0.0011299
0.5000	0.0429796	0.1028106	0.1556367	0.2932152	0.2171309	0.0000072	0.0114261	0.0940035	0.0173438	0.0640562	0.0011918
0.5500	0.0395652	0.0979570	0.1613680	0.2940594	0.2170837	0.0000074	0.0116285	0.0953562	0.0176511	0.0640773	0.0012477
0.6000	0.0364731	0.0934893	0.1668425	0.2949742	0.2170408	0.0000076	0.0118124	0.0965880	0.0179305	0.0640827	0.0012983
0.6500	0.0336594	0.0893553	0.1707159	0.2959530	0.2170016	0.0000078	0.0119804	0.0977161	0.0181856	0.0640823	0.0013441
0.8000	0.0265340	0.0785881	0.1814148	0.2991857	0.2169024	0.0000084	0.0124055	0.1005998	0.0188316	0.0640775	0.0014571
1.0000	0.0193279	0.0671307	0.1912316	0.3039470	0.2168025	0.0000092	0.0128336	0.1035760	0.0194824	0.0640977	0.0015631
1.2000	0.0139782	0.0580409	0.1974496	0.3090360	0.2167290	0.0000099	0.0131484	0.1058576	0.0199614	0.0641639	0.0016309
1.4000	0.0099499	0.0507307	0.2011451	0.3142111	0.2166748	0.0000106	0.0133809	0.1076317	0.0203153	0.0642803	0.0016713
1.6000	0.0069153	0.0447618	0.2029411	0.3194462	0.2166351	0.0000113	0.0135513	0.1090262	0.0205750	0.0644478	0.0016906
1.8000	0.0046372	0.0398855	0.2033472	0.3245999	0.2166065	0.0000119	0.0136735	0.1101188	0.0207617	0.0646650	0.0016945
2.0000	0.0029495	0.0358997	0.2028955	0.3296252	0.2165869	0.0000125	0.0137578	0.1109884	0.0208907	0.0649289	0.0016866
2.1500	0.0020001	0.0333311	0.2015636	0.3334521	0.2165768	0.0000129	0.0138007	0.1114845	0.0209567	0.0651533	0.0016735

POSITION	(VAPOR PRESSURE) FUEL1	FUEL2	ASH	COAL LAT HEAT	PF	(COAL COMPOSITION) ASH	FUEL	(VAPORIZED COAL) ASH	FUEL	(INTEGRATED PARAMS FOR MASS FRACTIONS) GAMMA(1)	GAMMA(2)	GAMMA(3)	GAMMA(4)
FEET	- - - LB/FT-2 - - -			BTU/LB	LB/SEC								
0.0000	12799.59	0.00	33.659	2511.2	0.21675	0.22500	0.77500	0.00825	0.99175	0.00000	0.00000	0.00000	0.00000
0.0000	10169.72	116.02	75.874	2486.4	0.23631	0.25838	0.74162	0.02206	0.97794	0.42494	-0.24534	-0.21926	0.02109
0.0005	10128.42	121.77	78.745	2484.8	0.23665	0.25958	0.74042	0.02293	0.97707	0.42305	-0.24330	-0.21924	0.02180
0.0010	10094.58	126.01	81.809	2483.4	0.23696	0.26078	0.73922	0.02385	0.97615	0.42119	-0.24130	-0.21922	0.02249
0.0015	10066.88	130.16	85.033	2481.5	0.23716	0.26193	0.73807	0.02480	0.97520	0.41938	-0.23934	-0.21921	0.02316
0.0100	9590.47	196.33	149.407	2466.7	0.23535	0.27951	0.72049	0.04416	0.95584	0.39335	-0.21127	-0.21896	0.03284
0.0200	8959.52	272.76	249.867	2390.5	0.22087	0.29633	0.70367	0.07546	0.92454	0.37005	-0.18616	-0.21874	0.04149
0.0300	8442.11	342.99	374.738	2340.2	0.19344	0.32080	0.67920	0.11568	0.88432	0.35192	-0.16817	-0.21856	0.04838
0.0400	7976.67	404.61	515.482	2232.8	0.15121	0.32051	0.67949	0.16325	0.83675	0.33621	-0.14966	-0.21842	0.05407
0.0500	6694.56	458.36	667.722	2138.4	0.11242	0.32824	0.67176	0.21582	0.78418	0.32331	-0.13575	-0.21830	0.05886
0.0600	5933.65	505.83	823.045	2039.9	0.06244	0.33308	0.66692	0.27064	0.72936	0.31231	-0.12389	-0.21819	0.06295
0.0700	5210.41	548.82	974.277	1996.2	0.01001	0.34594	0.65406	0.34501	0.65499	0.30286	-0.11370	-0.21810	0.06646
0.0800	4555.36	587.97	1115.087	1849.6	-0.04242	0.33418	0.66582	0.37660	0.62340	0.29469	-0.10490	-0.21803	0.06950
0.0900	3957.69	625.25	1240.448	1765.0	-0.09310	0.33060	0.66940	0.42371	0.57629	0.28701	-0.09726	-0.21796	0.07213
0.1000	3425.07	661.27	1346.796	1690.4	-0.14078	0.32447	0.67553	0.46524	0.53476	0.28142	-0.09058	-0.21790	0.07443
0.1500	1640.00	841.05	1534.747	1484.6	-0.31987	0.28188	0.71812	0.58075	0.41925	0.25925	-0.06701	-0.21769	0.08256
0.2000	812.67	1025.05	1326.111	1520.7	-0.37183	0.18193	0.81807	0.55976	0.44024	0.24573	-0.05210	-0.21756	0.08770
0.2500	449.00	1162.38	951.347	1748.2	-0.31710	0.11597	0.88403	0.43306	0.56694	0.23517	-0.04072	-0.21746	0.09162
0.3000	271.57	1206.00	677.959	2056.0	-0.18112	0.08059	0.91941	0.26171	0.73829	0.22625	-0.03110	-0.21738	0.09494
0.3500	174.49	1176.48	548.264	2229.0	-0.08115	0.06748	0.93254	0.12861	0.87139	0.21846	-0.02270	-0.21730	0.09783
0.4000	114.14	1119.47	493.393	2424.1	0.00853	0.06525	0.93475	0.05672	0.94328	0.21157	-0.01521	-0.21724	0.10039
0.4500	76.38	1052.95	472.965	2483.0	0.04378	0.06772	0.93228	0.02394	0.97606	0.20542	-0.00864	-0.21718	0.10268
0.5000	51.67	987.56	464.728	2508.7	0.06269	0.07231	0.92769	0.00962	0.99038	0.19990	-0.00269	-0.21713	0.10473
0.5500	35.21	928.00	461.077	2520.1	0.07415	0.07802	0.92198	0.00327	0.99673	0.19491	0.00270	-0.21708	0.10659
0.6000	24.12	868.80	459.299	2525.2	0.08405	0.08448	0.91552	0.00043	0.99957	0.19037	0.00759	-0.21704	0.10827
0.6500	16.58	815.63	458.304	2527.4	0.09232	0.09156	0.90844	-0.00076	1.00076	0.18622	0.01206	-0.21700	0.10981
0.7000	11.45	678.58	457.667	2526.0	0.11635	0.11633	0.88367	-0.00002	1.00002	0.17573	0.02338	-0.21690	0.11371
0.8000	5.45	533.16	457.121	2514.4	0.13613	0.15886	0.84114	0.00651	0.99349	0.16515	0.03478	-0.21680	0.11764
1.0000	1.23	416.18	462.521	2491.1	0.19527	0.21470	0.78530	0.01943	0.98057	0.15737	0.04317	-0.21673	0.12054
1.2000	0.27	316.94	467.480	2453.6	0.24951	0.26984	0.71016	0.04033	0.95967	0.15162	0.04937	-0.21667	0.12267
1.4000	0.05	228.66	474.125	2394.7	0.31972	0.39281	0.60719	0.07309	0.92691	0.14740	0.05392	-0.21663	0.12424
1.6000	0.00	145.84	482.445	2345.4	0.38248	0.53894	0.46106	0.12256	0.87744	0.14437	0.05719	-0.21660	0.12537
2.0000	0.00	63.53	492.738	2170.1	0.35966	0.75784	0.24216	0.19816	0.80184	0.14227	0.05945	-0.21658	0.12615
2.1500	-0.00	-1.21	502.216	2015.2	0.72100	1.00539	-0.00539	0.28439	0.71561	0.14120	0.06060	-0.21657	0.12655

VITA

William L. Holt was born August 13, 1940, in Whites Creek, Tennessee. He attended Vanderbilt University and received a Bachelor of Engineering degree in Mechanical Engineering in 1962. While employed by Pratt and Whitney Aircraft Company in West Palm Beach, Florida, he received a Masters of Engineering degree in Mechanical Engineering from the University of Florida.

He was awarded an Atomic Energy Commission Fellowship in 1965 and attended Vanderbilt University from 1965 until 1970 pursuing graduate studies in Mechanical Engineering. During this time he served as a teaching assistant at Vanderbilt and Tennessee State University.

During the period from 1970 to 1977 he was employed in industry in both technical and management positions.

In 1977 he was offered a Research Assistantship at the University of Tennessee Space Institute, Tullahoma, Tennessee, and pursued graduate studies in Mechanical Engineering. During 1978 he became a full-time employee of the Energy Conversion Division at UTSI and presently holds the position of Research Scientist.

He is married and has three children, Ashley, Katie and Lee.